Politecnico di Torino

POLITECNICO DI TORINO

Master of Science in Materials Engineering for Industry 4.0

Master's Degree Thesis

Effect of Processing Parameters on the Disintegration of PHA-Based Bio-Compounds

Supervisor:

Prof. Alberto FRACHE

Co-supervisors:

Mr. Amir NOORI

Mr. Alessio CARMINATI

Candidate:

Nazanin SEDGHI

Academic year 2025/2026

April 2026

Acknowledgement

First and foremost, I wish to express my sincere gratitude to my supervisor, Professor Alberto Frache, for his guidance, patience, and encouragement throughout this work. I am deeply grateful for the trust he placed in me by offering me the opportunity to collaborate with him, and for the dedication he showed at every stage of this journey.

I would also like to extend my heartfelt thanks to the entire team at MAIP Compounding Srl for their warm welcome and genuine consideration. The time spent within their company proved to be an incredibly valuable and formative experience, one that has left a lasting impression on both my academic and personal growth.

Abstract

Polyhydroxyalkanoates (PHAs) are becoming increasingly prominent as sustainable alternatives to conventional plastics, driven by growing demand for biodegradable materials. However, their overall processability and post-processing behaviour strongly depend on the manufacturing conditions. In this study, the effect of key extrusion processing parameters (barrel temperature, feed rate, and screw speed) on the disintegration of PHAs was investigated.

To address this, a combined numerical and experimental approach was adopted. The chosen material (IamNATURE B6 G713) was processed under controlled extrusion conditions by systematically varying screw speed, feed rate, and barrel temperature in five extrusion trials, then, using an injection moulding machine, it was moulded at 20°C and °C. The mechanical properties of the resulting material were characterised under tensile, three-point bending (flexural), and Charpy impact (notched and unnotched) loading.

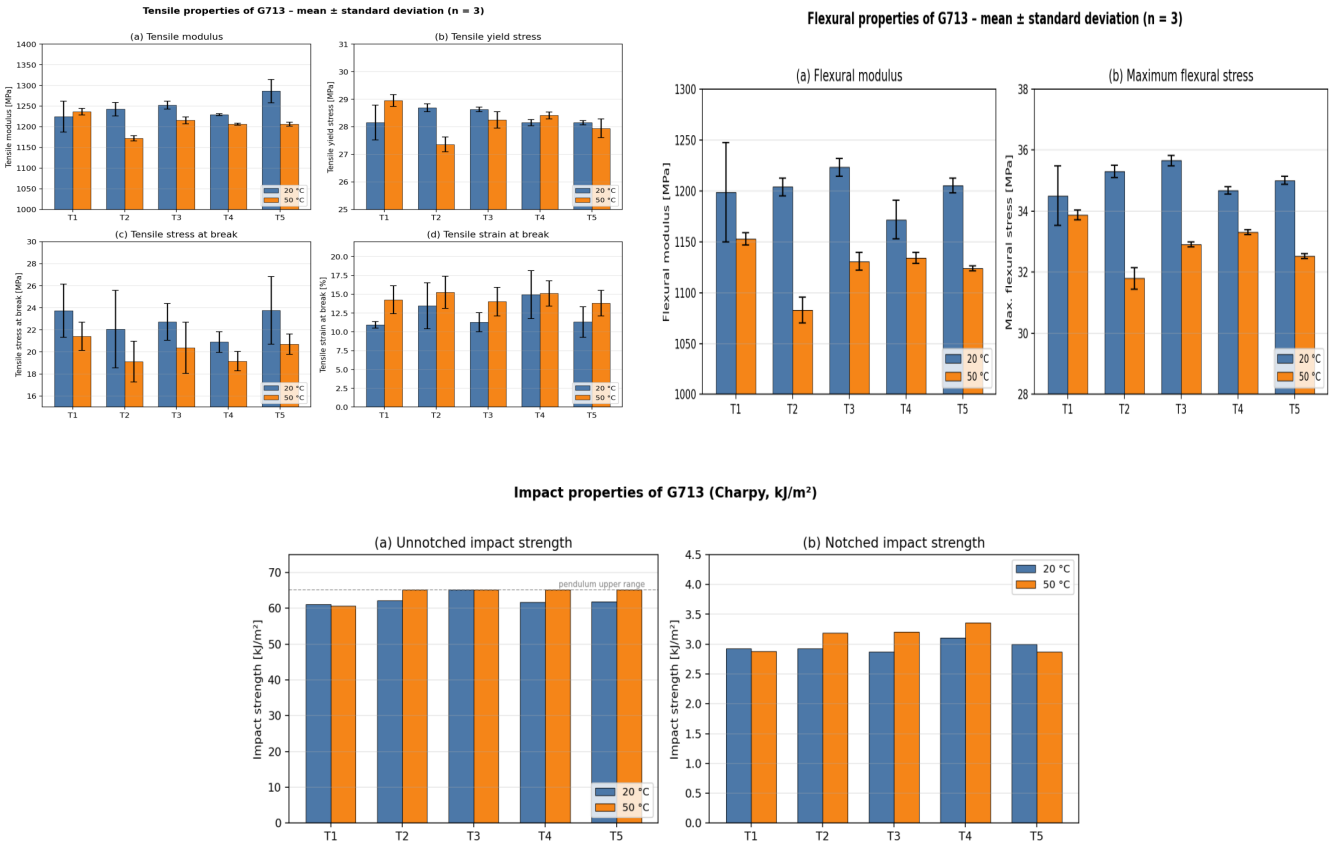

In all trials, the material exhibited semi-ductile thermoplastic behaviour, with a consistent yield stress of approximately 28 MPa, a tensile modulus in the range 1170 to 1290 MPa, a flexural modulus of 1083 to 1223 MPa, and Charpy impact energies of approximately 60–65 kJ/m² (unnotched) and 3 kJ/m² (notched). Increasing the mould temperature from 20 °C to 50 °C

produced a small but reproducible reduction in stiffness and stress at break accompanied by an increase in strain at break, while yield stress and flexural strain at maximum force remained essentially unaffected. The material displayed clear notch sensitivity, whereas temperature effects within each notch configuration were within experimental scatter.

In this study, besides the effect of independent processing parameters on disintegration, the effect of dependent variables which were related to the applied stress on the material was also investigated. These dependent variables were Specific Mechanical Energy (SME), torque, pressure, viscosity, shear rate, and residence time. Since these are the dependent variables on processing parameters, a simulation was conducted using Ludovic software to evaluate the effect of processing parameters on them.

In addition, standardised disintegration tests were carried out over a defined time period to assess the degradation performance of the samples with the thickness of 1mm and 2mm. It should be mentioned that all the 1mm samples were completely disintegrated over the time period of the disintegration test. These results were then further imported into the Minitab software to identify the most influential parameters governing the disintegration behaviour.

Results indicated that the only parameters which affect the disintegration behaviour of the material were the feed rate and the mould temperature. Based on the formula given by the Minitab software, increasing each of them will reduce the disintegration percentage of the material.

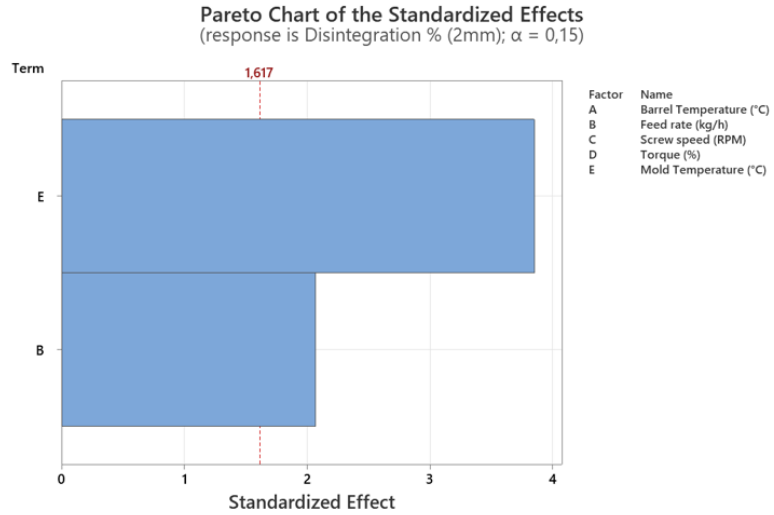

$$Disintegration\ \%\ (2mm) = 76.85 - 0.1129\ Feed\ rate\ (\frac{kg}{h}) - 0.2400\ Mould\ temperature\ (℃)$$

Table of Contents

1 Chapter 1 1

1.1 Introduction 1

1.2 Theoretical Fundamentals 3

1.2.1 Polyhydroxyalkanoate (PHA) 3

1.2.2 Chemical structure and classification of PHA 4

1.2.3 Biosynthesis of PHA 6

1.2.4 Physical, Thermal, and Mechanical Properties of PHA 8

1.2.5 Applications of PHA 11

1.2.6 Biodegradation of PHA 13

1.2.7 PHA blends, Bio composites, and Commercial Development 16

1.2.8 Challenges and Future Perspectives 17

1.2.9 Processing techniques and the effect of processing parameters on PHA during processing 18

2 Chapter 2 29

2.1 Experimental section 30

2.1.1 Materials and methods 30

2.2 Setting of the simulation with Ludovic software 43

2.2.1 “Extruder” Tab 43

2.2.2 “Product” Tab 44

2.2.3 Process tab 52

2.2.4 Design of Experiment (DoE) 53

2.3 Analysing the simulation results 107

2.3.1 Temperature 107

2.3.2 Pressure 110

2.3.3 Total Residence Time 112

2.3.4 Viscosity 113

2.3.5 Shear rate 116

2.3.6 Mechanical ΔT (°C) ($\boldsymbol{\Delta T meh}$) 117

2.3.7 Conclusion for all the simulation results for each trial 119

2.4 Disintegration Test 126

3 Chapter 3 137

3.1 Statistical analysis with Minitab software 138
3.2 Conclusion 146
4 References 148

Fig 1. Chemical structure of different types of PHA monomers [1] 5

Fig 2. An overview of the materials tetrahedron and the relationships between each aspect as applied to PHA biopolymer material design [2] 6

Fig 3. Three main pathways of PHA production [1] 7

Fig 4. Chemical, thermal, and mechanical characteristics of PHA-based biopolymers [1] 8

Fig 5. Overview of application areas for PHA-based biopolymers [1] 11

Fig 6. PHA Production and few material forms. Shown in figure: a. PHA granules in Halomonas bluephagenesis, b. PHA films, c. PHBV/PLA yarn, d. fermentation for PHA production from glucose, e. PHB powder for microsphere application, f.-g. PHBV adhesives, i. PHA paper coating [6] 13

Fig 7. Aerobic and anaerobic biodegradation pathways and end products of PHA-based biopolymers [1] 14

Fig 8. Schematic diagram of a typical extruder screw showing the feed zone, compression zone, and metering zone [20] 20

Fig 9. Typical cycle for an injection moulding process [20] 26

Fig 10. A sample of a dumbbell-shaped specimen, which was moulded at 50℃ 32

Fig 11. Tensile Test 33

Fig 12. Flexural Test 34

Fig 13. Impact Test 35

Fig 14. Tensile properties of G713 across the five trials at 20℃ and 50℃: a)tensile modulus, b)yield stress, c)stress at break, d)strain at break. Blue bars represent 20℃ and orange bars represent the 50℃ mould temperature 38

Fig 15. Flexural properties of G713: (a) flexural modulus, (b) maximum flexural stress. Blue bars = 20 °C mould temperature; orange bars = 50 °C mould temperature 40

Fig 16. Charpy impact strength of G713: (a) unnotched, (b) notched 41

Fig 17. Adding the used material to the software 44

Fig 18. DSC analysis 45

Fig 19. Second Cycle of the DSC test 46

Fig 20. Thermal Properties of G713 46

Fig 21. Available Viscosity laws 47

Fig 22. Rheology Test 48

Fig 23. Complex Viscosity Versus Angular Frequency curve 49

Fig 24. Carreau-Yasuda law Arrhenius for G713 51

Fig 25. The plotted viscosity curve of G713 using the Ludovic software 51

Fig 26. Added material to the software 52
Fig 27. The process tab of the Ludovic software 52
Fig 28. DoE parameters selection tab 53
Fig 29. Result Section of DoE 54
Fig 30. DoE "SME Results" at constant Barrel Temperature 56
Fig 31.DoE "SME result" at constant Barrel Temperature both in A)120 ℃ and B)145℃ 57
Fig 32. Comparison of the processing possibility of the material at A)120℃ and B)145℃ 58
Fig 33. DoE "SME Result" at constant Rotation Speed 59
Fig 34. DoE "SME result" at constant Rotation speed, both in A)150 RPM and B)518 RPM 59
Fig 35. Comparison of the processing possibility of the material at A)150 RPM and B)518 RPM 60
Fig 36. DoE "SME Result" at constant Feeding Rate 61
Fig 37. DoE "SME result" at constant temperature, both in A)30 kg/h and B)80 kg/h 62
Fig 38. Comparison of the processing possibility of the material at A)30 kg/h and B)80 kg/h 63
Fig 39. DoE "Torque Results" at constant Barrel Temperature 64
Fig 40. DoE "Torque result" at constant Barrel Temperature, both in A)120 ℃ and B)145℃ 65
Fig 41. Comparison of the processing possibility of the material at A)120℃ and B)145℃ 66
Fig 42. DoE "Torque Results" at constant Rotation Speed 67
Fig 43. DoE "Torque result" at constant Rotation Speed, both in A)150 RPM and B)518 RPM 67
Fig 44. Comparison of the processing possibility of the material at A)150 RPM and B)518 RPM 68
Fig 45. DoE "Torque Results" at constant Feeding rate 69
Fig 46. DoE "Torque result" at constant Feeding Rate, both in A)30 kg/h and B)80 kg/h 70
Fig 47. Comparison of the processing possibility of the material at A)30 kg/h B)80 kg/h 71
Fig 48. DoE "Pressure result" at constant Barrel Temperature 72
Fig 49. DoE “Pressure result” at constant Barrel temperature at both A)120℃ and B)145℃ 73
Fig 50. Comparison of the processing possibility of the material at A)120℃ and B)145℃ 74
Fig 51. DoE "Pressure result" at constant Rotation Speed 75
Fig 52. DoE "Pressure result" at constant Rotation Speed, both in A)150 RPM and B)518 RPM 76

Fig 53. Comparison of the processing possibility of the material at A)150 RPM and B)518 RPM 77
Fig 54. DoE "Pressure result" at constant Feeding rate 78
Fig 55. DoE "Pressure result" at constant Feeding rate, both in A)30 kg/h and B)80 kg/h 78
Fig 56. Comparison of the processing possibility of the material at A)30 kg/h and B)80 kg/h 80
Fig 57. DoE "Shear result" at constant Barrel Temperature 81
Fig 58. DoE “Shear rate result” at constant Barrel temperature at both A)120℃ and B)145℃ 82
Fig 59. Comparison of the processing possibility of the material at A)120℃ and B)145℃ ..83
Fig 60. DoE "Shear rate result" at constant Rotation Speed 84
Fig 61. DoE "Shear rate result" at constant Rotation Speed, both in A)150 RPM and B)518 RPM 84
Fig 62. Comparison of the processing possibility of the material at A)150 RPM and B)518 RPM 86
Fig 63.DoE "Shear rate result" at constant Feeding rate 86
Fig 64. DoE "Shear rate result" at constant Feeding rate, both in A)30 kg/h and B)80 kg/h ..87
Fig 65. Comparison of the processing possibility of the material at A)30 kg/h and B)80 kg/h 88
Fig 66. DoE "Viscosity result" at constant Barrel Temperature 90
Fig 67. DoE “Viscosity result” at constant Barrel temperature at both A)120℃ and B)145℃ 91
Fig 68. Comparison of the processing possibility of the material at A)120℃ and B)145℃ ..92
Fig 69. DoE "Viscosity result" at constant Rotation Speed 93
Fig 70. DoE "Viscosity result" at constant Rotation Speed, both in A)150 RPM and B)518 RPM 94
Fig 71. Comparison of the processing possibility of the material at A)150 RPM and B)518 RPM 95
Fig 72. DoE "Viscosity result" at constant Feeding Rate 96
Fig 73. DoE "Viscosity result" at constant Feeding rate, both in A)30 kg/h and B)80 kg/h 96
Fig 74. Comparison of the processing possibility of the material at A)30 kg/h and B)80 kg/h 97
Fig 75. DoE "Total Residence time result" at constant Barrel Temperature 98
Fig 76. DoE “Total Residence time result” at constant Barrel temperature at both A)120℃ and B)145℃ 99

Fig 77. Comparison of the processing possibility of the material at A)120℃ and B)145℃ 100
Fig 78. DoE "Total Residence time result" at constant Rotation Speed 101
Fig 79. DoE "Total Residence time result" at constant Rotation Speed, both in A)150 RPM and B)518 RPM 101
Fig 80. Comparison of the processing possibility of the material at A)150 RPM and B)518 RPM 102
Fig 81. DoE "Total Residence time result" at constant Feeding Rate.....103
Fig 82. DoE "Total Residence time result" at constant Feeding rate, both in A)30 kg/h and B)80 kg/h 104
Fig 83. Comparison of the processing possibility of the material at A)30 kg/h and B)80 kg/h 105
Fig 84. Comparison between the temperature plots of all the simulations.....107
Fig 85. Comparison between the pressure plots of all the simulations.....110
Fig 86. Comparison between the total residence time plots of all the simulations.....112
Fig 87. Comparison between the viscosity plots of all the simulations.....113
Fig 88. Comparison between the shear rate plots of all the simulations.....116
Fig 89. Comparison between the mechanical delta T plots of all the simulations.....118
Fig 90. The cut samples with the thickness of A)1mm and B)2mm.....128
Fig 91. The placement of 1mm samples inside the composting reactor.....128
Fig 92. The initial stages of the creation of the bacterial film on the samples 130
Fig 93. The samples are almost covered with the bacterial film.....130
Fig 94. weighting of the samples 130
Fig 95. Non-disintegrated dried samples 132
Fig 96. Pareto Chart of the standardised effects 145

Table 1. Comparison of Single- and Twin-screw Extruders [20].....22
Table 2. Conditions for each trial.....31
Table 3. Injection conditions for 20℃ mould.....32
Table 4. Injection conditions for 50℃ mould.....32
Table 5. Tensile properties of G713.....36
Table 6. Flexural properties of G713.....37
Table 7. Charpy impact strength of G713.....37
Table 8. Quantitative data of the Complex Viscosity Versus Angular Frequency curve.....50
Table 9. Setting of DoE based on selected parameters for 5 trials.....53
Table 10. Summary of the results observed from DoE.....106
Table 11. Composition of synthetic solid waste.....127
Table 12. dimensions of the pieces of the test material used in the disintegration test.....127
Table 13. Composting procedure.....129
Table 14. Disintegration Test results for G713 moulded at 20℃.....134
Table 15. Disintegration Test results for G713 moulded at 50℃.....135
Table 16. Selection Criteria.....139
Table 17. Coded Coefficient Table.....140
Table 18. Model Summary.....141
Table 19. Analysis of Variance.....142
Table 20. Explanation of the terms in the equation.....144
Table 21. Fits and Diagnostics for Unusual Observations.....144
Table 22. Summary of the results.....146

Table 1. Comparison of Single- and Twin-screw Extruders [20].....22
Table 2. Conditions for each trial.....31
Table 3. Injection conditions for 20℃ mould.....32
Table 4. Injection conditions for 50℃ mould.....32
Table 5. Tensile properties of G713.....36
Table 6. Flexural properties of G713.....37
Table 7. Charpy impact strength of G713.....37
Table 8. Quantitative data of the Complex Viscosity Versus Angular Frequency curve.....50
Table 9. Setting of DoE based on selected parameters for 5 trials.....53

Table 10. Summary of the results observed from DoE 106
Table 11. Composition of synthetic solid waste 127
Table 12. dimensions of the pieces of the test material used in the disintegration test 127
Table 13. Composting procedure 129
Table 14. Disintegration Test results for G713 moulded at 20℃ 134
Table 15. Disintegration Test results for G713 moulded at 50℃ 135
Table 16. Selection Criteria 139
Table 17. Coded Coefficient Table 140
Table 18. Model Summary 141
Table 19. Analysis of Variance 142
Table 20. Explanation of the terms in the equation 144
Table 21. Fits and Diagnostics for Unusual Observations 144
Table 22. Summary of the results 146

1 Chapter 1

1.1 Introduction

Biodegradable polymers have attracted significant attention recently as substitutes for conventional petroleum-derived plastics, driven by increasing environmental concerns and the demand for sustainable products. Polyhydroxyalkanoates (PHAs) are a promising type of biopolymer as they can degrade naturally, are safe for organisms, and can be made from renewable materials. PHAs are naturally occurring thermoplastic polyesters that have a wide range of physical and chemical properties depending on the monomers that are present in their structure. This makes them useful for a wide range of things, including packaging, agriculture, medical devices, and consumer goods. PHAs are completely biodegradable in both aerobic and anaerobic conditions, such as in soil, marine, and composting environments. This means that they have a closed-loop material life cycle and have a much smaller effect on the environment than petroleum-based materials.

PHA-based materials are beneficial for the environment and work well, but there are still a lot of challenges that make it difficult for industries to use them widely. These problems include high production costs, complicated fermentation and downstream processing needs, and performance issues caused by brittle materials and short processing windows. The relationship between processing parameters and the subsequent disintegration behaviour of PHA-based bio compounds under controlled and real-world conditions is a critical yet inadequately explored aspect influencing their practical applicability. During processing activities like extrusion, injection moulding, thermoforming, and mixing, the polymer matrix has to deal with mechanical shear, high temperatures, and different amounts of time spent in each stage. These variables can change the structure and characteristics of materials on both the molecular and macroscopic levels. These modifications, in turn, have the potential to significantly influence the rate and mechanism of biodegradation or disintegration of the final product.

The logical design of PHA-based products optimised for end-of-life biodegradation performance is constrained by an insufficient understanding of the processing-disintegration relationship. International standards (e.g. ISO 14855, EN 13432, and ASTM D6400) set the rate at which biodegradable materials degrade. If a material fails to meet the required degradation criteria when composting, it may not be considered compostable. This gap is especially important from a regulatory and sustainability point of view. Consequently, for both scholarly advancement and the practical application of PHA-based bio compounds, a scientific understanding of how processing parameters influence disintegration kinetics is essential.

This thesis's main goal is to examine how several processing parameters affect the rate at which PHA-based bio compounds disintegrate in controlled environments. A methodical technique that combines process modelling and appropriate parameter analysis is used to accomplish these goals. In order to clear the mechanisms causing disintegration, the study considers how SME, torque, pressure, shear rate, residence time, and viscosity change under various operating conditions. The findings are meant to help optimise processing parameters and aid in the creation of more dependable and effective manufacturing techniques for biodegradable polymers.

In conclusion, this thesis primarily contributes to a better understanding of the connection between PHA disintegration behaviour and processing parameters. This work attempts to close current knowledge gaps and provide useful advice for industrial applications by identifying crucial parameters and their relationships.

In the following, a review of the relevant literature on PHA materials, polymer processing techniques, and processing parameters will be presented.

1.2 Theoretical Fundamentals

1.2.1 Polyhydroxyalkanoate (PHA)

The production of traditional petroleum-based plastics has grown significantly over the past few decades and reached 400 million metric tons per year, and if this consumption trend continues, predictions indicate that this growth will continue. Plastics have become extremely important in almost every area due to their low bulk density, high durability, and excellent processability. Polyethylene (PE ~36%), polypropylene (PP ~21%), polyvinyl chloride (PVC ~12%), polystyrene (PS), and polyethylene terephthalate (PET) are the main polymers which represent the great majority of plastic manufactured globally. Although these conventional plastics have extensive use, they are non-biodegradable and present serious environmental risks. These materials have been demonstrated to remain for more than 450 years in the environment and accumulate in marine ecosystems, water bodies, and soils. 12 billion tons are expected to accumulate and end up in the landfills or natural environments by 2050. Additionally, more than 20 million metric tons of plastic waste, roughly 11% of all plastic trash produced, entered aquatic ecosystems in 2016 alone, and it is predicted that by 2030, this volume will be almost doubled. It should be noted that conventional plastics decompose into microplastics, which enter the world's soils, water, and air and eventually make their way into the human food chain, affecting ecosystems and human health. Since only 5 to 30% of virgin plastic may be recycled or used for other purposes, up to 95% of the original material's economic value is lost [1], [2], [3].

According to the mentioned concerns of petroleum-based plastics, a considerable interest in biodegradable, bio-based polymer substitutes has been shown. The market is predicted to grow significantly, with bioplastics production expected to reach 7.43 million tonnes by 2028 from 2.18 million tonnes in 2023. The main advantage of biodegradable polymers is their disintegration in ambient or industrial composting environments without producing pollutants. According to the European Committee for Standardisation (EN 13432:2000), at least 90% of the weight of biodegradable plastic should degrade in six months under composting environments and at least 50% in three months under anaerobic conditions. Common bio-based biodegradable plastics that make up 31%, 6.4%, 0.9%, and 4.8% of the market are polylactic acid (PLA), starch-containing polymer compounds (SCPC), polybutylene succinate (PBS), and polyhydroxyalkanoates (PHA), respectively. Among these alternatives, polyhydroxyalkanoates (PHAs) show great promise because of their unique combination of biodegradability, biocompatibility, and controllable mechanical and thermal properties [1].

Polyhydroxyalkanoates (PHAs) are a type of linear aliphatic polyesters, a large and structurally diverse family of biopolymers. They were first described in the early 20th century, and they have been extensively researched as model biologically derived polyesters. PHAs are created and accumulate in microbial cells as intracellular granules, where they serve as a carbon and energy reserve when there is a high level of carbon and a shortage of essential nutrients like nitrogen, phosphorus, oxygen, or sulphur. The general chemical formula of PHA is $[-O(R)CHCH, CO-]_n$, where n indicates the number of monomer repeat units and R represents the side chain group, which may be a saturated alkyl, unsaturated alkyl, branched alkyl, or substituted alkyl group. This adaptable side chain chemistry produces over 150 structurally unique PHA monomers that have been independently identified and biosynthesised, creating an extensive variety of possible polymer and copolymer combinations [1], [2], [4], [5], [6].

PHAs can be produced by a variety of Gram-positive and Gram-negative bacteria; around 92 bacterial species can do so in both aerobic and anaerobic conditions. PHAs are composed of 600 to 35,000 hydroxy fatty acid units and typically have molecular weights between 200 and 3,000 kDa. They are semicrystalline aliphatic polyesters, and PHAs produced by different microorganisms or under different working conditions can differ significantly in terms of their structure, molecular weight, and physical and chemical properties [1], [2], [3].

1.2.2 Chemical structure and classification of PHA

The structural diversity of PHAs is caused by three main sources of variation in the monomer, which are [2]:

I. Number of carbon atoms in the polymer backbone
II. Number of carbons in side chain branching from the backbone
III. The presence or absence of functional groups in the side chain

In general, PHAs are classified into three major categories based on the number of carbon atoms that are present in the monomer units [1], [2], [3], [6]:

1. Short-chain length PHAs (scl-PHAs, $C_3 – C_5$)
   This family of PHAs are characterised by high crystallinity (40-80%) and is brittle and stiff in their pure form. Some examples of this family can be: P3HB or PHB [poly(3-hydroxybutyrate)] and PHBV [poly(3-hydroxybutyrate-co-3-hydroxyvalerate)] [1], [2]
2. Medium-chain length PHAs (mcl-PHAs, $C_6 – C_{14}$)
3. Long-chain length PHAs (lcl-PHAs, $>C_{14}$)

Unlike scl-PHAs, both mcl-PHAs and lcl-PHAs have lower crystallinity (~25%), low tensile strength, higher elongation at break, and lower melting temperatures, making them rubbery and plastic. Some examples are PHBHHx [poly(3-hydroxybutyrate-co-3-hydroxyhexanoate) and PHO [poly(3-hydroxyoctanoate)] [1], [6]

It is possible to create copolymers and blends of PHA classes, which may have intermediate or even higher properties than their constituent homopolymers [2], [3]. Currently, the worldwide market is dominated by five different kinds of PHA-based biopolymers:

1. Poly(3-hydroxybutyrate) (PHB)
2. Poly(4-hydroxybutyrate) (P4HB)
3. Poly(3-hydroxybutyrate-co-3-hydroxyvalerate) (PHBV)
4. Poly(3-hydroxybutyrate-co-4-hydroxybutyrate) (P3HB4HB)
5. Poly(3-hydroxybutyrate-co-3-hydroxyhexanoate) (PHBHHx)

Which are marketed under brands such as Nodax™ (P&G), Enmat® (Tianan Biologic), and Biomer® (Biomer Inc) [1], [6].

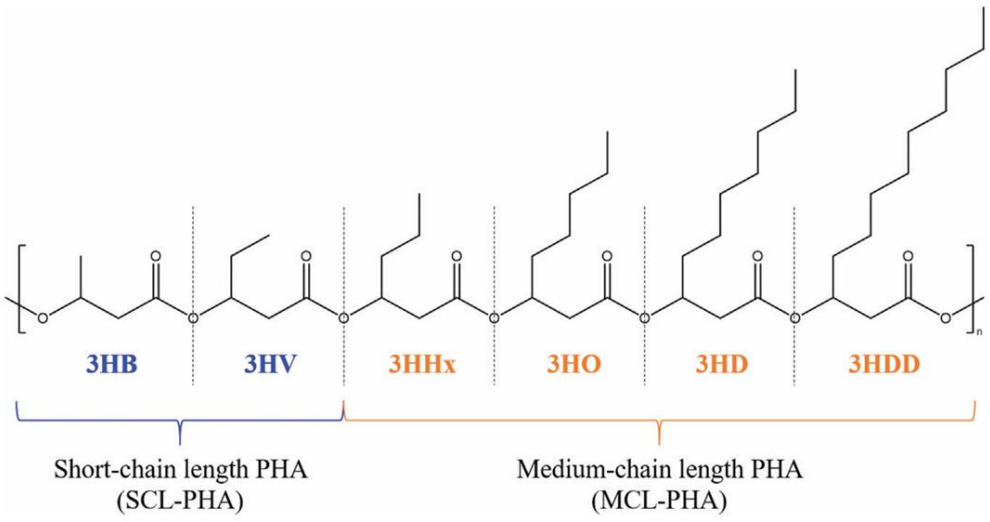

Fig 1. Chemical structure of different types of PHA monomers [1]

It should be noted that PHB, the most often produced and studied PHA, is produced by a variety of bacteria, including the Gram-negative Cupriavidus necator (Ralstonia eutropha), Ralstonia eutropha, Halomonas bluephagenesis, and several Gram-positive Bacillus and Streptomyces species. Despite being referred to as the "model PHA," PHB's high crystallinity, brittleness, and narrow processing window limit its use [1], [2], [7].

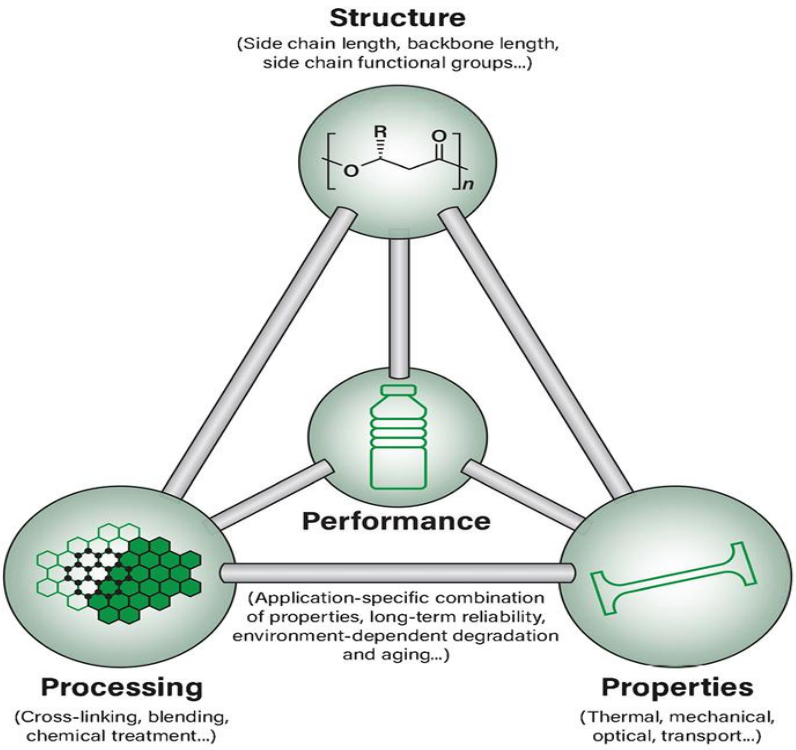

Fig 2. An overview of the materials tetrahedron and the relationships between each aspect as applied to PHA biopolymer material design [2]

1.2.3 **Biosynthesis of PHA**

Many different types of bacteria spontaneously produce PHA as a means of storing carbon and energy under unbalanced growth conditions. This typically occurs when there is a lot of carbon available together with deficiencies in nitrogen, phosphorus, oxygen, sulphur, or other essential nutrients. The intracellular PHA granules can be used as energy storage when external carbon sources run out. Thus far, at least three important metabolic pathways for the synthesis of PHA have been found [1], [4], [5]:

I. The sugar-dependent (glycolysis-based) pathway

   This pathway is the most studied route during which a hexose substrate, such as glucose, is metabolised through glycolysis into acetyl-CoA, which is subsequently condensed to acetoacetyl-CoA by PhaA (3-ketothiolase), then reduced to (R)-3-hydroxybutyryl-CoA by PhaB (NADPH-dependent acetoacetyl-CoA reductase), and finally polymerised into PHA by the PHA synthase (PhaC) [4]

II. The fatty acid β-oxidation pathway

In Pathway II, fatty acid substrates are metabolised through β-oxidation to yield enoyl-CoA intermediates, which are converted to (R)-3-hydroxyacyl-CoA by R-specific enoyl-CoA hydratase (PhaJ), and then polymerised by PhaC into PHA

III. The fatty acid de novo synthesis pathway [4], [5]

Finally, the third pathway, involving de novo fatty acid synthesis, is particularly important in Pseudomonas species for the production of mcl-PHAs from various carbon sources, including sugars and glycerol, where PhaG provides the critical link between fatty acid biosynthesis and PHA production [5]

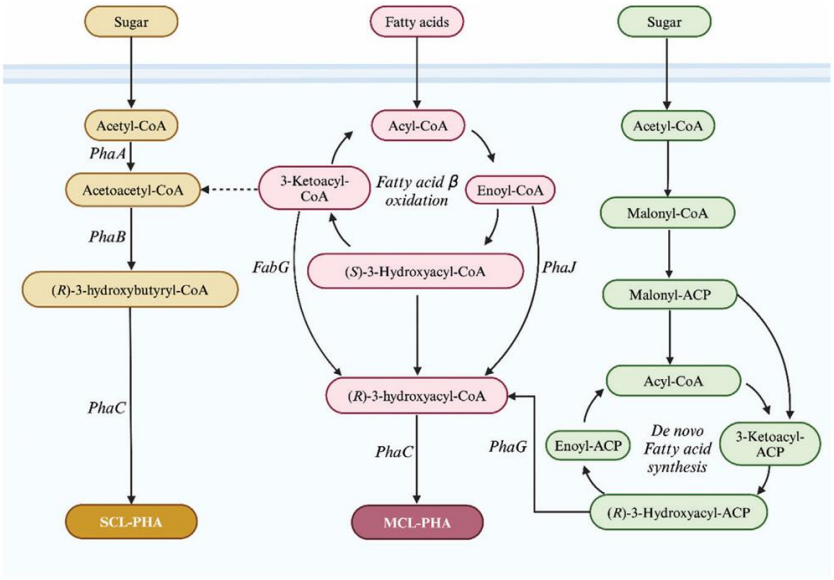

Fig 3. Three main pathways of PHA production [1]

Cupriavidus necator (formerly Ralstonia eutropha H16) is the most studied PHA producer. It can make more than 200 g/L of dry cell mass (DCM) with more than 70 wt% PHA accumulation when fermentation conditions are strictly controlled. Pseudomonas putida is particularly well-suited for producing mcl-PHAs from fatty acids and glycerol. It can yield 60–70% of the dry cell weight in PHA. Many Bacillus species, including Bacillus cereus, Bacillus megaterium, and Bacillus subtilis, offer advantages such as endotoxin-free PHAs, genetic tractability, and rapid growth. Additionally, photosynthetic cyanobacteria, such as Synechocystis sp. PCC 6803 can generate PHA from CO2 and sunlight, potentially reducing manufacturing costs and environmental impact. Methanotrophs, like Methylocystis sp., make PHAs from methane (CH_4), which is a way to make greenhouse gases more useful. Halophilic

organisms, like Halomonas bluephagenesis, can grow in non-sterile environments and have lower production costs [6].

Increasing the chemical diversity of accessible PHA structures and improving PHA production efficiency can be accomplished by genetic modification and metabolic engineering. PHA depolymerase genes are missing, despite a high number of PHA production genes. PHA synthase is modified to become more monomer-specific, and heterologous routes are introduced. Aeration, pH, and temperature must all be kept at specific values in order to maximise PHA extraction from the fermentation process. The biopolymer is then recovered through harvesting, cell disruption, and extraction/purification [5], [6].

1.2.4 Physical, Thermal, and Mechanical Properties of PHA

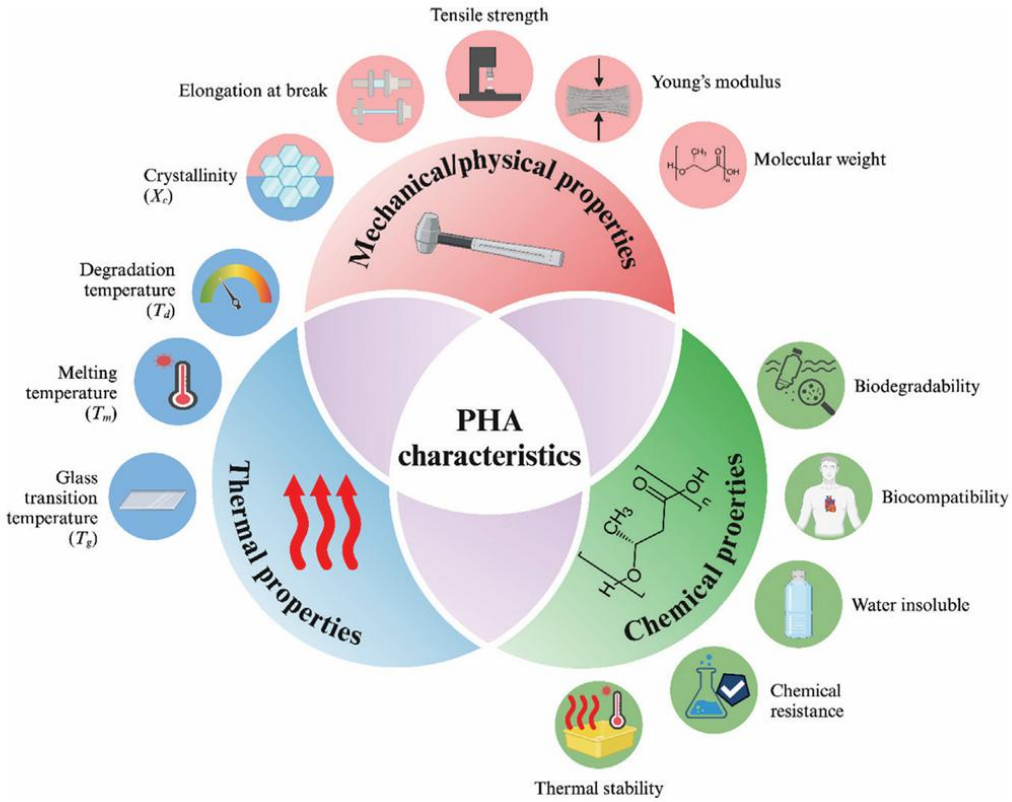

Fig 4. Chemical, thermal, and mechanical characteristics of PHA-based biopolymers [1]

1.2.4.1 *Crystallinity*

PHAs are semi-crystalline biopolymers characterised by the coexistence of ordered crystalline domains and disordered amorphous regions. The degree of crystallinity is a critical factor influencing both the mechanical and degradation behaviour of PHAs. Scl-PHAs (especially P3HB) have high levels of stereoregularity and a strong tendency to form large spherulites. This makes them very crystalline (40–80%) and therefore not highly beneficial for commercial applications. The 3-hydroxyvalerate (3HV) monomer in PHBV can co-crystallise within the 3-hydroxybutyrate (3HB) crystal lattice, making it the only PHA copolymer that exhibits true isomorphous behaviour. However, this isomorphism does not significantly improve the mechanical properties of pure P3HB. On the other hand, mcl-PHA copolymers like P3HB4HB and PHBHHx crystallise much more slowly. In P3HB4HB, the crystallinity decreases from about 55% to 14% as the 4HB content rises from 0 to 49 mol%. This shows how important the composition of the comonomer is to the crystalline morphology. To lower crystallinity, nucleating agents (such as cellulose nanocrystals and chitosan) can be used, either mixed with other polymers or copolymerized to disrupt the regularity of the crystal lattice [1], [2], [3].

1.2.4.2 *Thermal properties*

To evaluate processability and end-of-life performance, it is important to know the thermal properties of PHA biopolymers, such as the glass transition temperature (T^G), melting temperature (T_m), and degradation temperature (T^D). For most PHAs, the values of T^G, T_m, and T^D are usually between −52 and +4 °C, up to 177 °C, and 227 and 256 °C, respectively. Additionally, the degradation temperature (T^D) of PHB is between 200 and 300 °C. It should be said that there are two stages of thermal degradation, which are rapid chain scission starting at 160–180 °C and more intense random scission caused by β-elimination reactions starting at 180–200 °C [1], [2].

One of the most significant issues with thermally processing PHA is that the melting point (about 180 °C for PHB) and the temperature at which it begins to disintegrate are extremely close to each other. This makes the processing window very narrow and can cause the molecular weight to decrease, the colour to change, and the mechanical properties to be lost during melt processing. Adding comonomer units like 3HV, 4HB, or 3-hydroxypropionate to the P3HB backbone reduces crystal formation, lowers T_m, and widens the processing window. This makes these copolymers easier to work with using common polymer processing methods like extrusion, injection moulding, and blow moulding [1], [2], [7].

1.2.4.3 *Mechanical properties*

The mechanical properties of PHA biopolymers are primarily characterised by Young's modulus, elongation at break, and tensile strength. The molecular weight, crystallinity, and processing history of the monomer in the PHA family can all have a significant impact on these parameters. PHB, the simplest and most common scl-PHA, is a stiff and brittle material that breaks at an elongation of less than 15%, has a Young's modulus of more than 1 GPa, and a tensile strength of about 18–25 MPa. The fragility of P3HB is mainly due to secondary crystallisation, which is when the amorphous region slowly crystallises over time (physical ageing), and the presence of large spherulite crystals in its structure [1], [2].

Copolymers and mcl-PHAs show much more flexibility. For instance, adding 43% of 3-hydroxyvalerate (3HV) monomers to PHB made the elongation at break rise from 3–6% (pure PHB) to 58%, which is more than ten times higher. Similarly, adding 4-hydroxybutyrate (4HB) units to P3HB4HB copolymers can change their mechanical properties and make them either very stiff or very flexible, depending on how much 4HB is added. PHBHHx, a mcl-PHA copolymer, has a Young's modulus of 0.21–1.28 GPa and elongation at break of 3.6–177%, which makes it much more useful than pure PHB. PHAs have a wide range of mechanical properties, from hard thermoplastics to soft elastomers. This means they could replace many types of traditional plastics [1], [6].

1.2.5 **Applications of PHA**

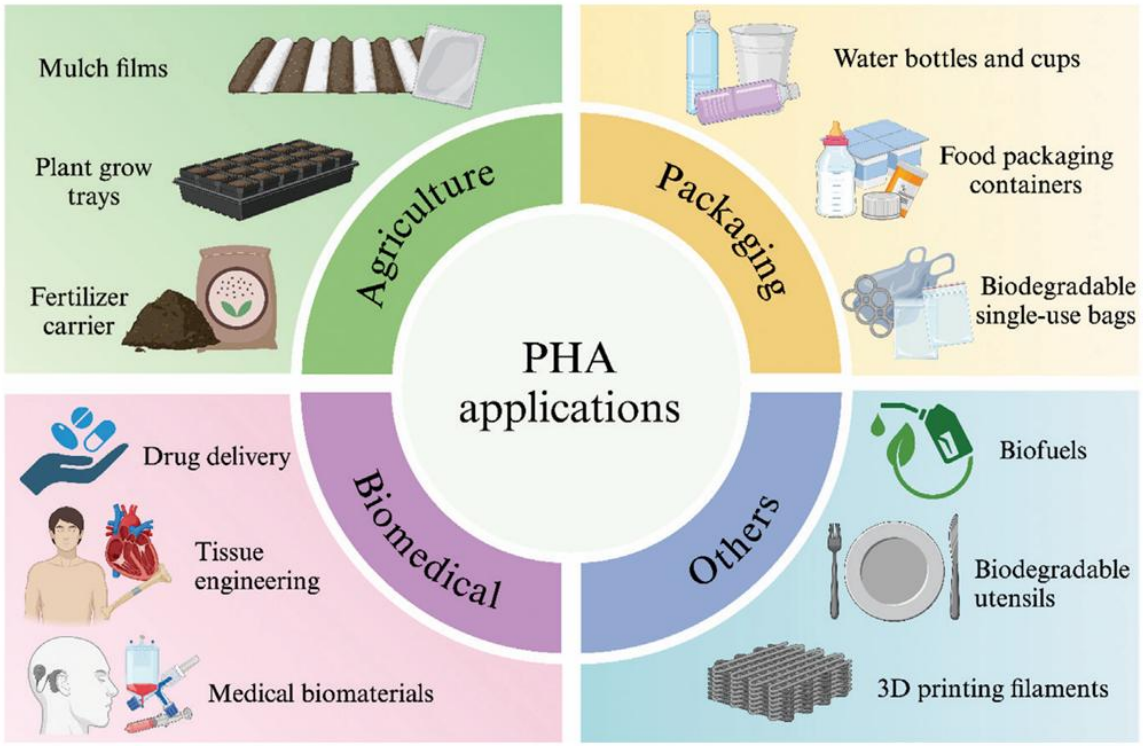

Fig 5. Overview of application areas for PHA-based biopolymers [1]

1.2.5.1 *Packaging*

Packaging represents one of the most important application sectors for PHAs, owing to their favourable mechanical properties, barrier properties against water vapour and oxygen, and full biodegradability. Scl-PHAs (particularly PHB and PHBV) exhibit Young's modulus (~1.2–1.7 GPa) and tensile strength (~25–35 MPa) comparable to typical packaging plastics. PHAs are currently used or explored for shampoo bottles, shopping bags, lids, coffee capsules, tea bags, paper cup linings, cosmetic containers, mulching films, and straws. Blending and copolymerization strategies have been applied to improve barrier and mechanical properties; for example, PLA/PHBV blends increased ductility and gas barrier properties by 26% and 70%, respectively [1], [6], [7].

1.2.5.2 *Agriculture*

In agriculture, PHAs are increasingly being considered as practical, sustainable alternatives for a range of applications, including mulching films, crop nets, grow bags, and coatings that control the release of fertilisers. For instance, fertiliser tablets coated with PHB have been shown to release nutrients much more gradually, extending over a period of more than two months, compared to uncoated versions. This slower release supports a more consistent nutrient supply during the early stages of crop growth. Beyond plant applications, P3HB has also attracted attention as a feed additive in aquaculture. Studies have shown that incorporating a small amount (1–2%) of crystalline P3HB into the diet of mussel larvae can nearly double their survival rate. Similar positive outcomes have also been reported in species such as the large yellow croaker, highlighting its potential benefits across different aquatic organisms [1], [4], [6].

1.2.5.3 *Biomedical applications*

The combination of biocompatibility and controllable biodegradation makes PHAs particularly well-suited for biomedical use. As a result, they are being explored in a wide range of applications, including drug delivery systems, tissue engineering scaffolds, medical implants, and surgical devices. For example, nanoparticles made from PHBV and loaded with the anticancer drug paclitaxel (PTX) have shown strong therapeutic performance in hepatocellular carcinoma (HCC) xenograft models, while also exhibiting lower toxicity in vivo compared to the free drug. In addition, PHAs are under investigation for several advanced medical applications such as orthopaedic implants, vascular grafts, nerve conduits, and controlled-release systems for anti-inflammatory drugs [1, 8]. Notably, P4HB has already received approval from the U.S. Food and Drug Administration for specific medical uses, further supporting the safety and effectiveness of PHAs in healthcare applications [1], [6].

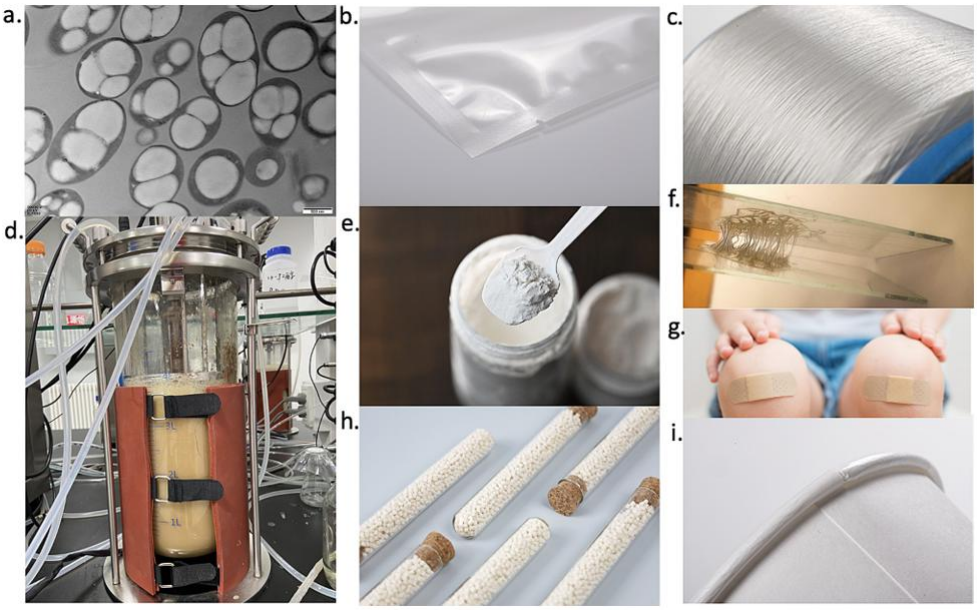

Fig 6. PHA Production and few material forms. Shown in figure: a. PHA granules in Halomonas bluephagenesis, b. PHA films, c. PHBV/PLA yarn, d. fermentation for PHA production from glucose, e. PHB powder for microsphere application, f.-g. PHBV adhesives, i. PHA paper coating [6]

1.2.6 **Biodegradation of PHA**

One of the most important and commercially valuable features of PHAs is their ability to biodegrade completely across a wide range of natural environments. Unlike many conventional plastics and even some bio-based alternatives, PHAs can be broken down by microorganisms in soil, compost, sediments, freshwater, and marine settings, under both oxygen-rich (aerobic) and oxygen-poor (anaerobic) conditions.

This biodegradation process takes place in three main stages. First, during bio-deterioration, microorganisms grow on the surface of the material, leading to initial physical and chemical changes. Next comes bio-fragmentation, in which the polymer chains are progressively broken down into smaller units, such as oligomers and monomers. Finally, in the assimilation stage, these smaller molecules are taken up by microbial cells and metabolised. Depending on the environment, this results in end products such as carbon dioxide, water, and microbial biomass under aerobic conditions, or carbon dioxide, methane, and water in anaerobic conditions [1], [2], [3].

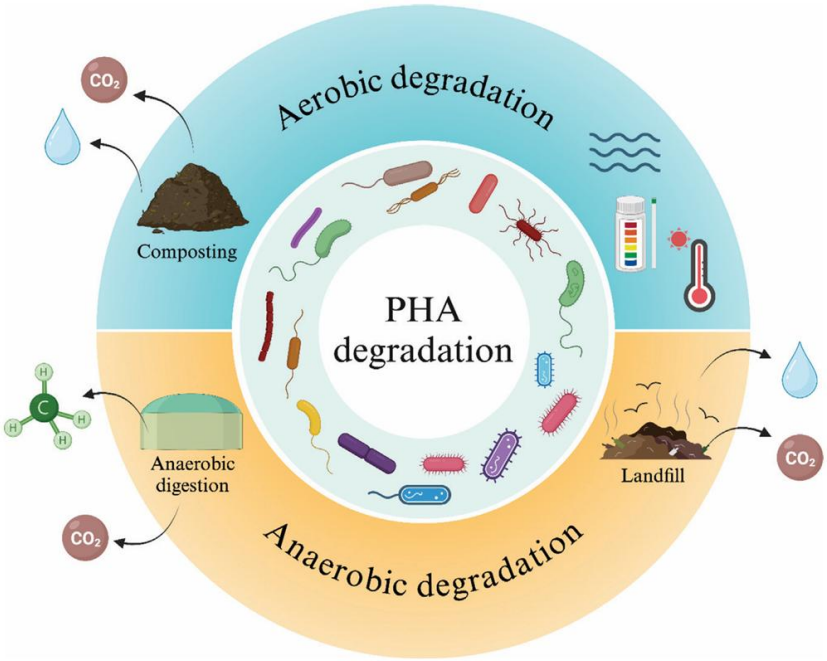

Fig 7. Aerobic and anaerobic biodegradation pathways and end products of PHA-based biopolymers [1]

1.2.6.1 *Aerobic and Anaerobic Biodegradation*

Under aerobic composting conditions, PHBV has demonstrated strong biodegradation performance. In pilot-scale composting systems, it has been observed to fully disintegrate, while laboratory-scale studies report around 81% degradation. In fact, under controlled composting conditions at 58 °C, PHBV can degrade relatively quickly, often within less than 80 days. Its performance under anaerobic conditions is even more notable. PHBV films have been shown to degrade almost completely within 20 days in simulated landfill environments at 35 °C. This behaviour highlights a clear advantage over other aliphatic polyesters such as PLA, PBS, and PBSE, which showed no significant degradation even after 100 days under the same conditions. The degradation of PHBV typically follows a two-phase pattern: an initial rapid degradation stage during approximately the first 10 days, followed by a slower degradation rate over the remaining period. A similar trend can be observed for P3HB under anaerobic conditions. For example, when degraded by sulfate-reducing bacteria such as Desulfotomaculum sp., the molecular weight of P3HB decreases early in the process and then stabilises after about 30 days. However, the overall mass loss continues up to around 60 days. This indicates that weight loss is not directly correlated with molecular weight reduction, suggesting that surface erosion and microbial consumption play a significant role even after the polymer chains have largely stabilised [1], [8], [9], [10], [11].

1.2.6.2 *PHA-degradation Microorganisms and Enzymes*

A wide variety of microorganisms are capable of degrading PHAs, highlighting their strong environmental compatibility. To date, more than 90 different types have been identified in natural settings, including aerobic and anaerobic bacteria, photosynthetic microorganisms, archaea, and even some lower eukaryotes. These organisms are found across diverse environments such as soil, sediments, marine ecosystems, and activated sludge systems. Several well-studied examples illustrate a capability that Pseudomonas mendocina is known to degrade P3HB4HB, while Bacillus sp. JY14 has been reported to degrade up to 98% of PHB films within just 14 days. Another important example is Schlegelella thermodepolymerans, a thermophilic bacterium that produces extracellular PHA depolymerases, enabling efficient degradation at higher temperatures. The degradation process itself is primarily enzymatic and occurs in two main stages. First, microorganisms secrete extracellular PHA depolymerases, which attach (adsorb) to the surface of the polymer. Next, these enzymes catalyse the hydrolysis of the polyester chains, breaking them down into smaller oligomers and monomers. These smaller molecules are then taken up by the cells and metabolised. It is also worth noting that ester bonds in PHAs can undergo hydrolysis through purely chemical (abiotic) processes in alkaline conditions, even in the absence of microbial activity [1], [12], [13], [14], [15].

1.2.6.3 *Factors affecting Biodegradation rate*

The biodegradability of PHAs is governed by a combination of material-related (intrinsic) and environmental (extrinsic) factors. Among the intrinsic properties, crystallinity plays the most decisive role. In general, degradation rates decrease as crystallinity increases, which explains the observed trend: P3HB4HB > PHBHHx > PHBV > PHB. Other important factors include molecular weight, surface morphology, and the presence of hydrophilic fillers such as wood flour, clay, or peat. These additives enhance water uptake into the material, which in turn accelerates hydrolytic degradation. From an environmental perspective, temperature is the dominant factor influencing PHA degradation. For example, in hardwood soil, PHB degradation has been reported at approximately 8%, 23%, and 26% at 15, 28, and 40 °C, respectively, showing a clear increase with temperature. The optimal degradation rate is typically observed around 30 °C, where it can be nearly twice as fast as at 20 ℃. In addition to temperature, several other environmental conditions play a significant role. These include pH (with alkaline conditions promoting abiotic hydrolysis), moisture content, the availability and activity of PHA-degrading microorganisms, and the specific environment in which degradation occurs, such as soil, compost, marine systems, or anaerobic digesters [1], [2], [3].

Besides the factors that are mentioned above, processing parameters also have their own influence on the disintegration of PHA, which will be discussed in the experimental part of this study.

1.2.7 PHA blends, Bio composites, and Commercial Development

To address the inherent limitations of neat PHAs, such as brittleness, high crystallinity, and a narrow thermal processing window, research has increasingly focused on blending PHAs with other biodegradable polymers and incorporating various fillers. Common blending partners include poly(ε-caprolactone) (PCL), polybutylene succinate (PBS), poly(butylene adipate-co-terephthalate) (PBAT), and polylactic acid (PLA). These materials help improve mechanical performance by adding properties like higher toughness and greater elongation at break. Two main processing approaches are typically used to produce these blends. The first is solution casting, where polymers are dissolved in a solvent before being combined, while the second is melt blending, which involves mixing the components at temperatures above their melting points. Melt blending is generally preferred in industrial settings because it avoids the use of solvents and is more scalable. However, a key challenge is that many PHA-based blends are thermodynamically immiscible, meaning they tend to separate into distinct phases. To overcome this, compatibilisers or reactive blending techniques are often required to improve interfacial adhesion and achieve better overall material properties [3].

From a commercial perspective, PHAs are gaining increasing traction. More than 25 companies worldwide are now involved in producing or incorporating PHAs into products, with over 30 different commercial brands available. Notable producers include Danimer Scientific, RWDC Industries, PhaBuilder, Kaneka, Biomer, Tianan Biologic, and Newlight Technologies. Despite this progress, large-scale production of PHAs still faces economic challenges. Their cost remains significantly higher than that of conventional plastics—for example, PHB typically ranges from about $1.81 to $3.20 per pound, compared to roughly $0.45 to $0.68 per pound for polypropylene (PP). These higher costs are mainly due to expensive feedstocks, complex downstream processing, and the lack of large-scale production efficiencies [2], [6].

1.2.8 **Challenges and Future Perspectives**

Despite their strong potential as sustainable and biodegradable alternatives to conventional plastics, PHAs still face several challenges that limit their large-scale commercial adoption. From a technical standpoint, key issues include the high crystallinity and brittleness of short-chain-length PHAs (especially PHB), which negatively affect both processability and mechanical performance. In addition, the narrow thermal processing window, due to the proximity between melting and degradation temperatures, makes processing more difficult. Other limitations include slow crystallisation kinetics and secondary crystallisation during storage, which can lead to embrittlement over time, as well as variability in biodegradation rates depending on environmental conditions [1], [2], [5], [6], [7], [16].

Economically, the relatively high production cost of PHAs remains a major obstacle. To address this, current research is increasingly focused on using low-cost, carbon-rich waste streams as feedstocks. These include agricultural residues, lignocellulosic biomass, agro-industrial by-products, volatile fatty acids derived from organic waste, and even greenhouse gases such as CO_2 and CH_4. Additionally, the use of mixed microbial cultures (MMCs) and non-sterile, open fermentation systems shows promise in reducing operational costs. Advances in metabolic engineering, such as designing more efficient PHA-producing microorganisms and optimising biosynthetic pathways, are also expected to improve yields and further lower production costs [2], [5], [6].

Looking ahead, future research is progressing along several important directions. These include expanding the range of commercially available PHAs beyond the currently PHB-dominated portfolio, improving the understanding of property–structure–processing–performance (PSPP) relationships through data-driven approaches, and developing more effective end-of-life strategies such as chemical and biological recycling. Together, these efforts aim to support the transition toward a circular bio-based plastics economy. At the same time, stronger global regulations on single-use plastics and growing environmental awareness among consumers are expected to act as key drivers, accelerating the adoption of PHAs in applications such as medical devices, food packaging, and agricultural materials in the coming years [1], [2], [5], [6], [7].

1.2.9 Processing techniques and the effect of processing parameters on PHA during processing

Within the PHA family, poly(3-hydroxybutyrate) (PHB) is by far the most studied material. It stands out because of its relatively high stiffness, good barrier properties, and a melting temperature of about 175 °C, which make it a promising alternative to conventional plastics like polypropylene and polyethylene, especially in rigid packaging, disposable products, and certain biomedical uses. At the same time, these advantages come with a significant drawback. PHB has a very narrow processing window, which means that the temperature at which it melts is uncomfortably close to the temperature at which it starts to degrade. In practice, this means there is very little margin for error during processing. Even small deviations in operating conditions, particularly during melt extrusion, can lead to thermal degradation and a loss of material performance. For this reason, precise control of processing parameters becomes essential to ensure that PHB-based products meet the desired quality standards. For instance, due to this narrow processing window, to maintain material integrity, extrusion temperatures must be meticulously regulated across the entire barrel, coupled with a tight residence time distribution to prevent any localised overheating. The physical design of the machinery, specifically the screw and die geometry, must be engineered to eliminate "dead zones" where the melt might otherwise stagnate and degrade. Even brief temperature fluctuations, such as those occurring during system startup or set-point transitions, can trigger a sharp decline in molecular weight. Ultimately, these deviations are more than just processing inconsistencies. They have a direct and detrimental impact on the mechanical performance of the final product [17], [18], [19].

Unlike the relatively straightforward processing of commodity polyolefins, the melt transformation of bio-based polyesters, specifically PHB, PHBV, and PHBHHx, presents a complex suite of technical challenges. Central to these challenges is the material’s precarious thermal stability. These polymers are prone to random chain scission almost immediately upon reaching their melting point, leaving a very narrow window for processing. This sensitivity is further increased by moisture, which triggers hydrolytic degradation throughout the drying and plasticization phases. Consequently, the resulting melt often suffers from erratic rheological behaviour; low molecular weight batches or partially degraded granules can lead to an extremely low melt viscosity, making the polymer difficult to shape effectively [17], [20].

Beyond these immediate constraints, the processing of PHAs is often hampered by the slow crystallisation kinetics typical of poly(3-hydroxybutyrate). In an injection moulding context, this necessitates extended residence times within the mould to ensure sufficient dimensional stability before the part can be safely removed. Perhaps most critically, because secondary crystallisation continues for days post-processing, the mechanical profile of the material remains a moving target. A sample tested shortly after moulding will appear deceptively soft and ductile, only reaching its true, more brittle equilibrium after roughly a week of ambient ageing. This lag means that early-stage measurements are often unreliable indicators of the material's long-term performance [21], [22].

1.2.9.1 *Processing techniques*

Conventional thermoplastic processing methods can generally be used for PHA, as long as the particular characteristics of these materials are carefully considered. In practice, the most common techniques include melt compounding (with both single-screw and twin-screw extruders), injection moulding, extrusion blow-moulding, blown film extrusion, compression moulding, melt blowing for fibres and nonwovens, and additive manufacturing via fused filament fabrication. Among all these options, extrusion plays a central role. It is not only used to compound PHA with additives and reinforcements, but also to directly produce semi-finished forms such as sheets, films, profiles, and pellets, which can then be further processed, for example, by injection moulding [19], [20].

Since only the extrusion technique and the injection moulding process were used in this project, to be more precise, only these two techniques will be explained briefly in the following.

1. Compounding

Extrusion is one of the most widely used and industrially important processes in plastic manufacturing. At its core, the system is relatively straightforward. An extruder consists of a rotating screw, or sometimes twin screws, housed in a heated barrel. The raw polymer is introduced through a hopper, and as it moves along the screw, it is gradually heated, melted, and mixed. By the time it reaches the end of the barrel, the material is in a fully molten state and is pushed through a die, which shapes it into a continuous product with a specific cross-section. Once the material exits the die, the extrudate is typically guided into downstream processing units depending on the final application. These can include cooling systems (such as water baths), pelletisers for producing granules, or additional forming processes like blow

moulding. This continuous nature of extrusion is what makes it especially efficient and versatile for large-scale production.

A standard extrusion screw is typically divided into three functional zones, each with a specific role in transforming the raw polymer into a processable melt. The first section is the feed zone, which usually accounts for about half of the total screw length. In this region, the polymer is still in solid form and is mainly conveyed forward while beginning to heat up. This is followed by the compression zone (~ 25–30% of the screw length), where the material is compacted, melted, and subjected to increasing pressure and shear. Finally, the metering zone (~ 20–25%) ensures that the melt is fully homogenised and delivered at a stable flow rate and pressure before exiting through the die. An important design parameter of the screw is the compression ratio, defined as the ratio between the flight depth in the feed zone and that in the metering zone. This parameter strongly influences how much shear heating and mixing the material experiences. Higher compression ratios generally lead to greater shear, improved mixing, and more efficient melting, but they can also increase the risk of thermal degradation, particularly for sensitive polymers like PHAs [20].

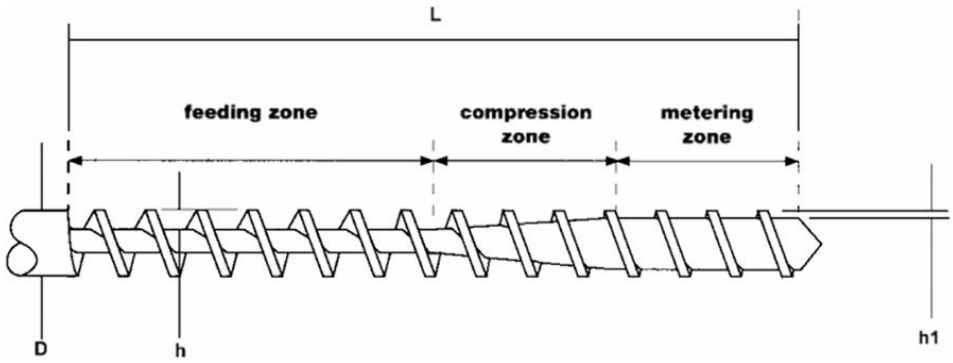

Fig 8. Schematic diagram of a typical extruder screw showing the feed zone, compression zone, and metering zone [20]

When it comes to the processing of PHAs by extrusion, operating conditions need to be carefully controlled to avoid thermal degradation. Typically, the barrel temperature is set with a gradual profile, starting from around 160 °C in the feed zone and reaching about 170–185 °C at the die. This is noticeably lower than the 190–200 °C commonly used for polyolefins, since PHAs are much more heat-sensitive and can lose molecular weight if processed too close to

those higher temperatures. Screw speed is another key parameter. Lower speeds are generally preferred when it is important to limit residence time and reduce thermal exposure, while higher speeds are only used when the material's viscosity is high, and additional shear is needed to ensure proper melting and mixing. At the same time, the feed rate must be carefully adjusted to strike a balance between maintaining a reasonable shear rate and avoiding excessive residence time inside the barrel.

To further improve material quality, many extrusion setups include vacuum venting in the metering zone. This allows the removal of residual moisture and low molecular weight volatiles generated during processing, both of which could otherwise accelerate degradation or negatively affect the final properties of the material [19], [22].

As it was mentioned above, there is a possibility of having a single or twin-screw extruder. In [Table 1], a comprehensive comparison between both of them is available. Single-screw extruders operate primarily under drag flow, resulting in a broader residence time distribution and higher shear levels within the channel, which can be advantageous for melting and processing relatively stable polymers. However, their output is more sensitive to back pressure, and their performance is constrained by limitations related to polymer thermal stability at higher screw speeds. In contrast, twin-screw extruders exhibit near-positive displacement flow, enabling more uniform and narrowly distributed residence times, which is particularly beneficial for precise thermal and mechanical control. Although they generate lower shear and have reduced thrust capacity, twin-screw systems are less affected by back pressure and allow for more controlled material conveying and mixing. These advantages come at the cost of increased mechanical complexity and higher initial investment. Overall, the choice between the two systems reflects a trade-off between simplicity and robustness in single-screw designs versus the enhanced control and processing versatility offered by twin-screw extruders.

Table 1. Comparison of Single- and Twin-screw Extruders [20]

Criteria	Single screw	Twin screw
Flow type	Drag	Near positive
Residence time and distribution	Medium and wide	Low and narrow
Effect of back pressure on output	Reduce output	Moderate effect on output
Shear in channel	High (useful for stable polymer)	Low
Maximum screw speed	High (limited by the melting and stability of the polymer)	Medium
Thrust capacity	High	Low
Mechanical construction	Robust, simple	Complicated
Initial costing	Moderate	High

The effect of processing parameters of compounding with an extruder on the PHA during processing can be explained by combining the chemical and physical mechanisms that the molten polymer will go through during the processing. The main processing parameters are melt temperature, screw speed, residence time, screw configuration, feed rate, and their effect on PHA will be explained in the following part of this section in brief.

Melt Temperature

Among all processing variables, melt temperature plays the dominant role in determining the extent of molecular weight degradation in PHA. Kinetic studies on PHB, based on a first-order model of random chain scission, show a strong temperature sensitivity. Around 180 °C, increasing the temperature by just 10 °C approximately doubles the degradation rate. A similar activation energy has been reported for related copolymers such as PHBV and PHBHHx, indicating a consistent behaviour across the PHA family. From a processing standpoint, this effect is substantial. For example, raising the processing temperature of PHB from 180 °C to 200 °C in a twin-screw extruder, even with a relatively short residence time of about one minute, can increase the molecular weight loss from roughly 10–15% up to 30–40%. This highlights how even moderate temperature increases can significantly accelerate polymer degradation during melt processing [17], [19].

Screw Speed

Screw speed is a key processing variable because it simultaneously influences the shear conditions experienced by the melt and the time the material spends inside the extruder. In single-screw systems, increasing the screw speed generally shortens the residence time, but at the same time, it intensifies viscous dissipation. This additional shear heating can significantly raise the local melt temperature, particularly in the compression zone, where it may exceed 200 °C even if the barrel set temperatures are lower. In twin-screw extruders, the situation is more nuanced. The residence time within the mixing sections tends to be only weakly affected by changes in screw speed, whereas the shear rate in elements such as kneading blocks increases almost linearly with it. As a result, the balance between mixing efficiency and thermal exposure becomes more complex to control [19].

From a practical standpoint, these effects lead to a preference for moderate screw speeds when processing PHA—typically in the range of 40–80 rpm for laboratory-scale single-screw extruders and 150–250 rpm for twin-screw systems. Moreover, it is essential to monitor the actual melt temperature directly, for example, using an infrared probe near the die, rather than relying solely on the barrel set temperatures. At high screw speeds, the discrepancy between

the set temperature and the true melt temperature can easily exceed 15 °C, which has important implications for thermal degradation [19], [22].

Residence Time

After temperature, residence time is the most critical parameter influencing the PHA during processing. In laboratory-scale extruders, it can be estimated through different approaches, such as assuming ideal plug flow, performing tracer experiments with colour markers, or using combined thermal–rheological models. For example, in a 25 mm single-screw extruder operating at a throughput of 2 kg/h, typical residence times range from about 1 to 3 minutes. On the other hand, in twin-screw extruders, the situation is slightly different. The average residence time is usually shorter, around 1 to 2 minutes, but the distribution is broader, meaning that some material elements may experience significantly longer or shorter thermal histories [19].

An important point is that different processing conditions can lead to the same level of molecular weight loss if they result in the same intensity. For instance, reducing the residence time by about 30% can have an equivalent effect to lowering the melt temperature by roughly 10 °C. This highlights the trade-off between thermal and time-based factors in controlling polymer degradation.

Feed Rate and Screw Configuration

The feed rate and screw configuration are the main factors influencing the residence time distribution in twin-screw extrusion. Increasing the feed rate typically results in a shorter average residence time, which helps reduce temperature exposure and, as a result, the polymer's degradation. A larger feed rate, however, reduces the filling degree of the kneading zones, which diminishes the effectiveness of dispersive mixing and may result in a less uniform distribution of fillers or additives. Equally significant is the screw configuration, especially when it comes to the quantity and arrangement of kneading blocks. Although these components are necessary to achieve sufficient mixing, too many of them might lengthen residence times and increase mechanical stress, which accelerates degradation. According to studies, an average feed rate combined with a screw design that employs a small number of carefully placed kneading blocks between conveying sections can produce the best possible balance. It

has been demonstrated that this arrangement offers a good balance between maintaining molecular weight and guaranteeing adequate dispersion of fillers [19].

2. Injection moulding

As it was stated above, injection moulding is another widely used technique for manufacturing plastic parts, especially when complex shapes, tight dimensional tolerances, and high-quality surface finishes are required. The process relies on two main components, which are the injection unit and the clamping unit. In the injection unit, a reciprocating screw melts the polymer at elevated temperatures and transports it forward. Once enough molten material has accumulated in front of the screw, the screw moves forward like a plunger, injecting the melt at high pressure into a mould cavity that is securely held closed by the clamping unit. The mould is kept at a controlled temperature to allow the material to solidify and, where relevant, crystallise before the finished part is ejected and the cycle starts again. The injection moulding cycle follows a well-defined sequence of steps [20]:

1. Mould clamping
2. Filling of the cavity
3. Application of holding or packing pressure
4. Cooling and solidification
5. Screw recovery
6. Mould opening
7. Part ejection

Among these, cycle time is particularly important from an industrial and economic perspective, as it directly affects productivity. From a design standpoint, a screw with a length-to-diameter (L/D) ratio of at least 20:1 is typically recommended. Longer screws can improve melt homogeneity by generating more shear heat, but they also come with trade-offs, including higher melt temperatures, longer cycle times, increased energy consumption, and a greater risk of thermal degradation, which is an especially critical concern when processing sensitive polymers like PHAs [20].

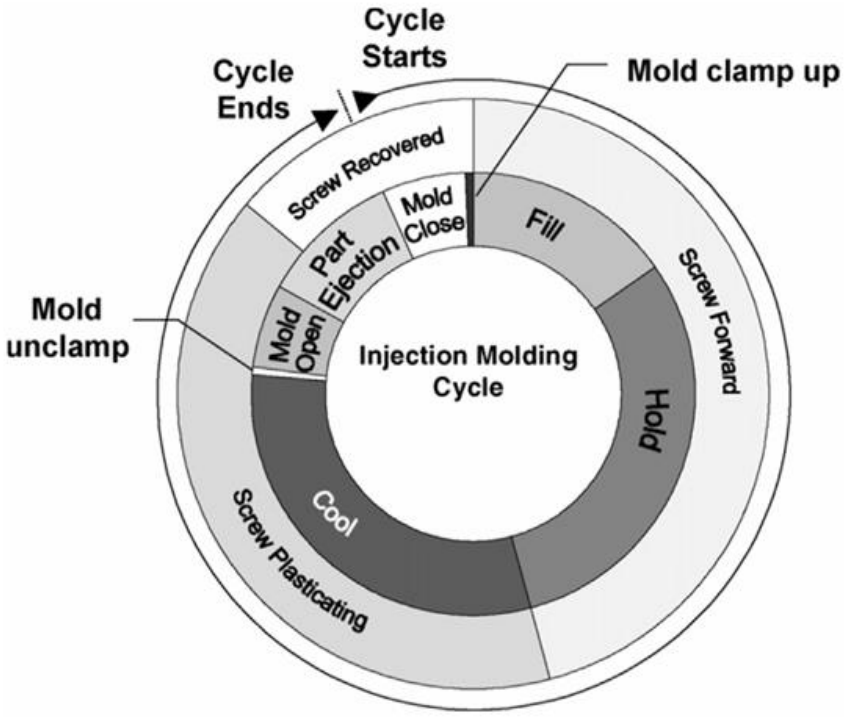

Fig 9. Typical cycle for an injection moulding process [20]

Experimental evidence indicates that the interaction between injection speed and mould temperature has a significant impact on the short- and long-term behaviour of moulded parts. When high injection speeds are combined with relatively cold moulds, the resulting components often appear stiff and brittle immediately after processing, while also exhibiting good geometric stability. However, this condition is not permanent. Over the course of several days, the material gradually recovers ductility as secondary crystallisation progresses. In contrast, processing at higher mould temperatures (for instance, 60 °C instead of 30 °C) allows the material to achieve its final degree of crystallinity much more rapidly, typically within a few hours. This accelerated structural stabilisation, however, comes at the expense of processability, as the reduced stiffness of the part makes demoulding more challenging. Consequently, the selection of mould temperature represents a critical trade-off, requiring a balance between minimising cycle time, ensuring dimensional stability, and achieving stable mechanical properties within an acceptable timeframe [21].

Just like compounding, the processing parameters of injection moulding also has its own influence on PHA during processing. Mould temperature and cooling time are the ones whose effect on PHA should be noted. In the following, their influence is briefly explained.

Mould Temperature and Cooling Time

The impact of mould temperature on thermal degradation in injection moulding is relatively low. This is primarily because there is little chance for substantial degradation to take place. After all, the polymer only stays at temperatures near the melt temperature for a very short period of time, usually one to two seconds, while passing through the hot runner. However, the ultimate morphology of the material is greatly influenced by the temperature of the mould. Incomplete crystallisation occurs during the cooling phase when PHB is injected into a cold mould (around 30 °C or lower). Consequently, after ejection, the material progressively continues to crystallise at ambient temperature. A gradual rise in stiffness (tensile modulus) and a corresponding decrease in ductility (strain at break) result from this post-crystallisation process, which can last for a few days or even up to a week. On the other hand, crystallization happens more quickly and is essentially finished before the portion is ejected when the mold temperature is higher (around 60 °C or above). In these circumstances, the material achieves its ultimate structure and mechanical characteristics significantly sooner, leading to more stable performance right after processing [21].

Up to this point, the main goal has been to provide an organised summary of the relevant theoretical background in order to provide the framework required for a better understanding of the study's later sections. The experimental examination is covered in the part that follows. It provides a thorough explanation of how the material used in this study was produced, as well as a description of its mechanical and chemical characteristics. Furthermore, a detailed explanation of the simulation methods used to examine the processing conditions is provided. Lastly, the methods and standards used in the disintegration tests are presented, allowing for a thorough assessment of the material's performance under various processing conditions.

2 Chapter 2

2.1 Experimental section

During this project, a bio compound was used to evaluate the effect of processing parameters on the disintegration rate. The first experimental part involved processing the bio compound in the MAIP Compounding Srl, and the next part was applying the conditions in the Ludovic software to simulate the process. In the following, there is a description of how these steps are done.

2.1.1 Materials and methods

With the use of an extruder present in the MAIP Compounding Srl, a PHA-based blend with the commercial name of IamNATURE B6 G713 was processed at five different conditions, which will be explained in the following.

2.1.1.1 Extruding the material and the parameters

PHA is the primary polymer in the bio compound that was used, which is marketed under the brand IamNATURE B6 G713. A range has been selected for both torque and specific mechanical energy to assess the impact of processing factors. When it comes to biopolymers, a torque of less than 60% is insufficient due to the small amount of material inside the extruder, which permits air to enter and subsequently causes the substance to degrade. Additionally, more than 80% indicates poor mixing because the extruder has an excessive amount of material. Thus, the torque range that was selected was [60-80%]. The screw speed, which was maintained between [150,518] Rpm, was the other regulated parameter. These variables were adjusted to provide the Specific Mechanical Energy within the range of [0.1,0.2], which represents the lowest and highest allowable stress on the material. Regarding the Specific Mechanical Energy, it is crucial to note that it almost entirely dissipates as heat within the system, which modifies the system's overall thermal energy [23]. Therefore, for biopolymers, it shouldn't be too high, or the polymer will degrade.

Five trials were completed to assess the processing parameters; these will be described below.

2.1.1.1.1 Five trials

The extruder was thoroughly cleaned before the experiments began to prevent any undesired materials from entering. Then, in order to complete all of the trials in a single run, 120 kilogrammes of the material were fed into the extruder. To ensure that all other parameters stay the same, this action was taken. The conditions for each trial are summarised in the table below [Table 2].

Table 2. Conditions for each trial

Trial	1	2	3	4	5
Torque (%)	60	80	60	80	65
Screw speed (RPM)	150	150	300	300	518
Output (kg/h)	30	41	48	60	80
Barrel Temperature (℃)	145	145	145	120	120
SME (kW/kg)	0.14	0.14	0.17	0.19	0.21

Certain points need to be mentioned. First of all, the first 5 kg of the extruded material will be discarded once all the materials have been fed and the first condition has been applied to ensure that all the parameters are established. Every time the circumstances change, this process is used. Furthermore, the specific mechanical energy, which is mentioned in [Table 2] was discovered using the following formula [Equation 1]:

$$SME = \frac{motor\ power\ (kW)}{Maximum\ torque(\%) * Maximum\ screw\ speed(Rpm)} * \frac{torque * screw\ speed}{output(\frac{kg}{h})}$$

Equation 1. SME formula

In the formula above, the extruder's motor power has a set term, which in this case is 30 kW. Also, the extruder's maximum torque and screw speed are defined as 100% and 600 RPM, respectively, for the extruder that was used. Note that the second term of torque and screw speed, the value is defined experimentally, and in this case, the values are shown in [Table 2].

The fact that the temperature is lowered to 120 degrees for trials 4 and 5 is another crucial detail regarding the trials. As seen in [Table 2], the temperature dropped to raise the torque and ultimately raise the SME because, up to trial 3, the SME did not reach 0.2.

Following the completion of all trials, the extruded G713 was dried and prepared for injection in an oven set to 80°C.

2.1.1.2 Injection of the bio compound

The MAIP company's injection equipment comprises five distinct zones. The temperature of the first three zones was set at 140°C, while the temperature of the final two zones was set at 145°C in order to inject the chosen compound. Furthermore, the mould's temperature, which is used to cool and shape the material, was set at two different temperatures, which were 20℃ and 50 °C. The injection machine's screw speed was set at 25 mm/s, and each trial's clamping force and duration were selected to produce the optimum outcomes. In the table below, there is a summary of the conditions that were used for the injection process.

Clamping force and time are decreased in trial 2, as shown in [Table 4]. Both of them were reduced because excessive material was extracted, which led to flaws in the finished shape. As a result, both the clamping force and its duration decreased.

Table 3. Injection conditions for 20℃ mould

Trial	**1**	**2**	**3**	**4**	**5**
Clamping force (MPa)	50	50	50	50	50
Time of the Clamping force (S)	10	10	10	10	10

Table 4. Injection conditions for 50℃ mould

Trial	**1**	**2**	**3**	**4**	**5**
Clamping force (MPa)	50	40	50	55	50
Time of the Clamping force (S)	15	10	10	10	10

Fig 10. A sample of a dumbbell-shaped specimen, which was moulded at 50℃

The following explains how the created samples are used to assess the chosen material's mechanical properties.

2.1.1.3 Mechanical properties of G713

Each material trial's mechanical characteristics were assessed using tensile, flexural, and impact tests, offering a thorough evaluation of structural performance. Because the generated data reflect the material's internal microstructure, these characterisations are essential. It should be noted that, for having more accurate results, each test was conducted three times.

1. **Tensile test**

   Tensile testing is an essential method for evaluating structural integrity since it offers quantitative insight into the material's deformation and failure behaviour under uniaxial force. Specifically, the degree of macromolecular orientation produced during processing and the quality of stress transmission across phase boundaries have a significant impact on the reported tensile modulus, strength, and elongation at break. [Fig 11].

Fig 11. Tensile Test

2. **Flexural test**

   When combined tensile and compressive stresses are applied to a material, flexural testing provides a sensitive probe of the material's overall homogeneity and mechanical integrity. The regularity of the interior morphology has a significant impact on the final

flexural modulus and strength because bending loads simultaneously contact the outside and inner areas of the sample cross-section. [Fig 12].

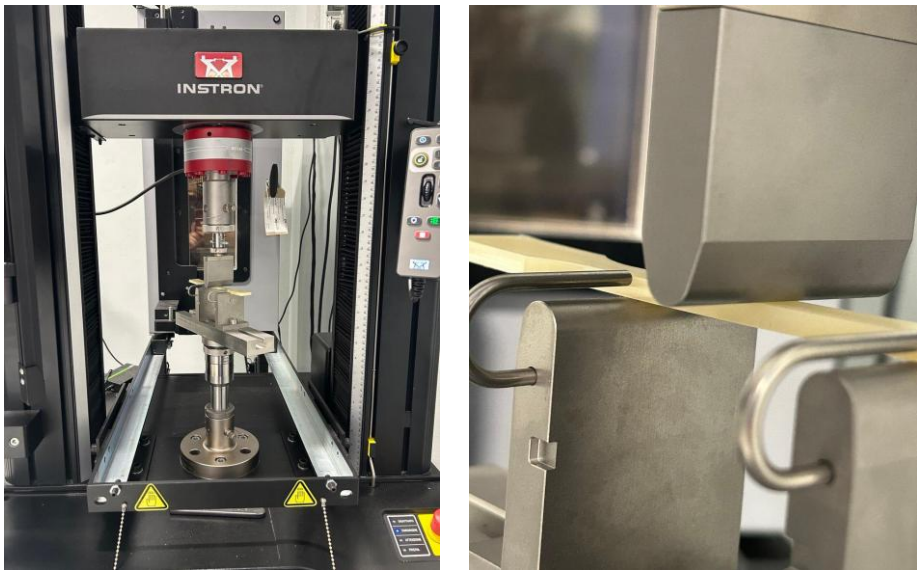

Fig 12. Flexural Test

3. Impact test

To elaborate, impact testing measures the material's capacity to absorb and release energy under fast loading, giving information on its durability and failure causes. Shear yielding, localised plastic deformation, craze initiation and propagation, and other microscopic energy-dissipation processes are all activated by the measured impact strength. The size, distribution, and connectivity of crystalline domains significantly influence these mechanisms. For each trial, this test was done with and without a notch. The specimen in an unnotched impact test has no pre-existing defects. The material's overall resistance to crack initiation and propagation under high-strain-rate loading is thus reflected in the measured impact energy. Intrinsic microstructural elements like voids, crystalline boundaries, weak interfacial areas, or processing-induced flaws must be the source of failure. As a result, unnotched impact strength frequently shows more variation in findings and is extremely susceptible to surface quality, internal flaws, and material homogeneity. The notched impact test, on the other hand, creates a distinct, sharp notch that serves as both a predetermined fracture initiation point and a stress concentrator. By focusing the measurement on the material's resistance to crack propagation after a defect is present, this design reduces the variability related to crack

initiation. As a result, the resulting impact energy is more repeatable and is highly dependent on notch sensitivity, interfacial adhesion, crystalline morphology, and the material's capacity for plastic deformation prior to the crack tip [Fig 13].

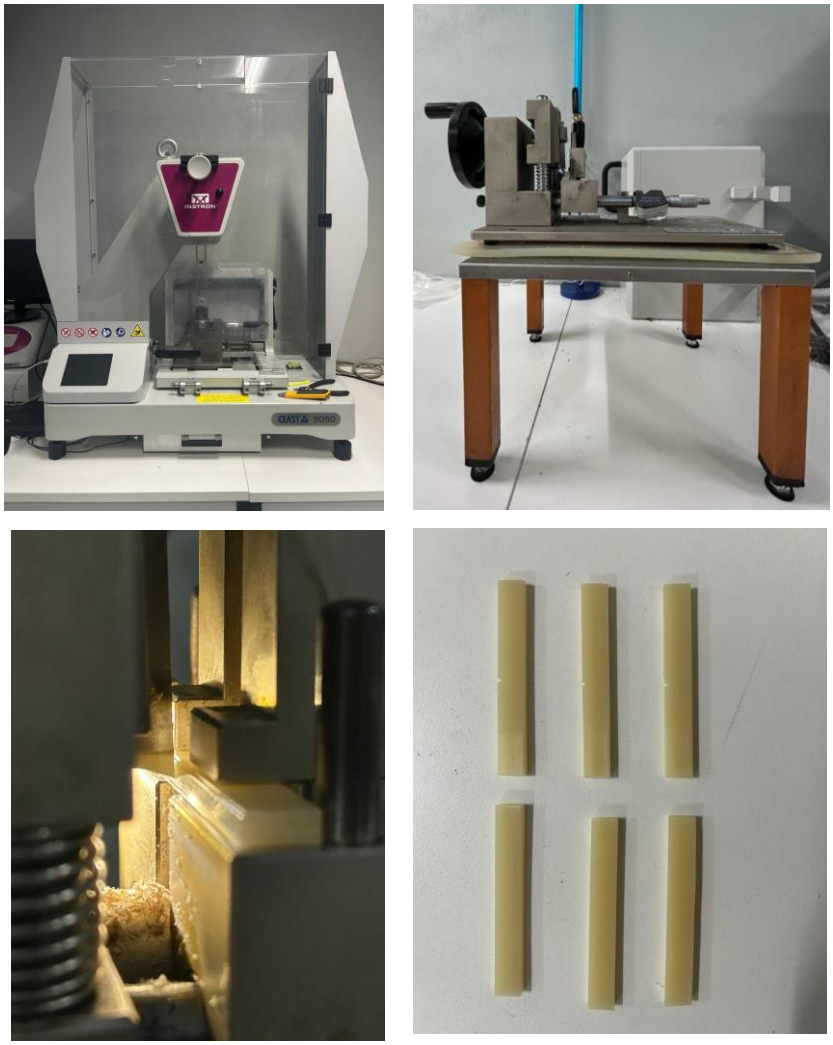

Fig 13. Impact Test

2.1.1.3.1 Mechanical characterisation of G713 (trial one to five, moulded at 20°C and 50°C)

Five trials of G713, which were moulded at 20°C and 50°C, were characterised in tension, three-point bending, and Charpy impact (notched and unnotched). For each combination, three specimens were tested, and the same qualitative response was observed in all trials. In tension, the specimens exhibited an initial linear-elastic region, a yield point, and post-yield softening; in flexure, extended plastic flow was observed without fracture, and good reliability up to yield, with larger scatter at break. Because this overall pattern is common to all trials, the individual

stress–strain curves are discussed jointly rather than trial by trial. The full per-trial data tables are reported in [Table 5], [Table 6], and [Table 7].

Table 5. Tensile properties of G713

Trial	T [°C]	E [MPa]	σ_yield [MPa]	ε_yield [%]	σ_break [MPa]	ε_break [%]
T1	20	1224.67 ± 37.09	28.15 ± 0.63	6.86 ± 0.15	23.74 ± 2.41	10.93 ± 0.45
T1	50	1236.55 ± 8.06	28.95 ± 0.21	7.00 ± 0.10	21.41 ± 1.28	14.27 ± 1.86
T2	20	1242.61 ± 16.14	28.69 ± 0.14	6.84 ± 0.13	22.06 ± 3.51	13.46 ± 3.07
T2	50	1172.02 ± 6.55	27.36 ± 0.27	7.03 ± 0.11	19.13 ± 1.85	15.26 ± 2.14
T3	20	1252.57 ± 9.42	28.63 ± 0.08	6.84 ± 0.10	22.72 ± 1.67	11.28 ± 1.28
T3	50	1215.70 ± 8.28	28.25 ± 0.30	6.84 ± 0.14	20.38 ± 2.32	14.02 ± 1.90
T4	20	1229.42 ± 2.54	28.15 ± 0.11	6.79 ± 0.04	20.90 ± 0.94	14.95 ± 3.20
T4	50	1206.30 ± 2.54	28.41 ± 0.13	7.25 ± 0.06	19.16 ± 0.87	15.11 ± 1.67
T5	20	1286.09 ± 28.35	28.15 ± 0.08	6.47 ± 0.18	23.77 ± 3.07	11.31 ± 2.04
T5	50	1206.12 ± 4.66	27.94 ± 0.34	6.92 ± 0.05	20.70 ± 0.93	13.82 ± 1.71

Table 6. Flexural properties of G713

Trial	T [°C]	E_flex [MPa]	σ_flex,max [MPa]
T1	20	1198.70 ± 49.10	34.51 ± 0.98
T1	50	1153.01 ± 6.06	33.88 ± 0.16
T2	20	1204.03 ± 8.76	35.30 ± 0.20
T2	50	1082.86 ± 12.81	31.80 ± 0.35
T3	20	1223.27 ± 8.71	35.66 ± 0.17
T3	50	1130.69 ± 8.89	32.91 ± 0.08
T4	20	1171.61 ± 19.05	34.69 ± 0.12
T4	50	1134.13 ± 5.67	33.32 ± 0.08
T5	20	1205.42 ± 7.29	35.01 ± 0.13
T5	50	1123.76 ± 2.39	32.54 ± 0.08

Table 7. Charpy impact strength of G713

Trial	Unnotched, 20 °C kJ/m²	Unnotched, 50 °C kJ/m²	Notched, 20 °C kJ/m²	Notched, 50 °C kJ/m²
T1	61.18	60.69	2.93	2.88
T2	62.24	65.24	2.93	3.19
T3	65.24	65.25	2.87	3.21
T4	61.77	65.24	3.11	3.36
T5	61.89	65.25	3.00	2.87

[Fig 14], shows a comparison between the tensile properties of G713 at two different mould temperatures. The material showed a typical behaviour of a semi-ductile thermoplastic. As previously stated, there was a common pattern in the experiments, and within this common pattern, the temperature of the mould had different effects on each property.

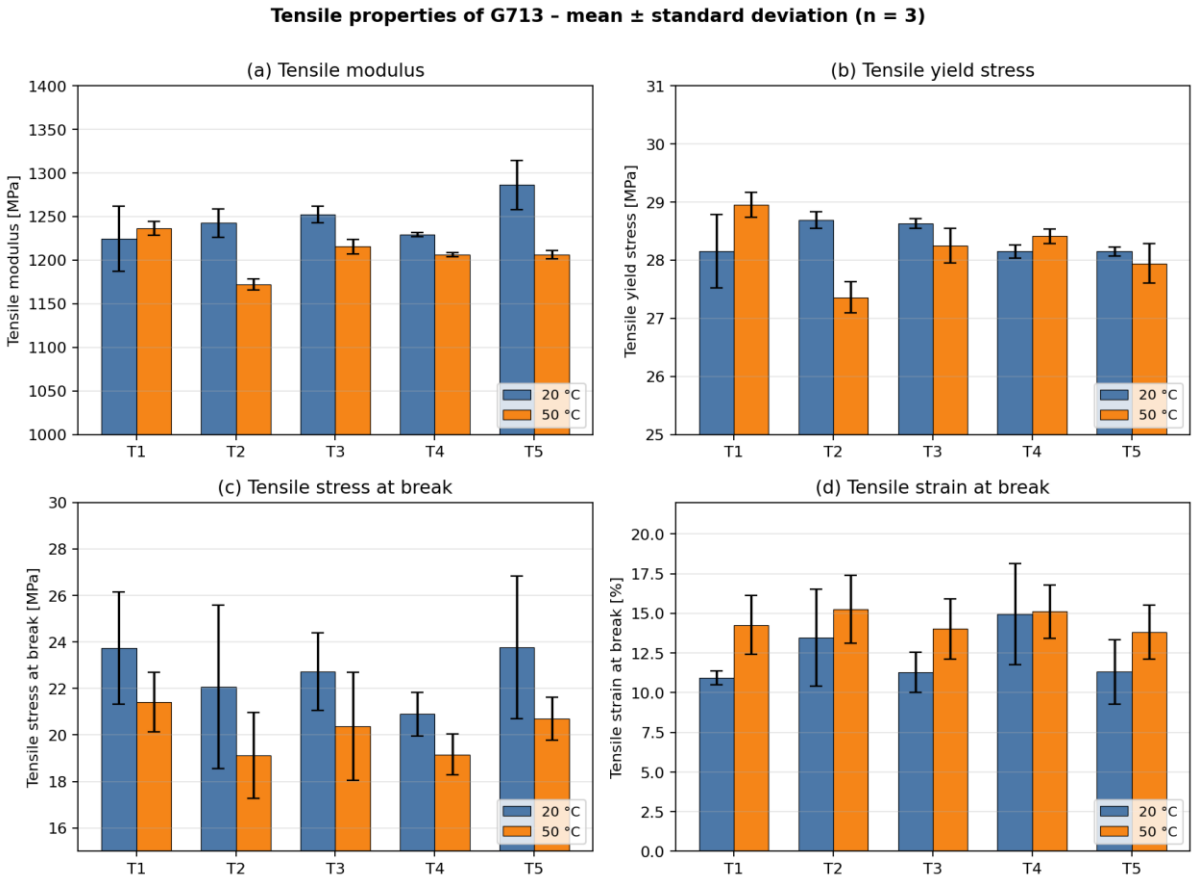

Fig 14. Tensile properties of G713 across the five trials at 20℃ and 50℃: a)tensile modulus, b)yield stress, c)stress at break, d)strain at break. Blue bars represent 20℃ and orange bars represent the 50℃ mould temperature

As can be seen in the tensile modulus [Fig 14.a], The mean values lie in a narrow band (≈ 1170–1290 MPa), and the 20 °C series is on average slightly stiffer than the 50 °C one, with the largest difference in trial five (1286 vs. 1206 MPa) and trial two (1243 vs. 1172 MPa). In trial one, the trend is reversed, but the difference is small and within the scatter of the 20 °C value (SD ≈ 37 MPa). Overall, the higher mould temperature tends to reduce the modulus, consistent with a slower cooling rate allowing more chain relaxation and a less ordered structure, but the magnitude of the change is moderate.

In [Fig 14.b], compare the yield stress of the trials at different temperatures. This is the most reproducible property in the whole figure. All the trials lie between 27 and 29MPa with small error. This indicates that this property is controlled by the intrinsic chemistry of the formulation rather than by the moulding condition. Yield strain shows a small but systematic increase at 50 °C, consistent with the slightly more compliant response observed in the modulus.

[Fig 14.c-d], shows the properties at break of the material. As is obvious, the stress at break is lower at 50 °C in every trial, while the strain at break is consistently higher at 50 °C. This is the clearest temperature effect observed in tension and corresponds to the conventional strength–ductility trade-off. This difference shows that at the higher mould temperature, the specimens stretch farther before failing but at a lower stress.

It should be said that trials two and five show the largest reductions in modulus and stress at break when the mould temperature is raised from 20 °C to 50 °C, which means that these extrusion conditions are the most temperature-sensitive in tension. On the other hand, trial one and trial four show the smallest property shifts between the two temperatures and can be regarded as the most thermally stable trials in tension.

Moving forward, [Fig 15] demonstrates the flexural behaviour of the material. In three-point bending, all specimens display a linear-elastic region followed by a non-linear phase without any sudden stress drop. None of the specimens fractured within the displacement range covered by the test, so the value reported as “maximum flexural stress” corresponds to the stop condition of the test rather than to an actual rupture. Strain and displacement at maximum force are identical in every condition, confirming that the test was stopped at the same limit in all cases.

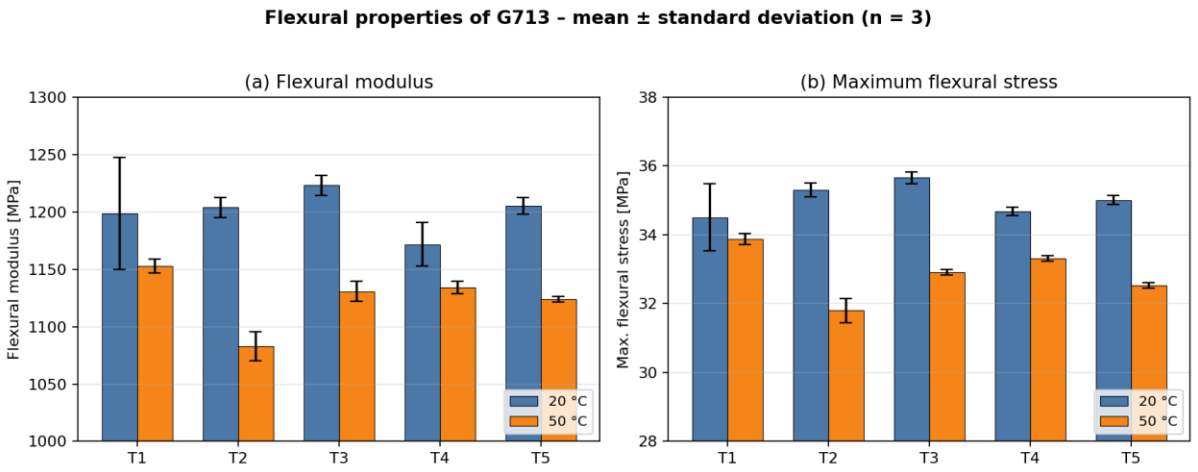

Fig 15. Flexural properties of G713: (a) flexural modulus, (b) maximum flexural stress. Blue bars = 20 °C mould temperature; orange bars = 50 °C mould temperature.

[Fig 15.a] demonstrates that the flexural modulus is between 1172 and 1223 MPa, and at 50 °C in the range of 1083 to 1153 MPa. As can be seen, for a given trial, the 50 °C value is lower than the 20 °C value by a few percent, and this reduction is consistent with the trend already seen in tension but again moderate in magnitude. It should be noted that trial two shows the highest reduction, which emphasises the sensitivity to temperature of this trial. On the other hand, trial four and one show the lowest reduction.

Flexural stress of the tested material is shown in [Fig 15.b]. As can be seen, for both temperatures, the values lie in a narrow band for all the trials. The 50 °C condition produces a small but systematic decrease with respect to 20 °C. Trial two again shows the largest reduction, while trial one and four show the smallest, generally consistent with the tensile trends.

The last mechanical property that should be mentioned is the impact property of the material.

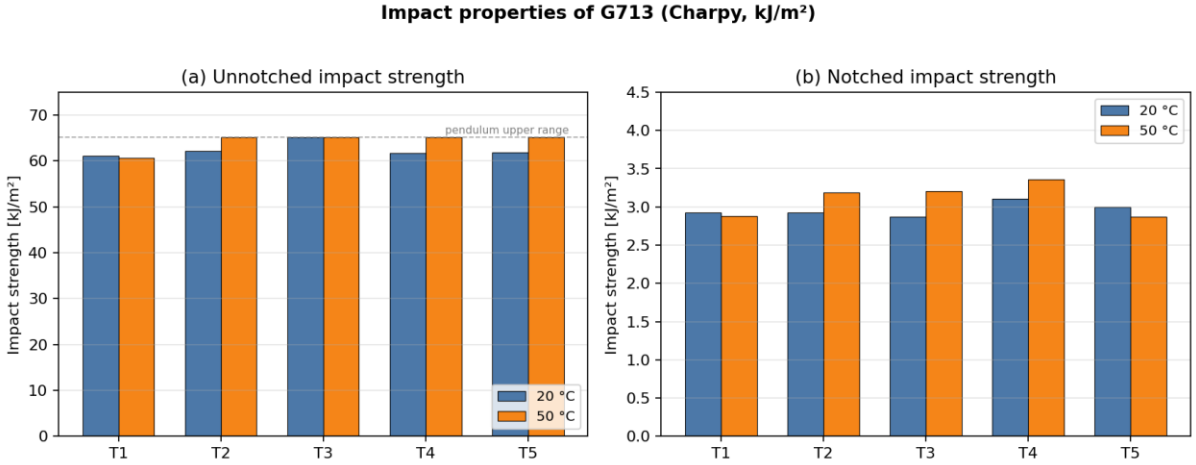

Fig 16. Charpy impact strength of G713: (a) unnotched, (b) notched

The impact test produces two clearly different families of results depending on the presence of the notch. Unnotched specimens absorb ~60–65 kJ/m², while notched specimens absorb only ~2.9–3.4 kJ/m². This factor of ~20 between the two configurations is by far the largest effect observed in the whole mechanical characterisation, and identifies the material as clearly notch-sensitive. The reduction in impact strength for the notched specimens can be explained by the fact that the presence of a sharp geometric discontinuity eliminates the crack-initiation phase and concentrates the stress at the notch tip, which strongly reduces the energy needed to propagate the crack.

It can be said that the effect of mould temperature within each notch configuration is much smaller. In the unnotched specimens, the differences between 20 °C and 50 °C are at most a few kJ/m², and the highest values are very close to the pendulum upper range (~65 kJ/m²), so part of the variation may simply reflect the limited resolution of the instrument in this region. Trial one is slightly lower than the others (~61 kJ/m²) at both temperatures. Overall, the differences between 20 °C and 50 °C for the unnotched configuration can be considered within experimental noise.

For the notched specimens, the values stay within 2.87 to 3.36 kJ/m² across all ten conditions. There is no clear evidence of the temperature effect. Trials two, three and four show a small increase at 50 °C, while trial one and trial five show a small decrease. Since the differences are small, the notched impact values can be considered constant for all the trials and temperatures, with the notch sensitivity itself.

In general, it can be said that with a yield stress of roughly 28 MPa, a tensile modulus of approximately 1200 MPa, a flexural modulus of about 1100 to 1200 MPa, and a Charpy impact strength of about 60–65 kJ/m² unnotched and about 3 kJ/m² notched, G713 exhibits semi-ductile thermoplastic behaviour across the five extrusion experiments and the two mould temperatures. Increasing the mould temperature from 20 °C to 50 °C results in a slight decrease in stiffness (both tensile and flexural) and stress at break, along with an increase in strain at break. This is a typical strength–ductility trade-off that is consistent with a slower cooling rate and a less ordered crystalline microstructure. In bending, yield stress and the parameters at maximum force are basically unaffected by mould temperature. In addition, among the trials, the second trial is the one which is most affected by the change in mould temperature in both tension and flexure. The smallest property shifts between 20 °C and 50 °C are observed on trial one and trial four, which can therefore be regarded as the most thermally stable extrusion conditions. T3 shows the highest absolute flexural properties at 20 °C but only intermediate temperature sensitivity. The impact test confirms a clear notch sensitivity of the material, with a reduction of about one order of magnitude between unnotched and notched specimens, and the temperature difference has no meaningful effect on the impact strength. At the end, it should be said that the anomalies in the results can be considered as test noise since they do not follow a clear path.

2.2 Setting of the simulation with Ludovic software

SC-Consultants created the proprietary simulation program Ludovic (v. 7.0) specifically for the global thermo-mechanical analysis of the co-rotating twin-screw extrusion process. The program models material behaviour under stationary (steady state) conditions from the feed zone through the die using a 1D numerical technique. Ludovic is a very effective predictive tool for quick process screening, even if the 1D simplification and stationary limitations naturally limit the absolute precision of local flow dynamics compared to 3D models.
This software's computational efficiency is one of its main advantages; a full simulation can be finished on a typical laptop in a matter of seconds. On the other hand, a 3D unstationary local analysis, like the one carried out by the XimeX software, demands a lot more resources; on specialised high-performance hardware (such as 16-core microprocessors), the computation time frequently exceeds 10 hours. Because of this speed, researchers may theoretically iterate through a variety of screw designs, temperature profiles, and rotation rates to find the best process windows without having to pay the exorbitant costs associated with actual laboratory experiments.

In order to produce detailed information on energy consumption (SME), residence time distribution (RTD), and axial profiles for temperature, pressure, and viscosity, the simulation workflow requires the definition of particular operating parameters. These results can be examined using the software's internal comparison tools or exported in the.xls format for processing by third parties. Additionally, Ludovic has a dedicated Design of Experiments (DoE) tool that automates simulation repetition by methodically changing independent variables. This goes beyond the conventional trial-and-error method by allowing the precise determination of the parameters needed to accomplish particular material targets. The hierarchical structure of "Projects" and "Databases," which makes it easier to manage big datasets and guarantees efficient backup processes, is used to manage simulations and DoEs for organisational efficiency.

2.2.1 **“Extruder” Tab**

The first step in using the Ludovic software to simulate the process is to define the extruder geometry. In general, a few key factors should be specified when establishing the extruder's geometry. Diameter, centreline, and screw/barrel leakage are the parameters that should be imported in the “Extruder” Tab. The design of the screw elements was added to the screw profile section because the screw profile used to process the material was new. In general, the

extruder is assembled from a series of elements mounted on a central shaft. Moving from the feed zone towards the die, first of all, there is a flighted conveying element. These elements are located near the feed zone to efficiently intake and transport the material forward. After these elements, there are kneading blocks, which are responsible for dispersive and distributive mixing. A left-handed conveying element is also present in the structure of the extruder, which acts as a flow restriction that forces material back and increases the local pressure, residence time and improves mixing.

The other information that should be specified in this tab is the different processing zones. Since no fillers or additives were used in the processing of G713, the only zone that exists is the feeding zone, which was considered at the beginning of the extruder. The final item to import into the program in this tab is the die's geometry. Since the die geometry was not accessible in this case, the simulation was run without the die at the extruder's end without affecting the results.

2.2.2 **"Product" Tab**

This section defines the characteristics of the material that was utilised. To assess a material's characteristics, the Ludovic program needs its density, thermal conductivity, and heat capacity in both liquid and solid phases. Moreover, melting temperature and melting enthalpy are also needed. The rheology of the utilised polymer should be defined in another tab using SoP or analytical law.

Different characterisation tests were conducted for each required data since the software does not contain the polymer that was used.

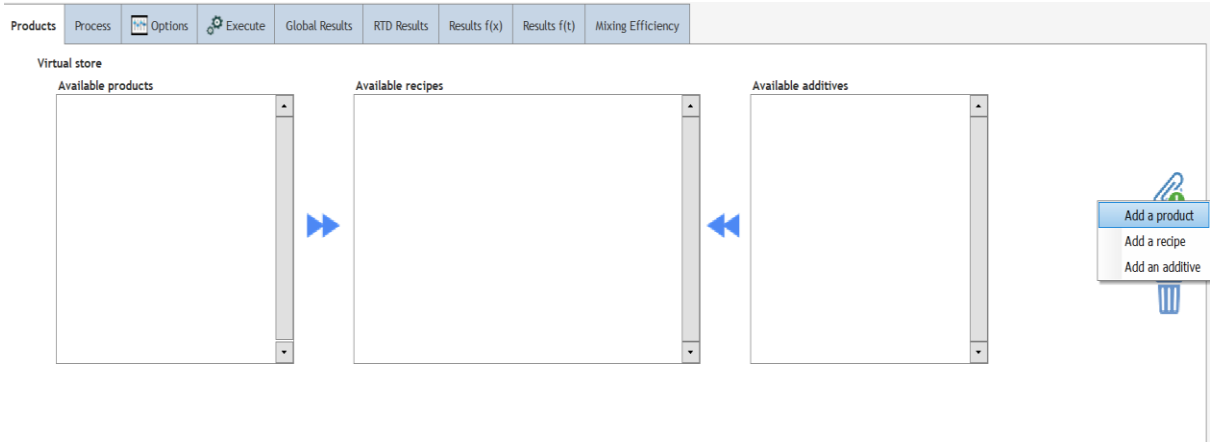

Fig 17. Adding the used material to the software

The software initially requests the thermal parameters of the material for analysis. The melting temperature and melting enthalpy were determined by performing DSC analysis, but the density and heat capacity in both the solid and liquid phases were imported based on the material's data sheet.

2.2.2.1 **Differential Scanning Calorimetry of G713**

Using a TA Instruments DSC Standard Cell FC, the Differential Scanning Calorimetry (DSC) analysis was carried out at the Alessandria Laboratory. A 7.2000 mg sample of G713 was encapsulated and heated linearly at a rate of 10°C per minute over a temperature range of 25°C to 220°C. To separate the material's processing history from its intrinsic thermodynamic properties, the approach suggests a two-cycle (heat-cool-heat) process. A cell constant of 1.0488 was used to guarantee the quantitative precision of the heat flow measurements (W/g), and data collecting was set up with the exothermic direction facing upward. It should be noted that the whole procedure was carried out under the Nitrogen gas to provide an inert atmosphere and prevent the material oxidation and degradation during the heating cycle. The result of the DSC test can be seen in [Fig 18].

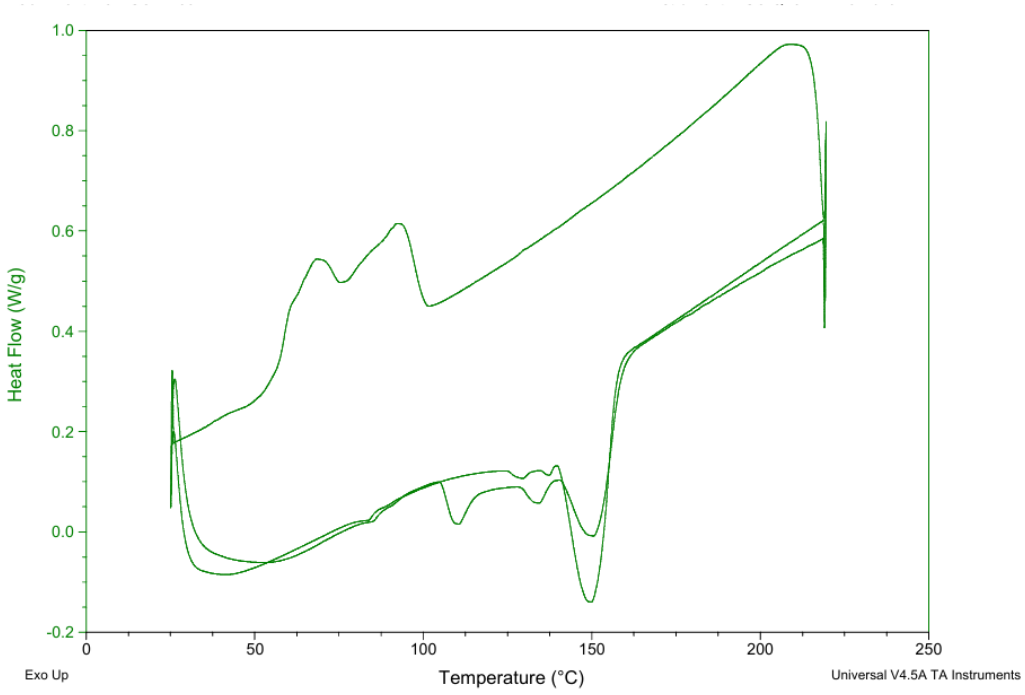

Fig 18. DSC analysis

Since the second heating curve erases the material's "thermal history" and discloses its inherent thermodynamic features, it is the one that is used for analysing [Fig 19]. After the sample has been melted and cooled under controlled conditions, the second heating cycle gives a "reset" molecular state, whereas the first cycle reflects the effects of prior manufacturing methods,

storage conditions, and internal tensions. Furthermore, "noise" from moisture evaporation or leftover solvents is frequently present in the first heat and is eliminated before the second run starts. This leads to clearer, more repeatable peaks and a much cleaner baseline.

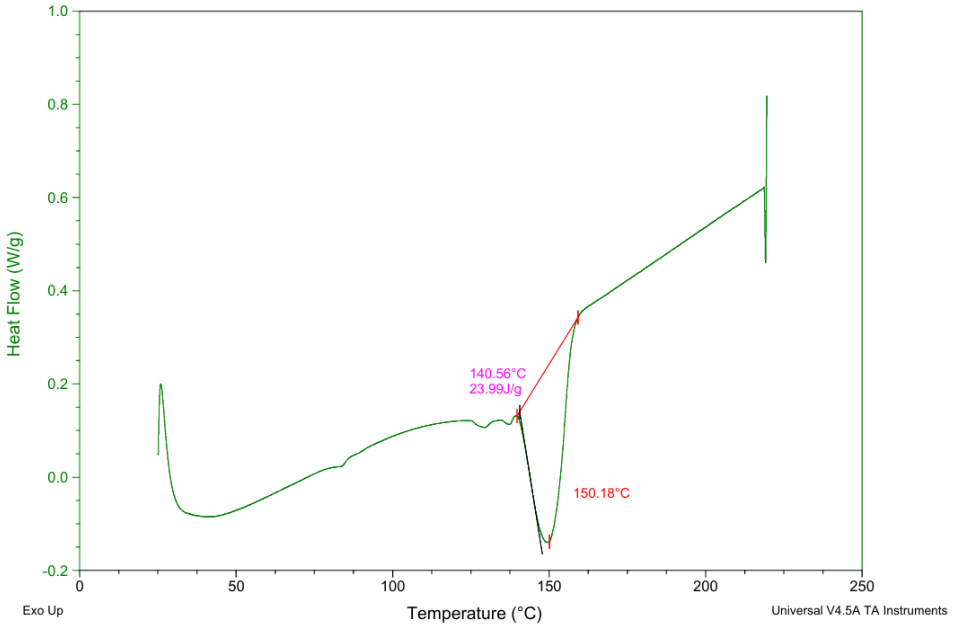

Fig 19. Second Cycle of the DSC test

As it can be seen in [Fig 19], the melting temperature is 150.18℃ and the melting enthalpy is 23.99 J/g.

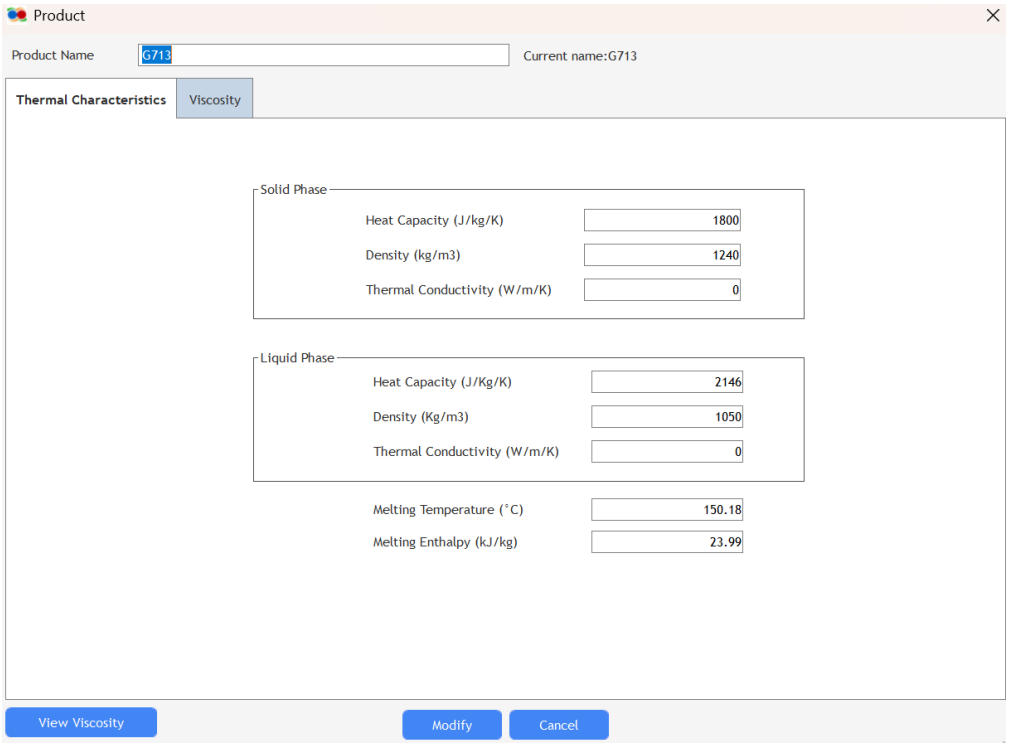

Fig 20. Thermal Properties of G713

Now that all the required data are available, the next step is to define the viscosity of the polymer.

2.2.2.2 **Viscosity of G713**

The right equation for the material must be chosen in order to specify the melt behaviour of G713. The software's available viscosity laws are displayed in [Fig 21], but since this polymer is not available in references using Loi Sop, the user must define the appropriate one for G713.

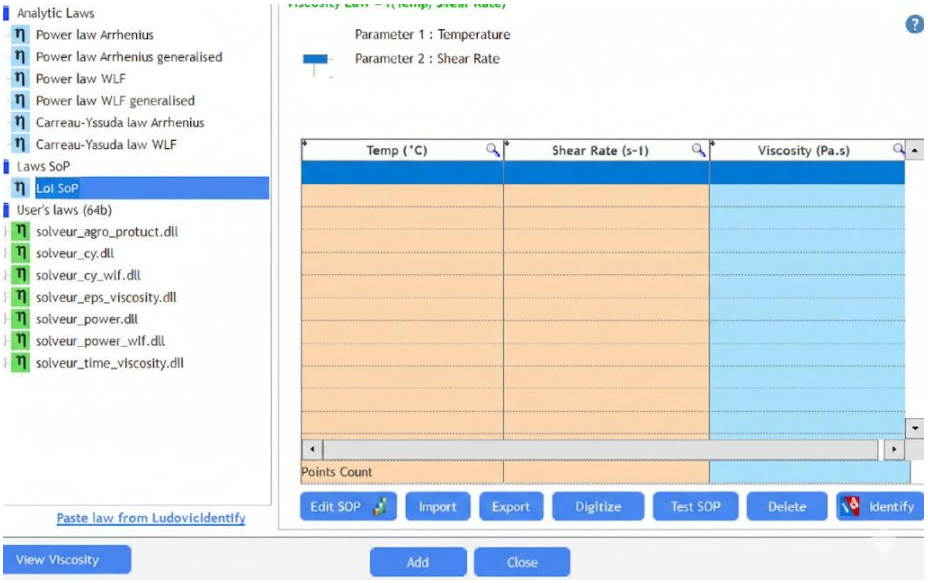

Fig 21. Available Viscosity laws

In order to find the required data on [Fig 21], rheological characterization was carried out at the Alessandria Laboratory. In the following, there is a description of how the rheology test was conducted.

Rheology test

A rotational rheometer was used to describe the rheological characteristics of G713. Prior to testing, samples were vacuumed and dried for six hours at a temperature below the melting point of the polymer (80°C) to prevent hydrolytic degradation. To find the Linear Viscoelastic Region, a Dynamic Strain Sweep test was first performed from 0.01 to 100 rad/s strain at a fixed frequency, 1.0 Hz. The Storage Modulus (G') and Loss Modulus (G") are linear in the Linear Viscoelastic Region. Determining this region is crucial because it establishes the maximum amount of deformation that the material can withstand without breaking structurally. 10% strain is permitted to do the Dynamic Frequency test based on the test's findings. The dynamic frequency sweep test is the main mode of the characterisation test that helps to identify the material’s behaviour over different time scales.

The Storage Modulus (G'), Loss Modulus (G''), and Complex Viscosity (η*) were measured using a Dynamic Frequency Sweep test (from 1 to 100 rad/s) inside the identified Linear Viscoelastic Region. All additional information was removed from the findings because the Ludovic software just requires (η*). In order to identify the non-Newtonian behaviour of the polymer and fit the data to a suitable equation for melt processing analysis, a Flow Curve was ultimately produced by varying the shear rate.

It should be noted that 100g of polymer granules were inserted between the rheometer's discs using a lab spatula to begin the Dynamic Strain Sweep Test and Dynamic Frequency Test. Excessive melted materials were cleaned during both tests to prevent test errors.

Fig 22. Rheology Test

Since the melt behaviour of the material in its processing condition is required, the rheology test was carried out at temperatures higher than the melting point. Additionally, three distinct (η*) at temperatures at least 10°C apart are needed by the Ludovic software. Thus, the test was conducted at 155, 165, and 175 degrees Celsius. The result of the test can be seen in [Fig 23] and [Table 8].

The material's rheological characterisation shows a pseudoplastic response across the temperature range under investigation, as demonstrated by a gradual decrease in complex viscosity as angular frequency increases. This shear-thinning response suggests that dynamic

loading significantly alters the material's interior structure, and it is evident that the total viscosity significantly drops with increasing temperature.

Additionally, when the degree of non-Newtonian character decreases, the material exhibits a shift toward more Newtonian-like flow at higher temperatures. In order to facilitate flow, this transition is usually linked to increased molecular mobility and a decrease in the density of intermolecular entanglements. Accordingly, the rheological profile indicates that although the material retains its structural stability in low-deformation conditions, thermal application greatly enhances its processability, making it extremely susceptible to the combined effects of temperature and shear rate during processing.

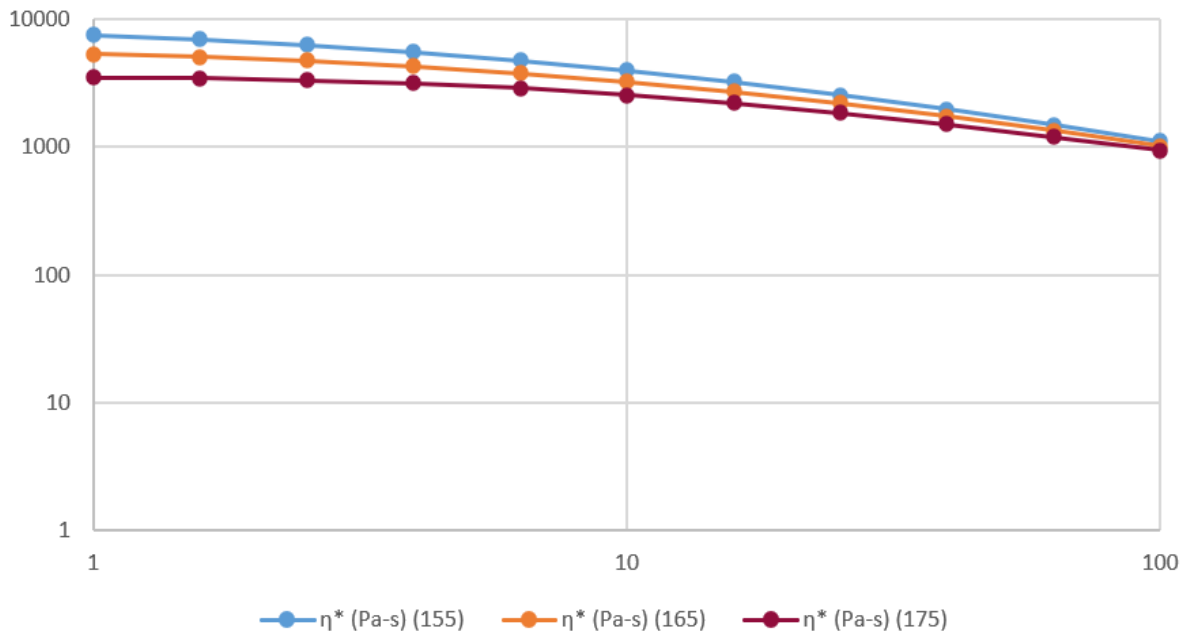

Fig 23. Complex Viscosity Versus Angular Frequency curve

Table 8. Quantitative data of the Complex Viscosity Versus Angular Frequency curve

w (rad/s)	η* (Pa-s) (155)	η* (Pa-s) (165)	η* (Pa-s) (175)
100	1113.43	1015.15	935.191
63.0957	1497.93	1340.71	1195.3
39.8107	1978.52	1738.09	1503.58
25.1189	2556.44	2201.19	1846.88
15.8489	3225.31	2716.4	2208.87
10	3969.37	3260.31	2562.18
6.30957	4752.55	3799.91	2878.74
3.98107	5539.18	4304.74	3143.45
2.51189	6284.56	4745.13	3333.19
1.58489	6954.36	5095.66	3445.89
1	7522.26	5339.65	3481.56

After importing the data from [Table 8] into the software, the process of identifying the experimental model began. Carreau-Yasuda Williams-Landel-Ferry (Carreau-Yasuda WLF) and Carreau-Yasuda Arrhenius (Carreau-Yasuda ARR) were the two methods that may be used to determine the material's melt behaviour. Carreau-Yasuda ARR was the choice that was chosen in order to make the process of determining the appropriate equation simpler.

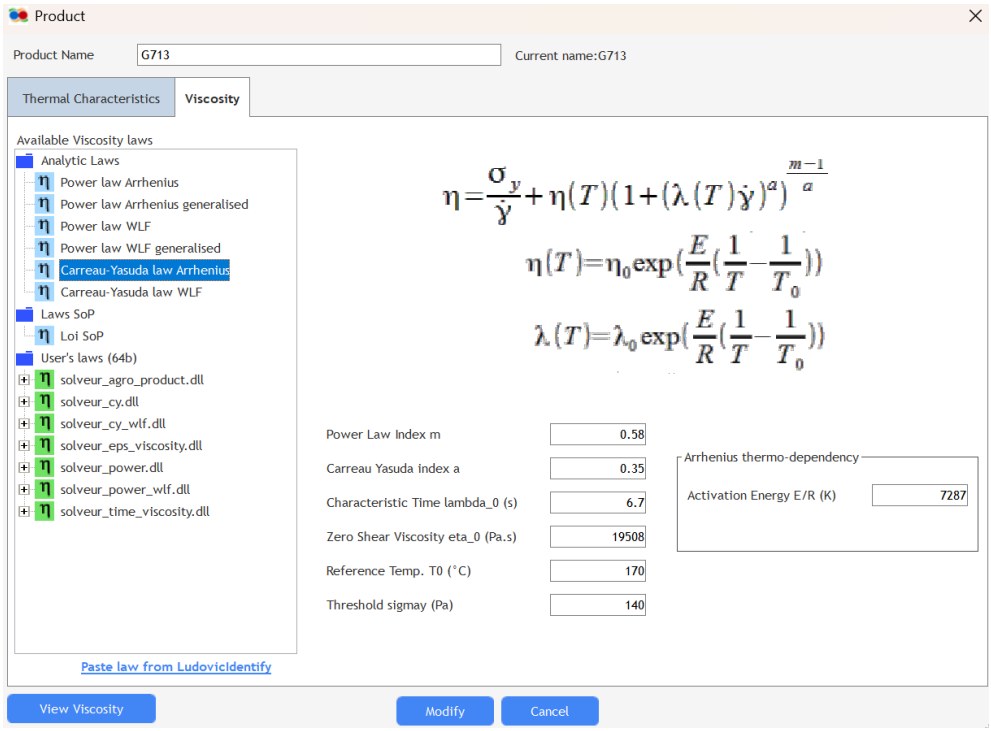

Fig 24. Carreau-Yasuda law Arrhenius for G713

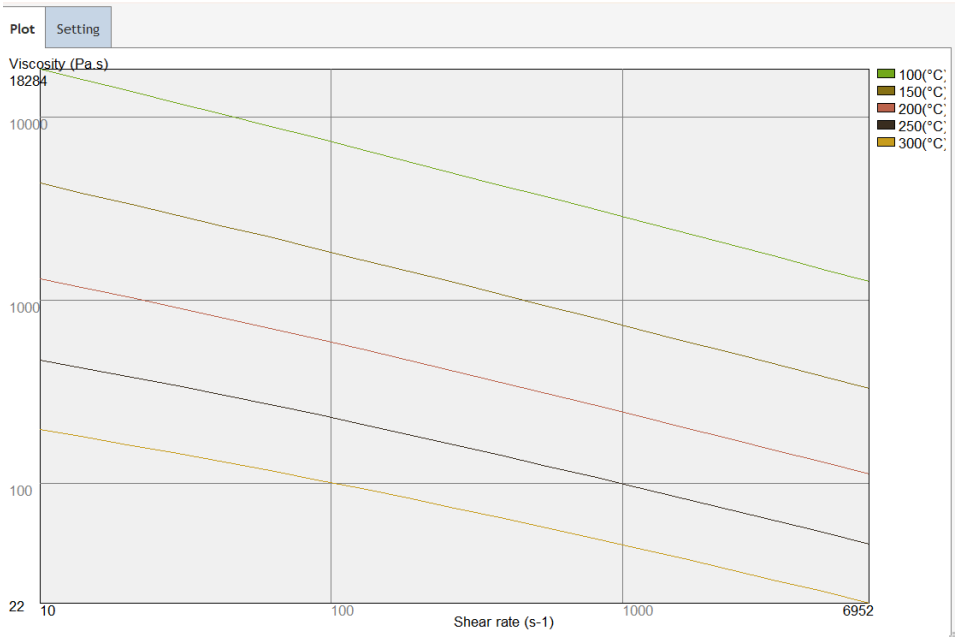

Fig 25. The plotted viscosity curve of G713 using the Ludovic software

After that all the needed information was inserted, the material will be added to the Product Tab.

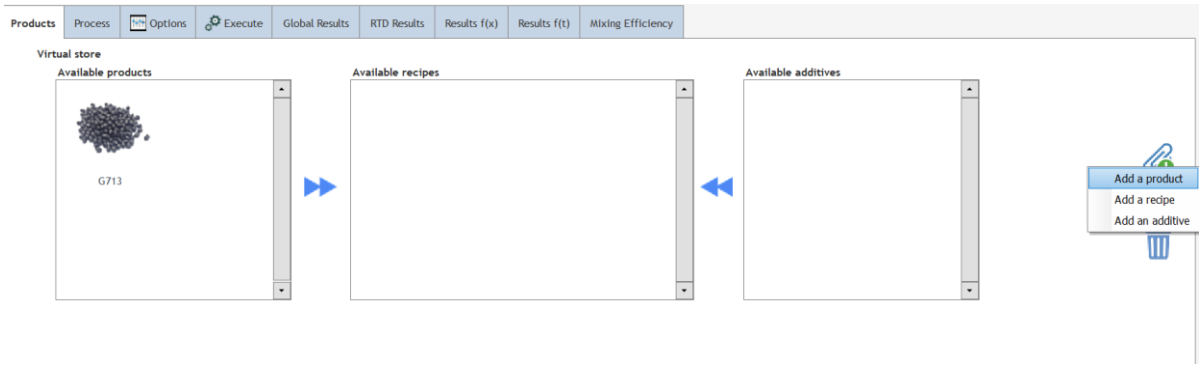

Fig 26. Added material to the software

2.2.3 **Process tab**

An explanation of the working parameters set for the experimental phase is given in this section. The study was organised around five separate trials, each of which was intended to isolate particular variables and track the material's behaviour under different processing parameters, as previously mentioned in [Table 2].

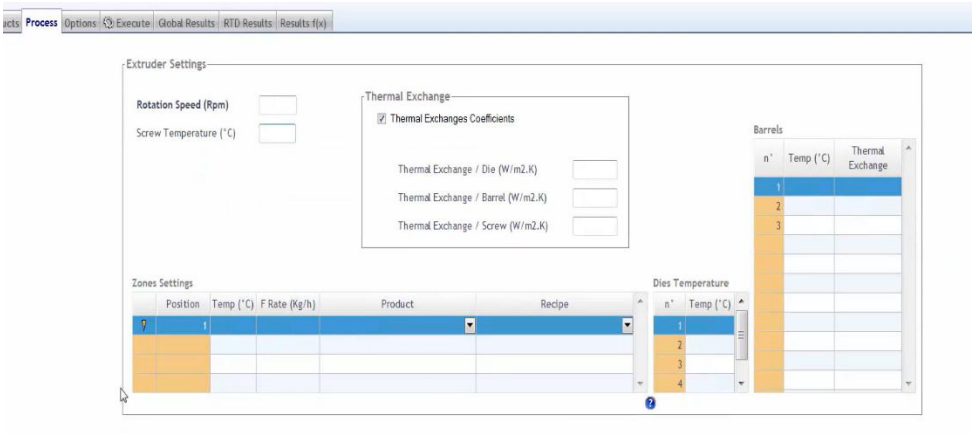

Fig 27. The process tab of the Ludovic software

As seen in the image, the window's "Zone Settings" tab should be used to specify several zones. The types of material and their flow rates in the different extruder sections should also be defined. Since no fillers or additives were used, the feeding zone was the only zone considered. The barrel temperature should also be specified here. The temperature of the barrels was considered constant throughout the processing of the material. Another important point is the die temperature, and as was mentioned before, since the die has not been considered, this section can be left blank. Finally, the die, barrel, and screw thermal exchange coefficients should be specified. The screw has a thermal exchange coefficient of zero, while the die and barrel have a thermal exchange coefficient of 1000. In the event of a medium and good exchange, the developers recommend these figures.

2.2.4 **Design of Experiment (DoE)**

The name of this section makes it clear that DoE should begin with an existing model. Here, it is necessary to specify the parameters that have been altered. There are two categories of parameters, referred to as "Primary" and "Secondary" parameters, as shown in the [Fig 28]. Primary parameters are independent, secondary parameters are dependent and will change when the primary parameters are altered. This is how they differ from one another. Actually, the user can specify how many steps are needed to modify the value of the first ones, whilst the number of steps for the second ones is equal to the value supplied for the amount to which they are tied. The data entered for the DoE is reported in

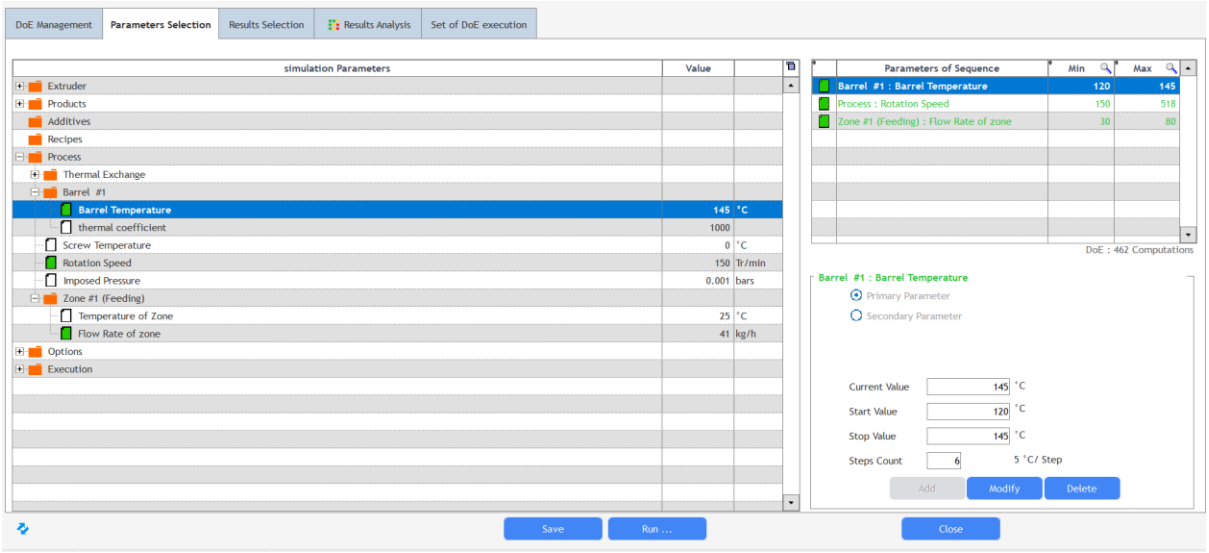

Fig 28. DoE parameters selection tab

Table 9. Setting of DoE based on selected parameters for 5 trials

	Type of parameter	**Start value**	**Stop value**	**Steps count**
Barrel temperature	**primary**	**120**	**145**	**6**
Rotation speed	**primary**	**150**	**518**	**8**
Flow rate of zone 1	**primary**	**30**	**80**	**11**

The DoE is utilised in this work to examine the impact of specific processing parameters on various outcomes, which are displayed in the [Fig 29] and will be discussed in the sections that follow. Additionally, DoE was utilised to establish an operative window for the G713 bio compound and identify the single parameter that has the greatest impact on each of the chosen outcomes.

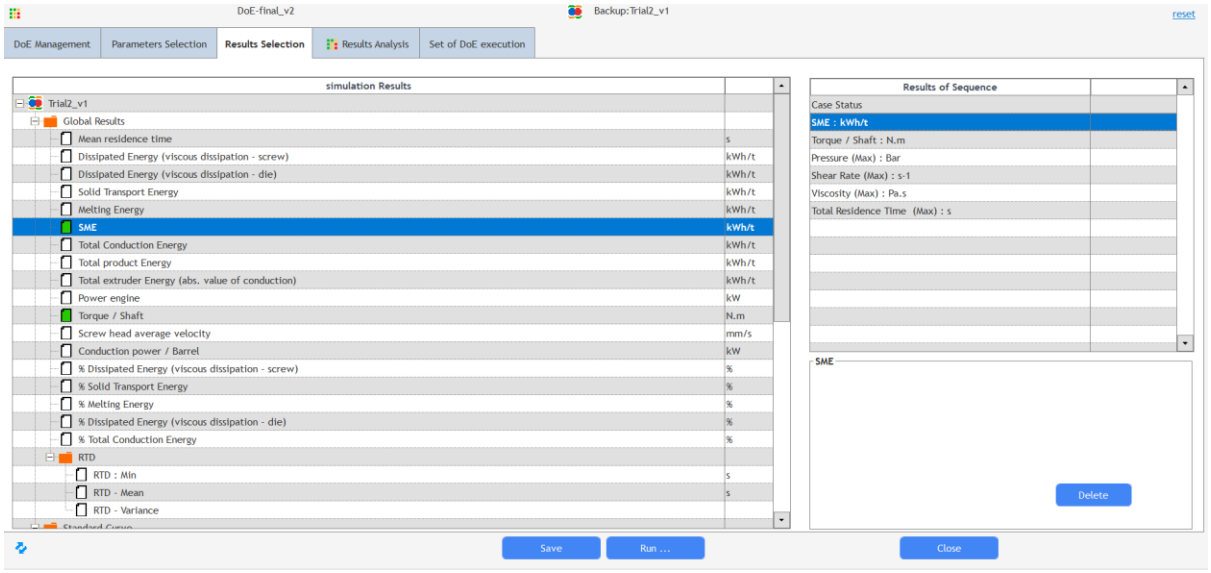

Fig 29. Result Section of DoE

As can be seen, the results of interest are chosen. The quantities that vary along the extruder are selected in the form of their maximum. All these parameters were selected since they are somehow related to the stress that will be applied to the polymer due to changes in processing parameters. In the following, the selected quantities with an explanation of why they were chosen can be seen:

- Specific Mechanical Energy (kWh/t): This is the stress result from mechanical work input. In other words, SME indicates how much polymer is being worked.
- Torque (N.m): Torque is the rotational force needed to turn the screw. So, it can be said that torque is somehow a measurement of the stress that is applied inside the barrel to the polymer.
- Pressure (Bar): The molten polymer will resist the pressure exerted by the screw as it pulls it ahead. The molten polymer will experience stress as a result, and increased pressure is frequently associated with increased stress.
- Shear Rate (s^{-1}): In rheological aspects, for polymer melts which are considered to have Pseudoplastic behaviour, the stress is defined as: $\tau = \eta(\dot{\gamma}, T)\,\dot{\gamma}$. It can be seen that the stress is in relation to the shear rate, and without it, the stress cannot be defined.

- Viscosity (Pa.s): Applied stress and viscosity are correlated in polymer melts. The polymer exhibits increased flow resistance and viscosity as the stress rises. In other words, too high viscosity means high stress, and too low viscosity means lower stress.
- Residence Time (s): Understandably, longer residence time means that the polymer is subjected to stress for a longer period of time.

It is now possible to run the DoE and get the computed data in the "Result Analysis" tab.

2.2.4.1 **The analysis of DoE Results**

The aim of creating DoE was to find the relation between the three variables (barrel temperature, screw speed, and feeding rate) and the selected results, which were mentioned in the previous part. With the use of the Ludovic software, it was possible to have the results of the DoE in both 3-D space (Graphical Analysis) and listed in a table (Results Data). In this section, graphical analysis is used to give a better understanding of the relation between the selected parameters and the selected results. Each result was plotted three times, and each time one of the processing parameters was considered constant, and the relation between the selected result and two other variables was considered.

2.2.4.1.1 *Specific Mechanical Energy (SME kWh/t)*

Specific mechanical energy is the first result which was considered. For starting the analysis, the first parameter, which was considered a constraint, was the **Barrel Temperature**.

The Z-axis is SME, which is the selected result, and the 3-D curve is plotted [**Error! Reference s ource not found.**].

There is a clear inverse relationship between the mass **feeding rate** and Specific Mechanical Energy (SME), as seen in [Fig 30]. This pattern suggests that the SME decreases in proportion to an increase in throughput. The principles of energy distribution throughout the volume of treated material are essentially responsible for this phenomenon. In an extrusion system, the material absorbs the mechanical energy from the motor through shear forces and viscous heating. Although the total volume of material flowing through the screw assembly grows with an increase in flow rate, the mechanical power input from the motor usually does not scale proportionately with the mass throughput. Consequently, the net mechanical work must be distributed over a larger mass of material. In addition, this relation can be explained according to [Equation 1] in which the inverse relation between SME and flow rate can be clearly seen.

Furthermore, considering the **Rotation speed**, the possibility of processing the material at a high feed rate and low rotation speed decreases, which is understandable according to the missing parts of the 3-D curve. But it can be said that at low feeding rates, the effect of rotation speed can be almost neglected since the curve is linear.

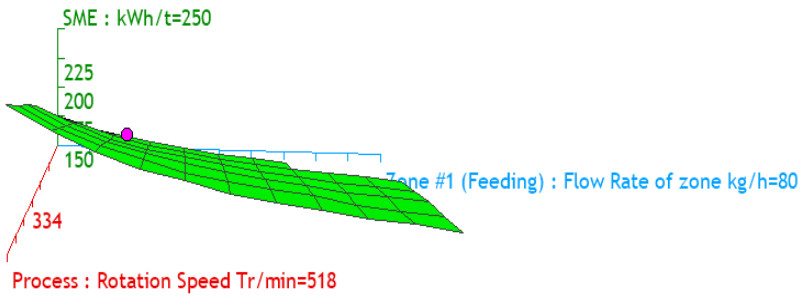

Fig 30. DoE "SME Results" at constant Barrel Temperature

The last point that should be mentioned is that it is also possible to see the trend of the curve as a video in this section. The curve showed a downward trend as the barrel temperature increased, which again emphasises that there is an inverse relation between the SME and barrel temperature. This effect can be explained by the increase in viscosity of the polymer. By increasing the temperature, the viscosity of the polymer starts to drop, and consequently, the stress needed to shape the material decreases [Fig 31].

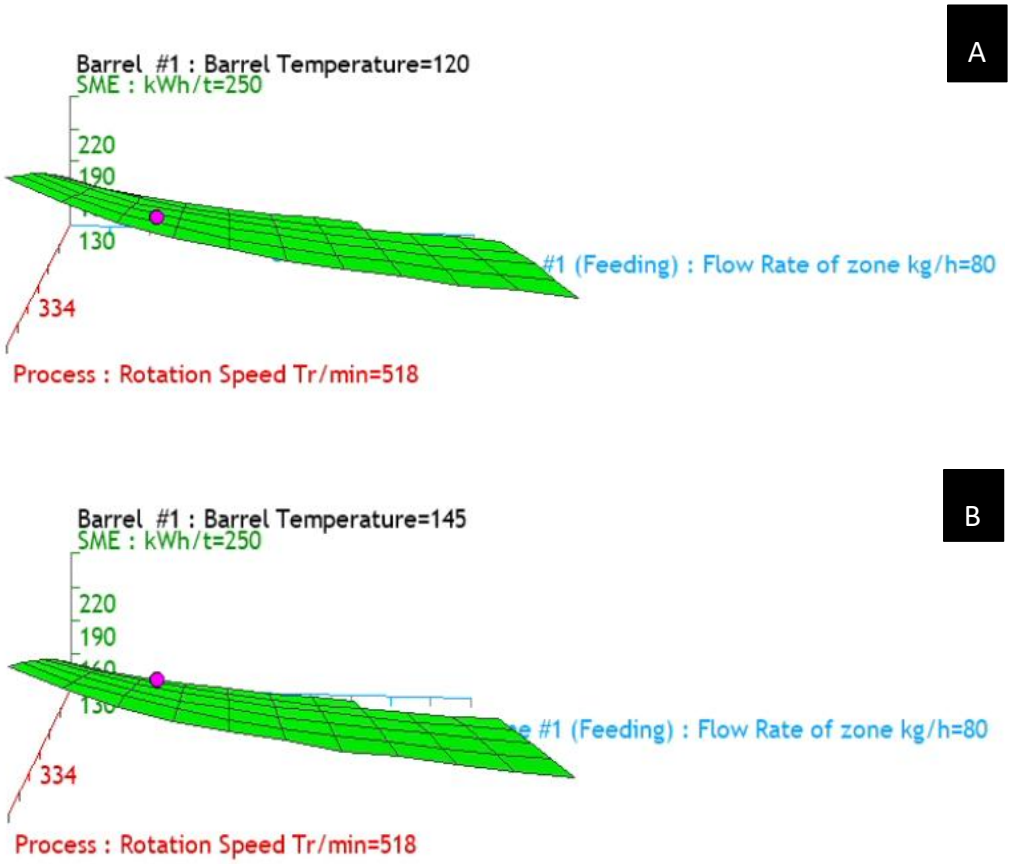

Fig 31.DoE "SME result" at constant Barrel Temperature both in A)120 ℃ and B)145℃

In addition, at low temperature, the processing of material is not possible at low feeding rate and low rotation speed, but by increasing the temperature of the barrel, the possibility of processing the material will also be available at low feeding rate and rotation speed [Fig 32]. Moreover, it can be seen that the highest value of SME can be achieved in the area related to the low feeding rate and low screw speed while the barrel temperature is constant. This is because a significant amount of mechanical power is still needed to overcome viscous resistance and internal friction within the melt when both the feeding rate and screw speed are low, which results in a relatively low mass flow rate. This leads to a large rise in the power to throughput (SME) ratio.

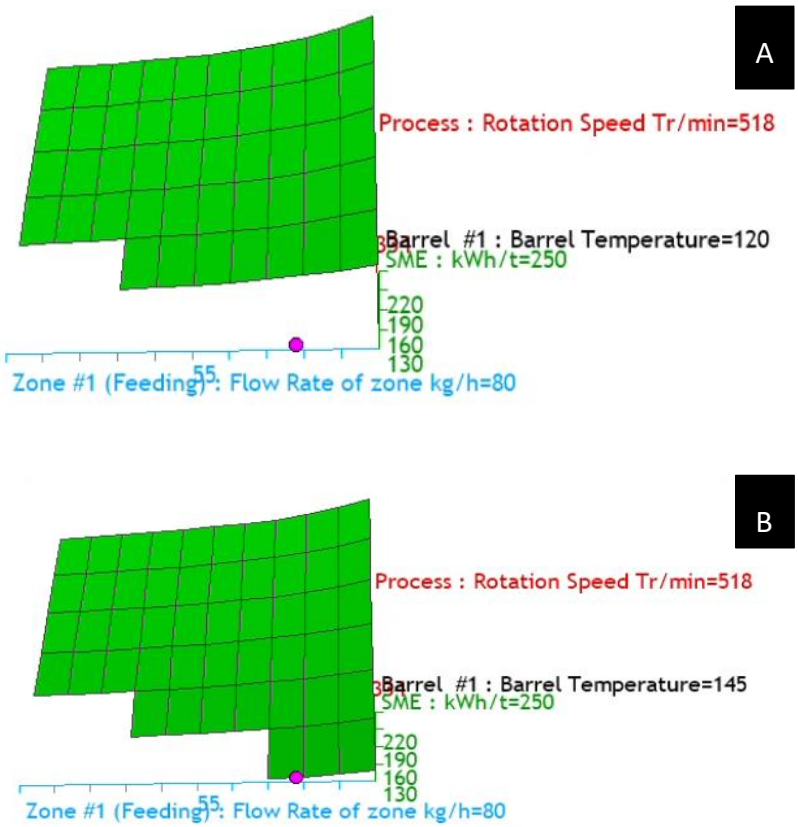

Fig 32. Comparison of the processing possibility of the material at A)120℃ and B)145℃

The 3-D curve for the SME was analysed once more by considering the **Rotation Speed** as a constant parameter [Fig 33]. According to [Fig 33Fig *33*], the plotted curve has a downward slope as the **feeding rate** increases. So, again, the maximum SME can be reached at low feeding rates. The reason for this trend can also be explained by the principles of energy distribution throughout the volume of treated material and the mathematical relation of SME. Additionally, the effect of **Barrel Temperature** can be neglected since there is an almost constant slope of the curve according to barrel temperature.

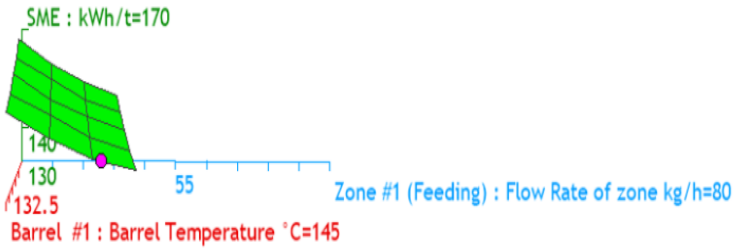

Fig 33. DoE "SME Result" at constant Rotation Speed

By analysing the video associated with the 3D curve, a clear upward trend can be observed as the rotation speed increases. This demonstrates a direct relationship between rotation speed and SME [Fig 34]. The reason for this behaviour is that increasing the rotation speed enhances the amount of mechanical work applied to the material, which in turn elevates the SME. This direct relationship between the two parameters becomes even more apparent when [Equation 1] is examined once again.

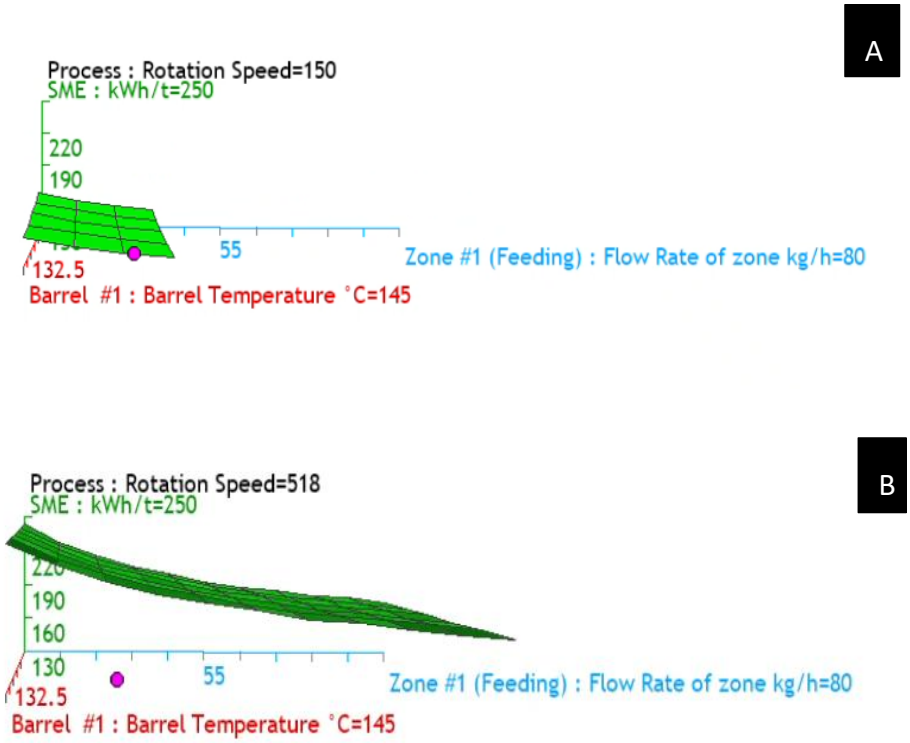

Fig 34. DoE "SME result" at constant Rotation speed, both in A)150 RPM and B)518 RPM

In addition, in [Fig 35] is obvious that at higher rotation speed, the possibility of processing the material is increased. This effect can be explained according to the throughput of the process. Higher volumes of materials require a higher screw speed to be processed and to be able to move forward. So, considering the screw speed as a constraint, it is possible to process the material only at low feed rates. It is also clear that the highest value for SME at constant rotation speed is achievable when the feeding rate is low and the barrel temperature is relatively high. This results from both efficient energy transmission to the melt and decreased throughput. By reducing polymer viscosity, a higher barrel temperature improves melt homogeneity and eliminates partially solid areas that would otherwise restrict the passage of mechanical energy. In these circumstances, a totally molten material successfully converts the majority of the mechanical work imposed by the screw into viscous dissipation. Concurrently, a low feeding rate lowers the mass flow rate, distributing the mechanical power over a smaller volume of material, while it may not be at its maximum, and SME rises significantly as a result.

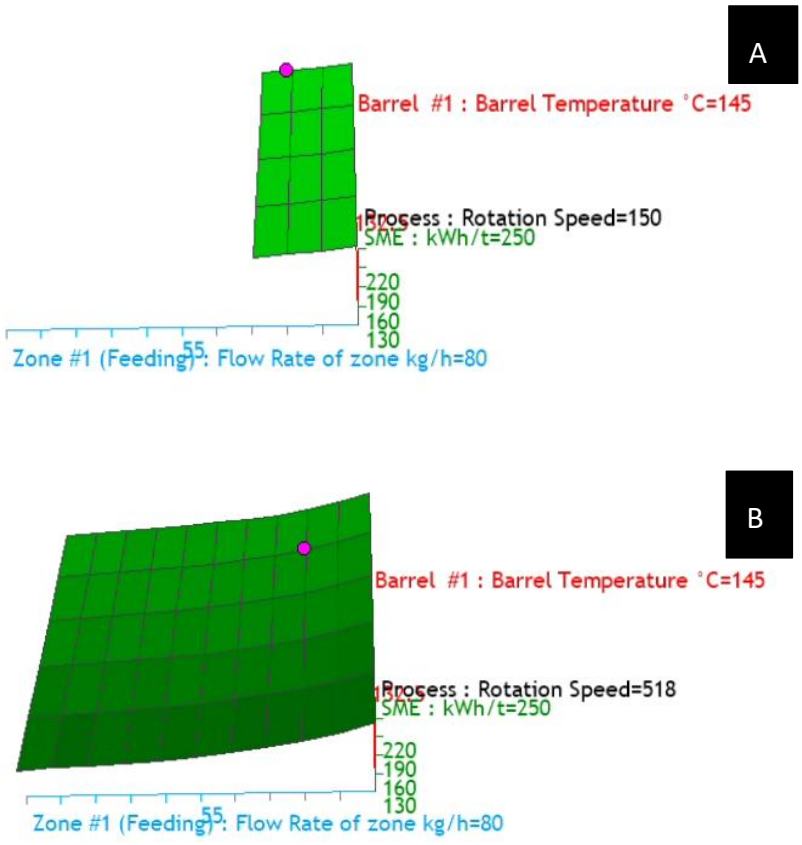

Fig 35. Comparison of the processing possibility of the material at A)150 RPM and B)518 RPM

The last parameter, which was considered as a constant, was the **Feeding Rate** [Fig 36]. It is obvious that the highest SME can be reached at high **Rotation Speed**. So, the direct relation between the screw speed and the SME can be seen here again. As expected, and by analysing the previous curves, again the effect of **Barrel Temperature** can be neglected since the slope of the curve is almost linear and no significant effect on SME can be seen by changing the barrel temperature.

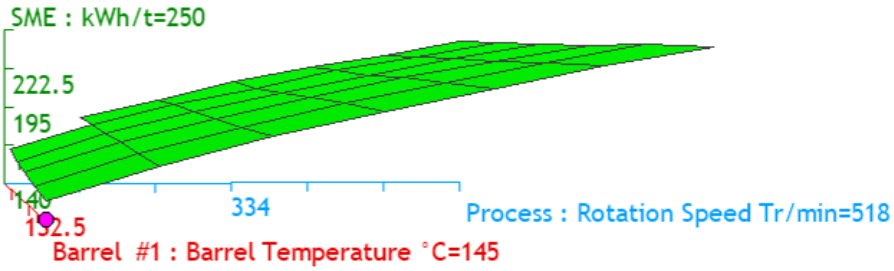

Fig 36. DoE "SME Result" at constant Feeding Rate

Based on the available video of the curve at this section, a higher feeding rate causes a downward shift of the curve. This behaviour was predictable in accordance with all the previous curves and their trends. An important thing that should be mentioned is that by increasing the feeding rate, a severe reduction was seen for SME [Fig 37].

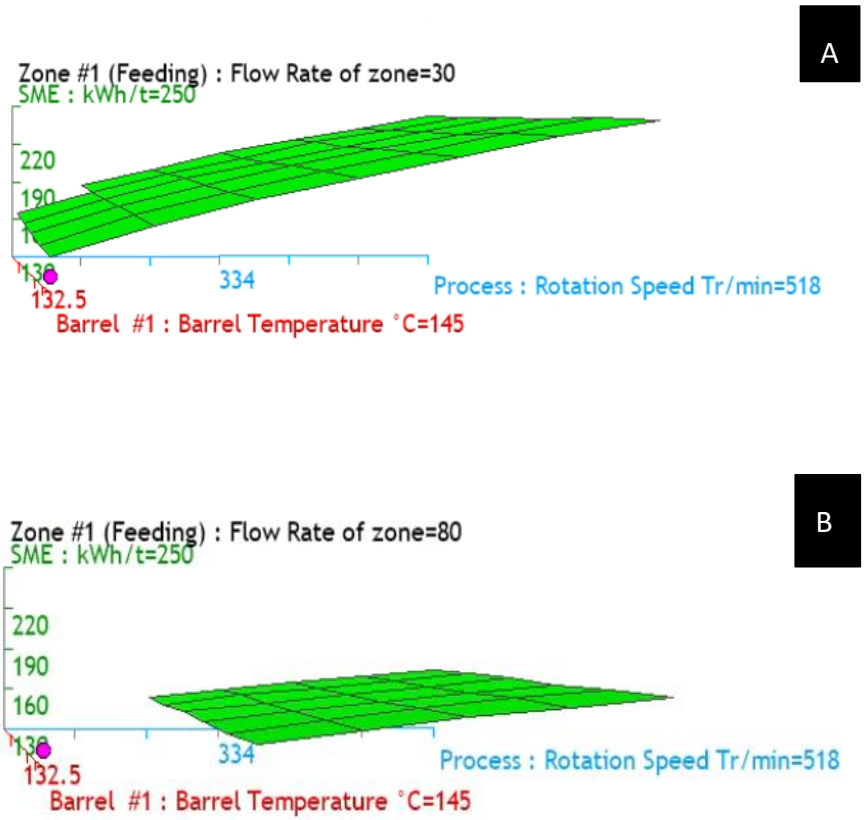

Fig 37. DoE "SME result" at constant temperature, both in A)30 kg/h and B)80 kg/h

The reduction of processing possibilities is obvious in [Fig 38]. This emphasises that even at high rotation speed, there is a limit for the highest processable amount of material. As can be seen here, the maximum value of SME was reached when the barrel temperature is high, and the rotation speed is low. This is because of the balance between mechanical power input and the viscous behaviour of the melt. Raising the barrel temperature lowers the viscosity of the polymer, resulting in a fully molten, continuous phase where shear stresses are effectively transferred throughout the material instead of dissipating at solid-melt transitions. In this situation, the screw's deformation is more evenly transformed into viscous dissipation inside the melt, even at low screw speeds. Lowering the screw speed also increases the amount of internal resistance and shear stress per unit of throughput by decreasing the drag flow component in comparison to pressure-driven flow. Because the feeding rate is constant, the

mass flow rate stays constant, and the mechanical energy is more efficiently dispersed inside the material, even if it is supplied at a slower speed.

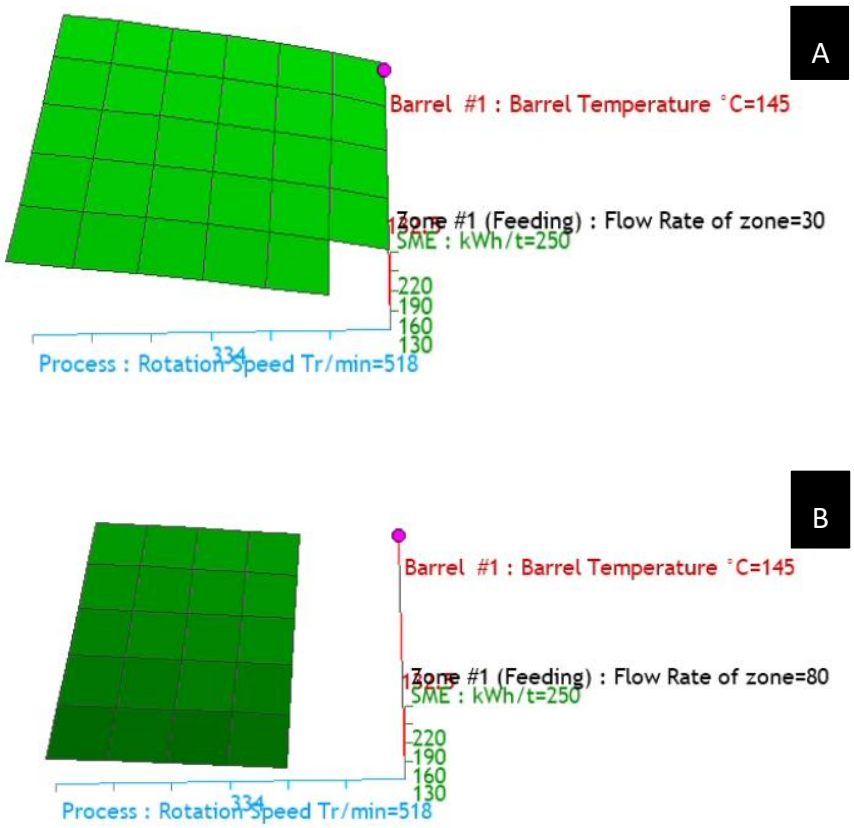

Fig 38. Comparison of the processing possibility of the material at A)30 kg/h and B)80 kg/h

In conclusion, the graphical trends of Specific Mechanical Energy (SME) provide a clear and consistent picture of how each process parameter contributed to its overall value. While all investigated parameters exerted a measurable influence on SME, the analysis reveals that feeding rate emerged as the most dominant significant factor. As illustrated in the 3-D curves, SME exhibited a strong inverse relationship with feeding rate; as feeding rate decreased, SME values increased substantially. Therefore, if the primary objective is to maximise SME, the feeding rate should be maintained as low as practically feasible within the operational constraints of the system.

2.2.4.1.2 *Torque (N.m):*

First, it should be noted that the torque's precise number was assessed using the software, in contrast to the experimental section, where the torque's percentage was displayed. Since the goal of this analysis is to identify the parameter that has the greatest influence on torque to vary it, it is not a problem that the percentage cannot be calculated in this section due to the absence of data regarding how the extruder converts the precise value of torque to percentage.

Starting with considering the **Barrel Temperature** as a constraint [Fig 39], it is obvious that there is an inverse relation between the torque and the rotation speed. This can be explained by the fact that increasing screw speed increases the shear rate inside the barrel, which reduces apparent viscosity due to the shear-thinning behaviour of most polymer melts. The reduced viscosity lowers the torque demand by reducing pressure build-up along the screw channel and the material's resistance to screw rotation. In addition, there is a slight downslope regarding the feeding rate, which can be explained again according to the redistribution of mechanical energy over a larger material throughput. So, it can be said that increasing both rotation speed and feeding rate will lower the torque.

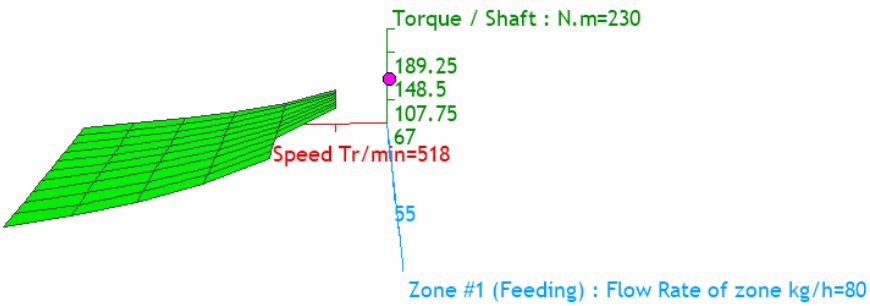

Fig 39. DoE "Torque Results" at constant Barrel Temperature

By analysing the obtained video of the trend for the 3-D curve, it can be seen that [Fig 40], at elevated temperature, there is a downward trend of the curve, which emphasises that increasing the barrel temperature decreases the torque. This inverse relationship between temperature and torque can be attributed to the fundamental thermophysical behaviour of polymer melts. As the Barrel temperature escalates, the viscosity of the melt decreases, and consequently, there is a reduction in the torque demand of the extruder.

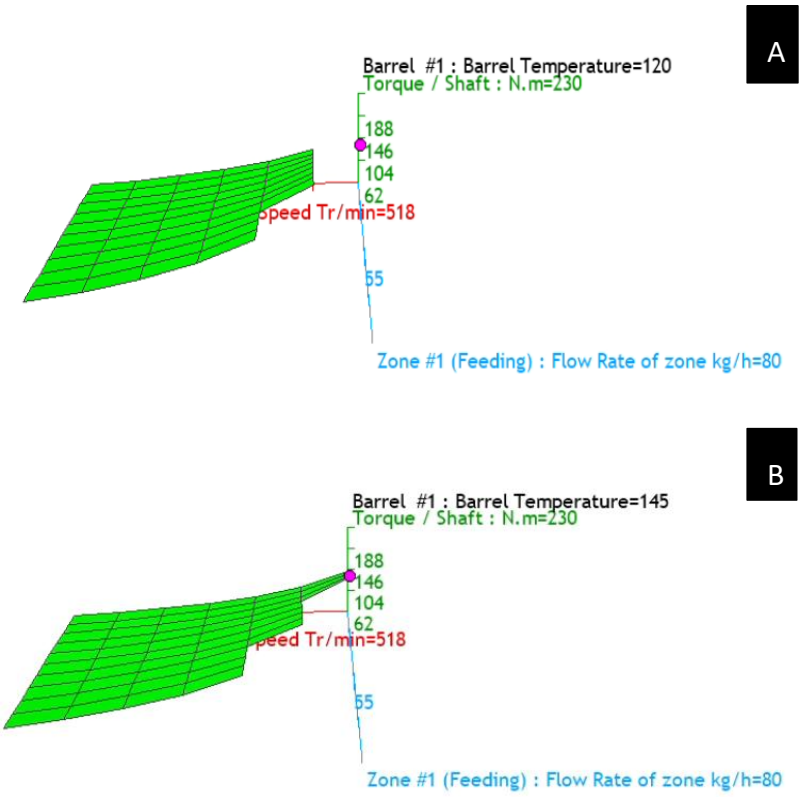

Fig 40. DoE "Torque result" at constant Barrel Temperature, both in A)120 °C and B)145°C

The last important thing is the processing possibility that should be analysed [Fig 41]. It is clear that the processing of the material at both high and low temperatures, while the feeding rate is moderate to high, is not possible unless the rotation speed is high. Under conditions where the screw rotational speed remains low, the resultant shear rate and the associated viscous dissipation are insufficient to fully melt the incoming material. This thermal and mechanical deficiency leads to incomplete melting, non-uniform material flow, and ultimately unstable conveying behaviour; consequently, processing becomes practically impossible unless an increase in screw rotational speed is applied to restore the needed level of specific mechanical energy. At elevated temperature, there is the possibility of processing the material even at low feeding rate and rotation speed. The extent of the processing window is due to the reduction of viscosity of the melted polymer, which facilitates the processing.

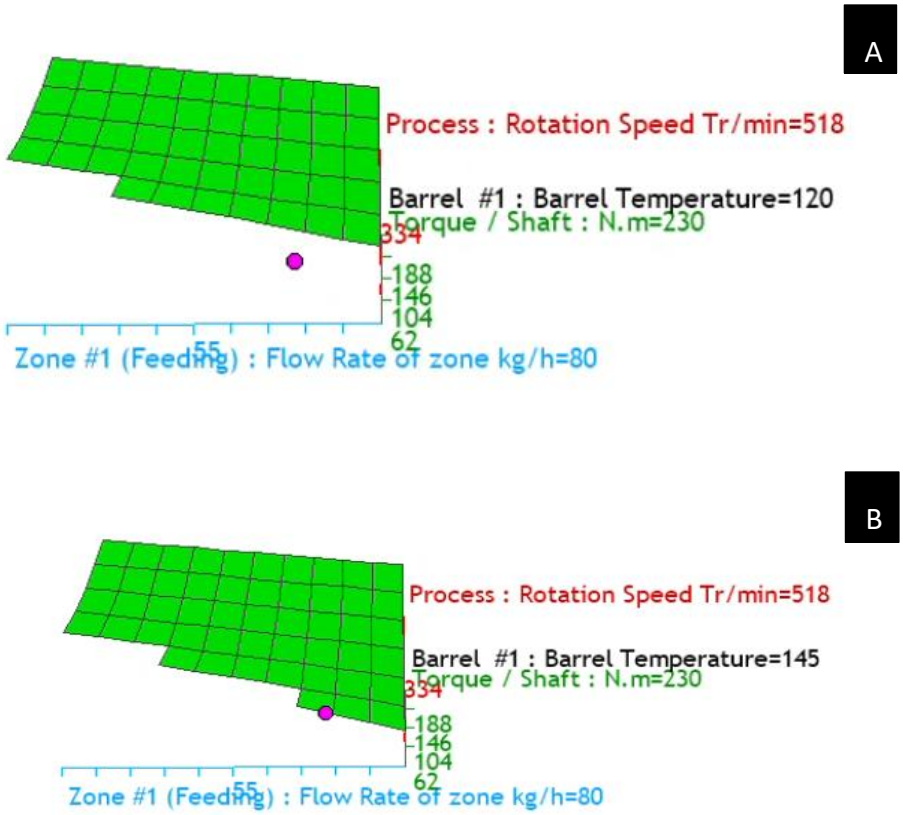

Fig 41. Comparison of the processing possibility of the material at A)120℃ and B)145℃

The next parameter, which was considered a constraint, was the **Rotation Speed**. As can be seen in [Fig 42], the effect of Barrel Temperature is almost nil since the slope of the curve at the relative axis is constant. On the other hand, there is a dramatic upward slope for Feeding Rate. It can be clearly seen that by increasing the feeding rate, the torque will increase too. This is due to the fact that at constant rotation speed, a high volume of material requires a higher torque to overcome the flow resistance of the material.

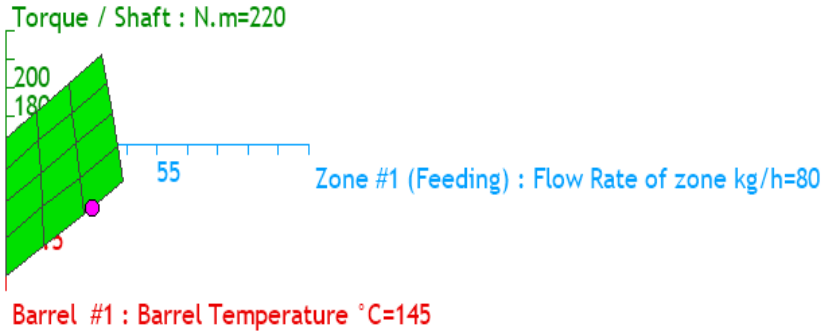

Fig 42. DoE "Torque Results" at constant Rotation Speed

By following the trend of the curve with the associated video, there is a sudden decrease in torque, which clarifies the inverse relation between torque and rotation speed. This can be explained by considering that high rotation speed causes more shear on the material, which decreases the viscosity of the material, and consequently, the amount of needed torque to compensate for the flow resistance of the material decreases.

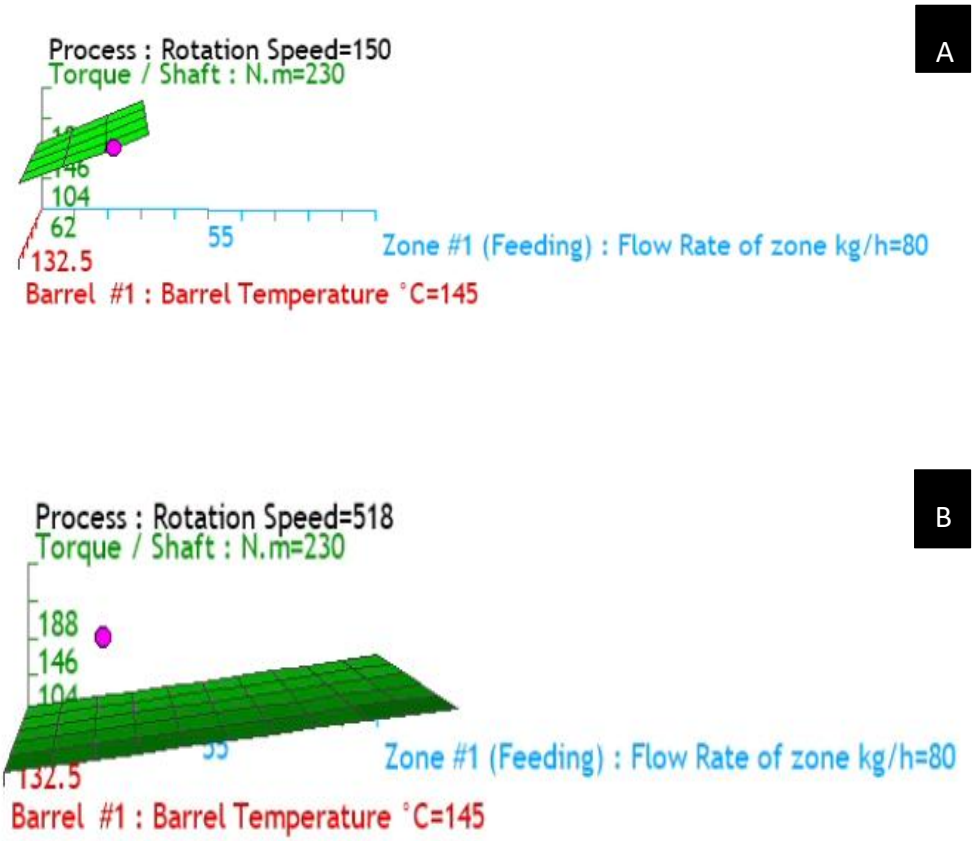

Fig 43. DoE "Torque result" at constant Rotation Speed, both in A)150 RPM and B)518 RPM

The last aspect is the possibility of processing the material, which is shown in [Fig 44]. As it is illustrated, the processing of the material at low rotation speed is only possible at a low feeding rate. It was mentioned before that a high volume of material shows higher resistance to flow, so at low screw speed, it is not possible to process a large volume of material since the flow resistance is high. In general, although a high level of rotation speed causes a reduction in torque, the processing of a considerable amount of material is possible only at a greater rotation speed. It is also clear that when the rotation speed is considered as a constant parameter, the maximum achievable torque is when the barrel temperature is high, and the feeding rate is relatively low. This is because stresses can be efficiently transferred along the screw without being influenced by unmelted or weakly plasticised areas, thanks to a high barrel temperature, which guarantees that the polymer is completely molten and homogeneous. The screw functions in a partially filled area at low feeding rates, where pressure-driven backflow rather than pure drag flow progressively controls the flow. Because of the increased resistance to forward conveying, more torque is needed to sustain the required rotation.

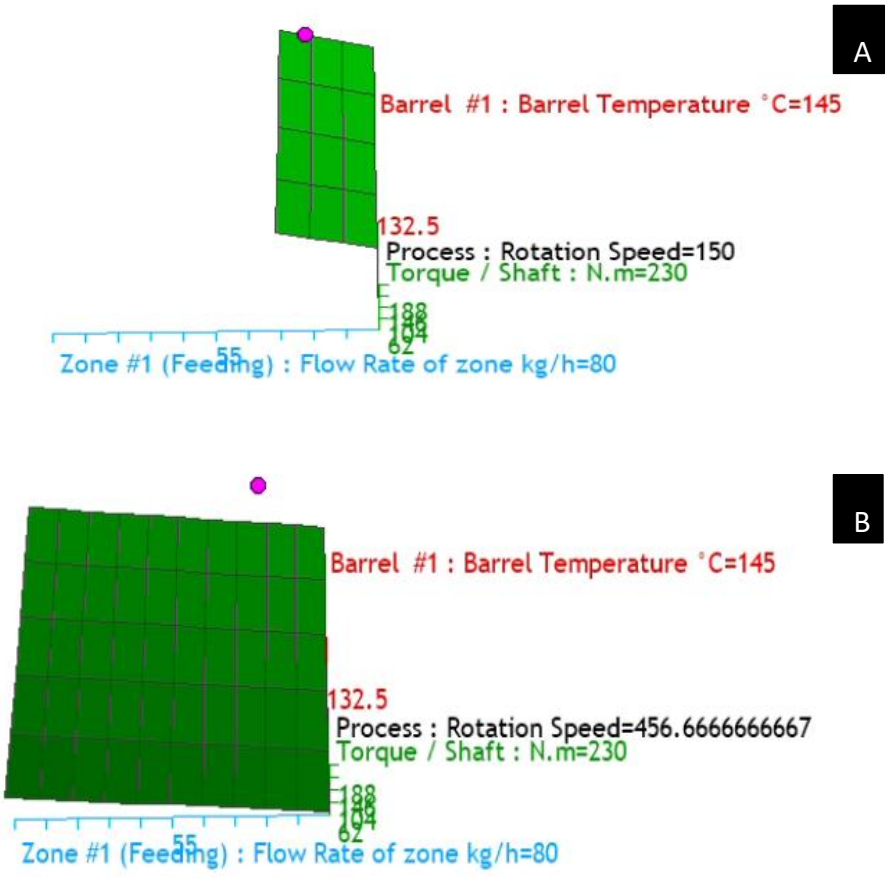

Fig 44. Comparison of the processing possibility of the material at A)150 RPM and B)518 RPM

The last constraint for analysing the effect of processing parameters on the torque is the **Feeding Rate**. The resultant curve [Fig *45*] demonstrate the inverse relation between torque and rotation speed. As it was expected, the effect of Barrel temperature is nil due to the linearity of the related curve.

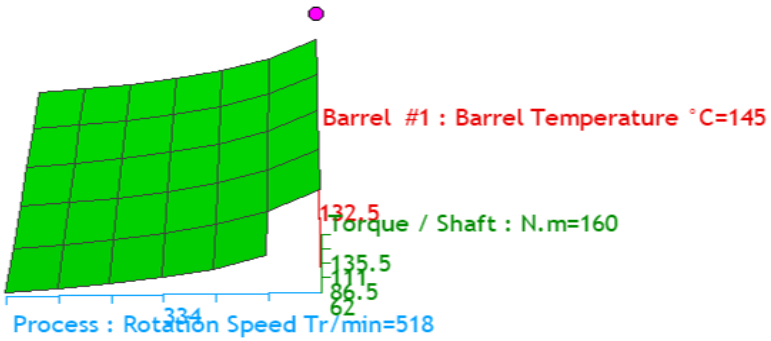

Fig 45. DoE "Torque Results" at constant Feeding rate

According to the overall trend for the 3-D curve, the curve will be shifted upward by increasing the feeding rate. The reason for this effect was mentioned before, which was the higher resistance to flow of a large volume of the material and consequently a higher needed torque for melting and processing the material. This trend can be seen in [Fig 46].

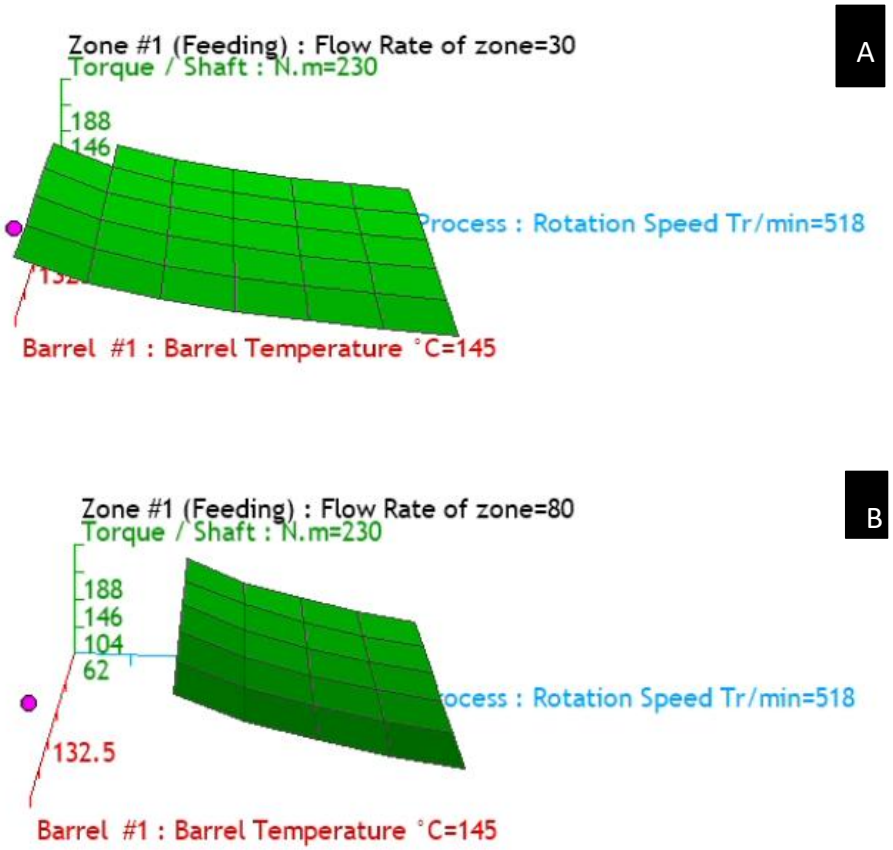

Fig 46. DoE "Torque result" at constant Feeding Rate, both in A)30 kg/h and B)80 kg/h

The possibility of processing the material regarding the feed rate decreases with increasing throughput. This can be seen in [Fig 47]. Please keep in mind that the reduction in processing window at high feeding rate is due to the need for high screw speed, as it was mentioned before. A considerable point about this curve is that the processing of material is not possible until the screw speed and barrel temperature reach a minimum level, even at low feeding rates, which can be explained by the high viscosity of the material at low screw speed and low temperature. While both of them are low, the viscosity is extremely high even at a low feeding rate, so that the inherent resistance to flow of the material overcomes the torque, and the extrusion of the material will not be possible. It can also be seen that the highest value for torque is when the barrel temperature is high, and the rotation speed is low. It is a known fact that the drag flow produced by the screw drops as the screw speed is lowered while keeping the feeding rate

constant. A greater pressure gradient must form along the barrel to force the material forward to meet this requirement. The resistance to screw rotation is greatly increased by this pressure build-up, which immediately results in increased torque. Consequently, the necessity to resist a larger pressure-driven flow at low screw speed results in the highest torque under these circumstances, despite the lower viscosity at high temperatures.

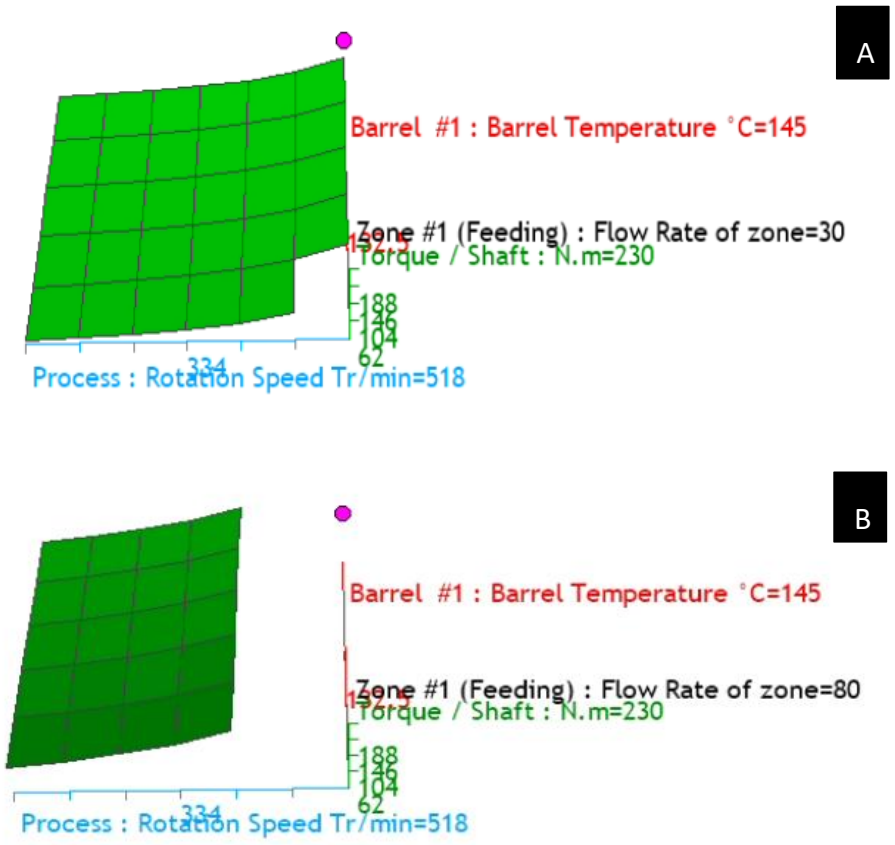

Fig 47. Comparison of the processing possibility of the material at A)30 kg/h B)80 kg/h

All things considered, Rotation Speed is the main parameter which has influence on torque. The reason is that screw speed controls the applied shear on the material, and due to the shear-thinning behaviour of the melted polymer, a small change in the screw speed has a significant effect on the viscosity of the material. The reduction of viscosity lowers the flow resistance of the material, and as a result, the torque will be changed. As it was stated, rotation speed and torque have an inverse relation, which means that for higher torque, the rotation speed has to be as low as possible.

2.2.4.1.3 *Pressure (Bar)*

Pressure is the other selected interesting result. Starting with the **Barrel Temperature** as a constraint [Fig 48], it can be seen that there is a direct relation between pressure and the **Feeding rate.** The viscous nature of the polymer melts and the constant resistance imposed by the die geometry are the main factors that control the correlation between feeding rate and pressure. High volume of material must be conveyed and forced through a constant cross-sectional area (die) as mass throughput rises, necessitating a higher-pressure gradient to overcome viscous flow resistance. Therefore, an increase in feeding rate requires an increase in pressure. On the other hand, the inverse relation between the pressure and **the Rotation Speed** can be concluded according to the downward slope of the related axis. Considering the fact that the increase in rotation speed increases the shear applied to the polymer melt and decreases the viscosity, this inverse relation can be explained.

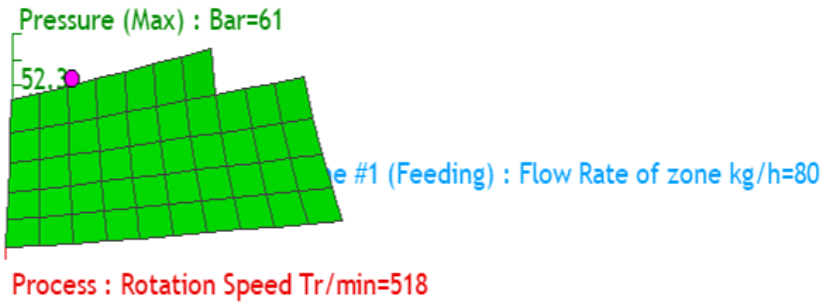

Fig 48. DoE "Pressure result" at constant Barrel Temperature

Following the overall trend of the 3-D curve [Fig 49], the slight downward shift by increasing the temperature can be seen. This can be explained by the reduction of viscosity at higher temperatures, which causes the need for lower pressure for processing.

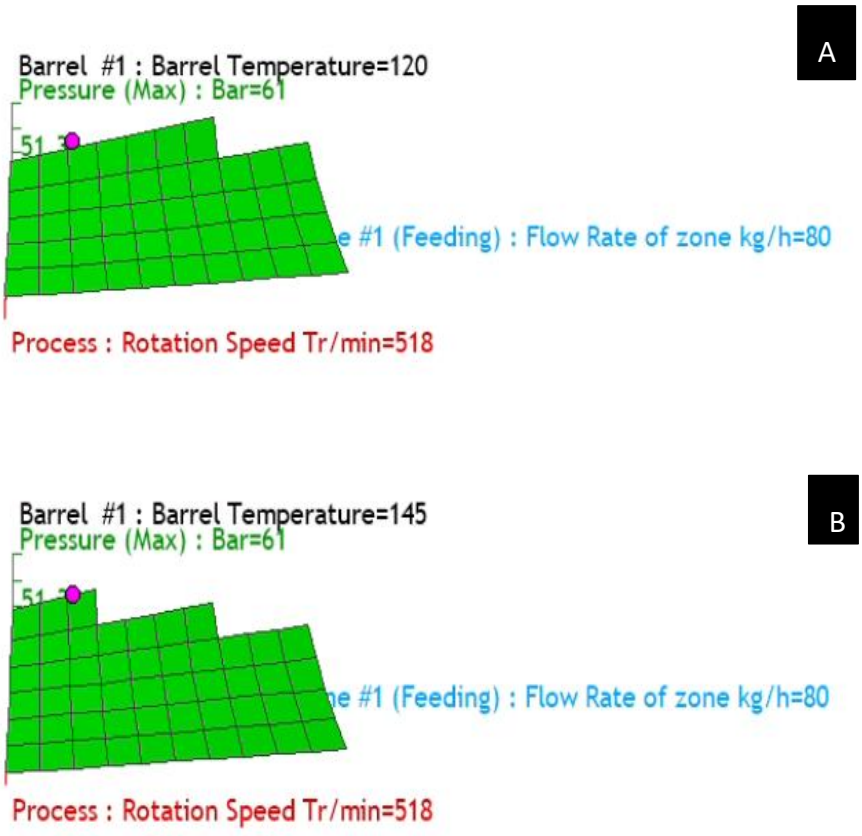

Fig 49. DoE "Pressure result" at constant Barrel temperature at both A)120℃ and B)145℃

The last aspect that should be pointed out, according to constant Barrel Temperature, is the processing possibility of the material. According to [Fig 50], by increasing the Barrel temperature, the processing window of the material will extend to lower flow rate and rotation speed, which again is understandable due to the reduction of the viscosity of the polymer melt. [Fig 50] also shows that while the barrel temperature remains constant, low rotation speed and feeding rate produce the highest possible pressure. This is because the material is not efficiently pushed forward when the screw speed is low, because the drag-induced transport capability of the screw decreases drastically. Simultaneously, a low feeding rate results in a poorly filled screw channel, where backflow and pressure-driven mechanisms progressively regulate flow instead of smooth drag transport. In these circumstances, even a small amount of material must be transported past the die or downstream limits by creating a reasonably strong pressure gradient. The system cannot lower resistance through thermal softening since viscosity is fixed

due to constant barrel temperature; raising pressure is the only method to preserve flow continuity.

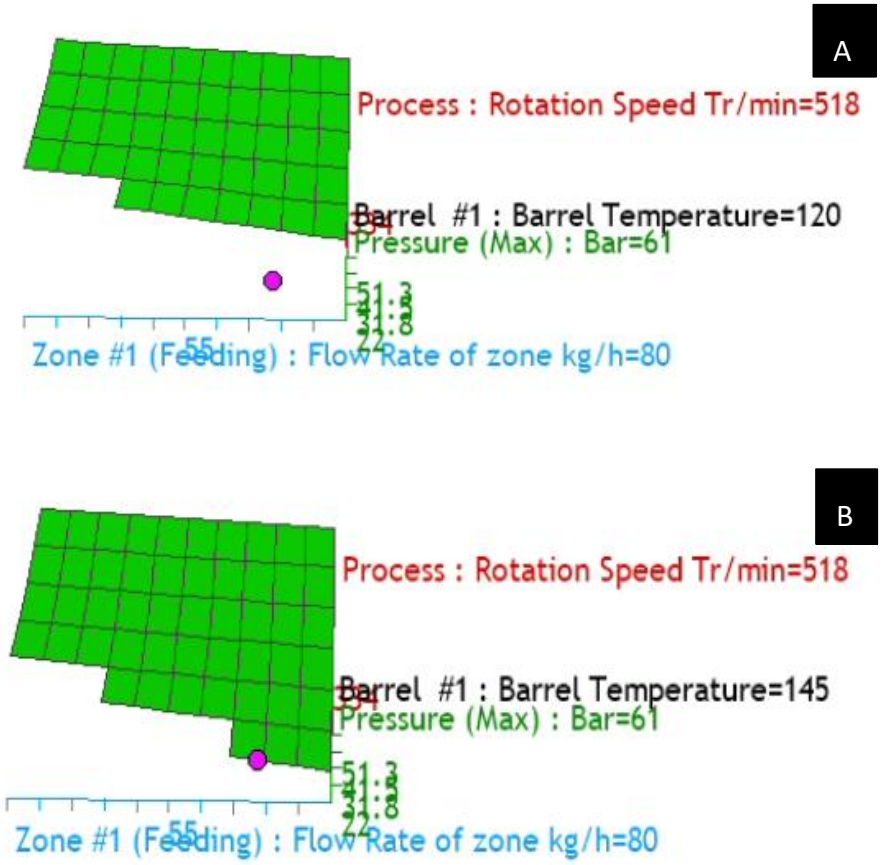

Fig 50. Comparison of the processing possibility of the material at A)120℃ and B)145℃

The next parameter, which was considered constant, is the **Rotation speed** [Fig 51]**.** As can be seen, the slope of the curve related to the **Flow Rate** has an upward slope. Thus, an increase in the feeding rate increases pressure. This relation between them can be explained due to the higher volume of the material inside the extruder, which cause to need for more pressure to overcome the flow resistance of the material. While the Rotation is constant, the effect of barrel temperature can be neglected as it is obvious from the linear slope of the related plot. This can be explained by the fact that the mechanical conveying action of the screw and the imposed throughput, rather than just temperature, are the main factors controlling pressure generation in a screw extruder. The volumetric displacement of the screw stays almost constant when the screw speed is constant, which means that the material flow rate through the barrel is essentially fixed. The polymer melt does indeed become less viscous when the barrel temperature is raised, which frequently reduces the pressure required to move the material forward, but this effect is frequently offset by the fact that the die still imposes the same flow resistance, and the screw

continues to deliver roughly the same material throughput. There is little to no noticeable change in the measured pressure as a result of the system reaching a new equilibrium where the decreased viscosity balances with the screw's constant mechanical pumping capacity. Consequently, barrel temperature may only slightly affect the pressure profile within the extruder under conditions of constant rotation speed.

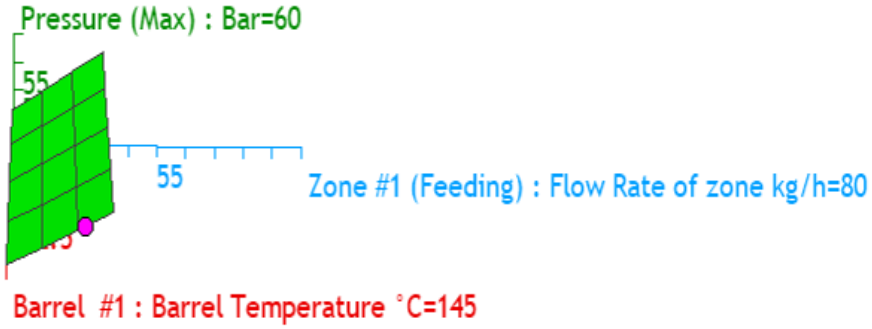

Fig 51. DoE "Pressure result" at constant Rotation Speed

A comparison of the 3D curve at both 150RPM and 518RPM is illustrated in [Fig 52]. The downward shift of the curve from 150RPM to 518RPM is obvious, which means that the increase in rotation speed will decrease the pressure. This is because at higher screw speeds, the conveying capacity of the screw increases and the shear introduced by the system to the material will increase accordingly. Higher shear rate on the material, even at high flow rates, causes a reduction in viscosity and consequently, the needed pressure will be reduced.

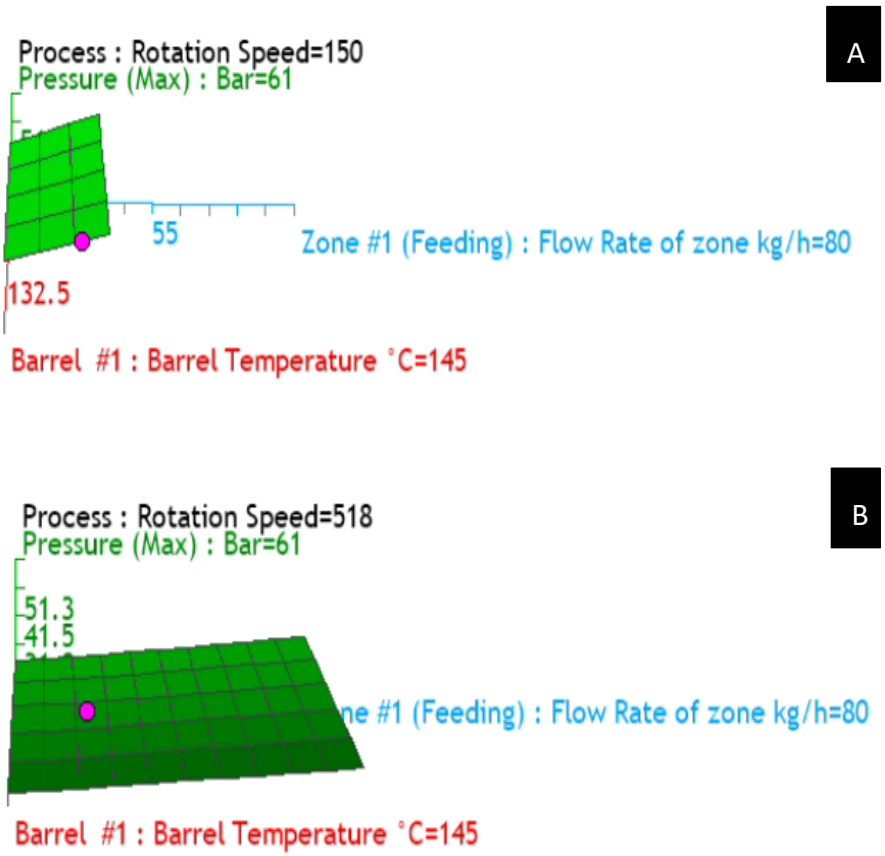

Fig 52. DoE "Pressure result" at constant Rotation Speed, both in A)150 RPM and B)518 RPM

The processing possibility of the material is shown in [Fig 53]. The expansion of the processing window is obvious from 150 RPM to 518 RPM, which is due to the increase in conveying capacity and the mechanical energy input into the polymer melt. Moreover, higher screw speed means higher shear rate and lower viscosity, which allows the processing of a higher volume of material. It can be seen that under these conditions, high barrel temperature and low flow rate lead to the maximum value of the pressure. A higher barrel temperature guarantees a fully molten, homogenous phase and lowers viscosity, enabling effective pressure transmission down the screw without losses from slip or unmelted areas. At the same time, the forward drag flow produced by the screw surpasses the required throughput when the flow rate is low. As a result, the system creates a powerful opposing pressure gradient to counteract this mismatch and lower the net flow to the necessary low level. So, consequently, the pressure will be increased inside the system.

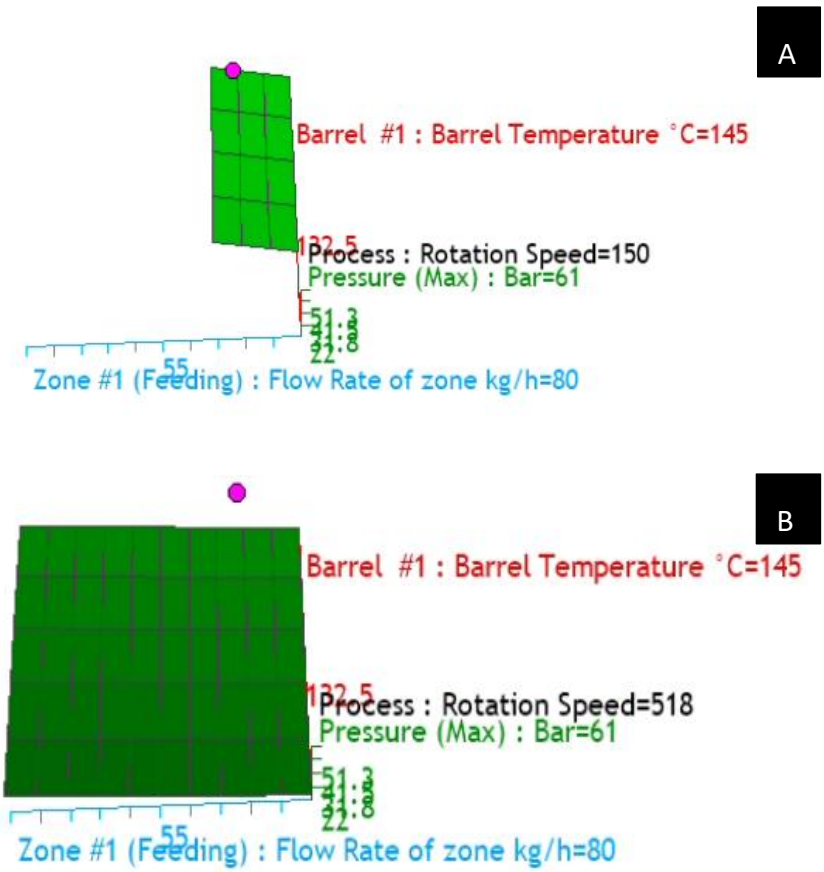

Fig 53. Comparison of the processing possibility of the material at A)150 RPM and B)518 RPM

The last parameter, which was considered a constraint, was the **Feeding Rate**. [Fig 54], shows that at a constant Feeding rate, the increase of rotation speed will lower the pressure dramatically since a higher shear rate will be applied to a fixed amount of material and causes a higher reduction in the viscosity. According to this curve, the effect of Barrel temperature is nil due to the flat slope of the related curve. This can be explained by the fact that, when it comes to constant feeding rate, the dominant factor that causes the pressure is the volumetric conveying capacity of the screw rather than the rheological properties of the polymer melt. As a result, the resistance to flow and the pressure needed to propel the material forward are not considerably changed by the decrease in viscosity caused by temperature variations.

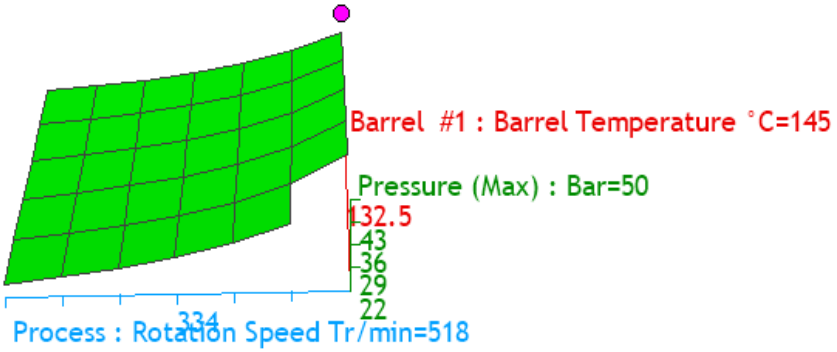

Fig 54. DoE "Pressure result" at constant Feeding rate

According to the overall trend of the 3D curve [Fig 55], there is a slight upward shift of the curve, which means that the increase in flow rate causes an increase in pressure. This can be explained by the fact that a higher volume of material needs a higher pressure to overcome the flow resistance.

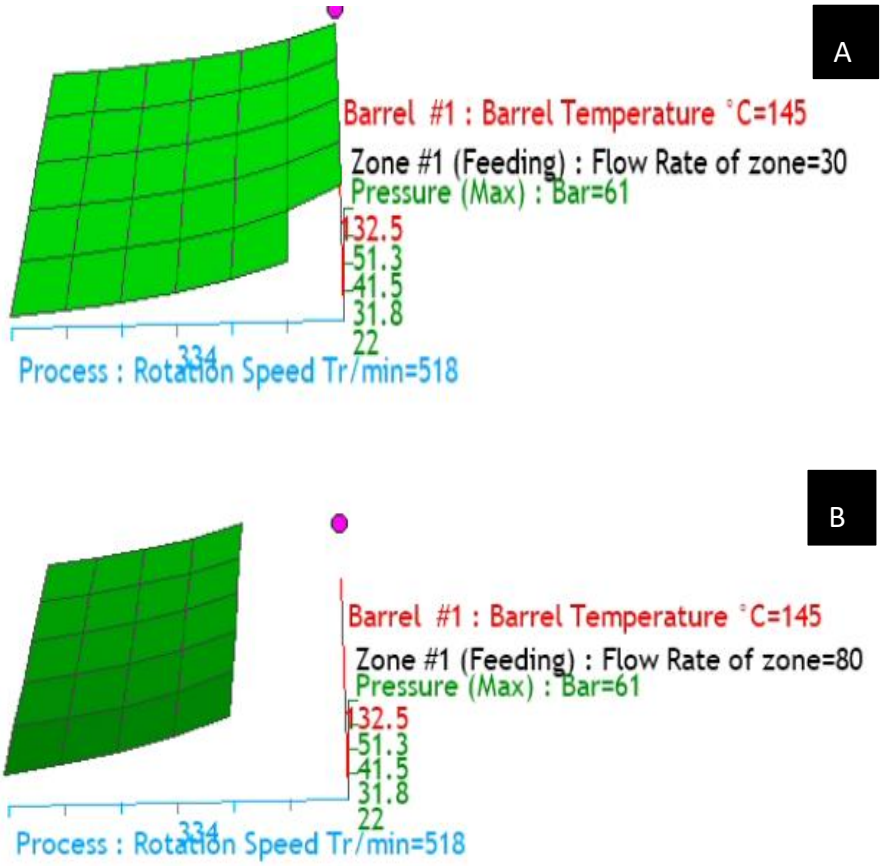

Fig 55. DoE "Pressure result" at constant Feeding rate, both in A)30 kg/h and B)80 kg/h

The last important thing about the pressure 3D curve at constant feeding rate is the processing possibilities of the material. [Fig 56] clearly demonstrates it is not possible to process the material at very low barrel temperatures and rotation speed since the viscosity of the material is too high. By increasing the feed rate, the processing of the material is possible only at high rotation speed since a higher amount of material requires a higher shear rate, and at low screw speed, it is not possible to lower the viscosity of a high amount of material. It is also clear that low screw speed and high barrel temperature ensure the maximum level of pressure. The drag flow produced by the screw is insufficient to move the required mass flow rate when the screw speed is low. The mechanism compensates for this by creating a significant pressure along the barrel, which pulls the material forward and maintains the fixed throughput. As screw speed drops, this pressure build-up becomes more noticeable since the drag contribution keeps getting reduced. In addition, a high barrel temperature guarantees a completely melted and continuous phase, which enables effective pressure transmission without dissipation from solid pieces or inadequate melting. As a result, even if viscosity is reduced, the necessity to overcome the restricted drag flow at low screw speed takes priority, resulting in the highest-pressure levels in these circumstances.

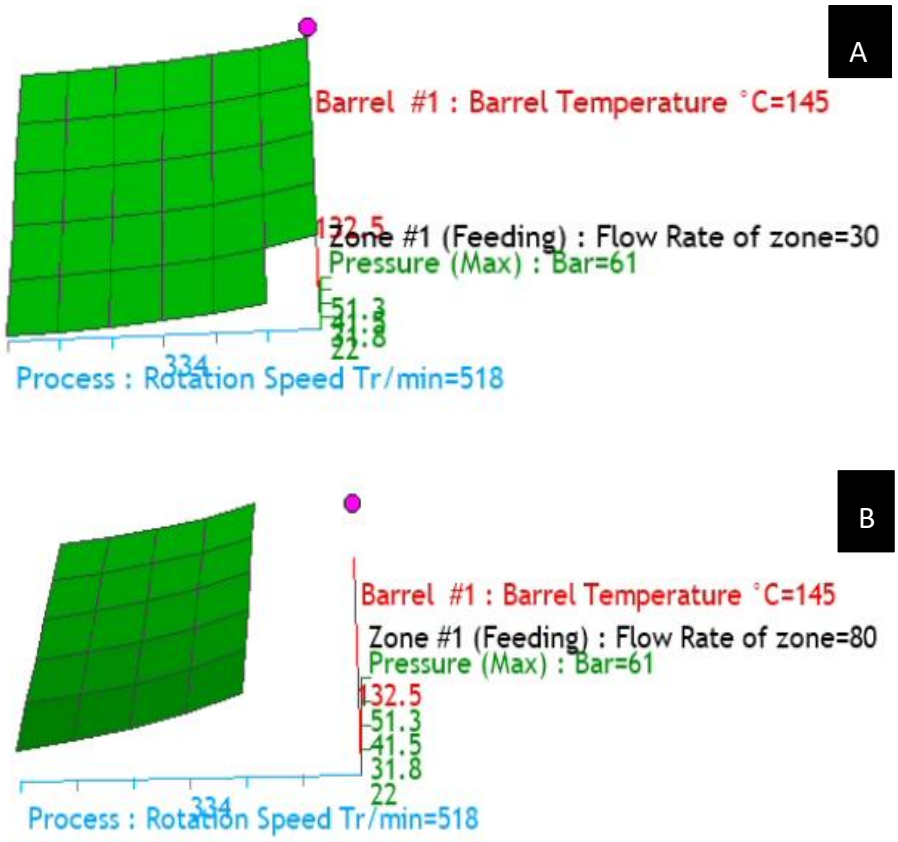

Fig 56. Comparison of the processing possibility of the material at A)30 kg/h and B)80 kg/h

In conclusion, by analysing all pressure curves, it can be concluded that rotation speed had the greatest effect on pressure, and a slight change in its value caused a dramatic change in pressure. As noted previously, these two parameters are inversely related; increasing pressure requires reducing the rotation speed as much as possible.

2.2.4.1.4 *Shear rate (s^{-1})*

The next selected result is the **Shear rate,** which will be applied to the molten polymer inside the extruder. As can be seen in [Fig 57], the axis related to the **Rotation speed** has an upward slope, while the axis related to the **Feed rate** has an almost constant slope.

The direct relation between the rotation speed and the shear rate can be explained by the velocity gradient established within the flow channel. According to the fact that the velocity of the melted polymer at the barrel wall is equal to zero, and its velocity at the screw surface is equal to the screw's velocity, a velocity profile is generated across the molten polymer, which is characterised by the "no-slip" condition. Since the spatial derivative of velocity with respect to the channel height is the definition of the shear rate, any increase in rotation speed causes an increase in the shear rate. By this definition, almost zero influence of the feeding rate can be understood. While the shear rate is related to the velocity gradient established between the rotating screw surface and the stationary barrel wall, the feeding rate determines the degree of screw fill, and it doesn't change the channel height; consequently, the shear rate is not influenced by the feeding rate.

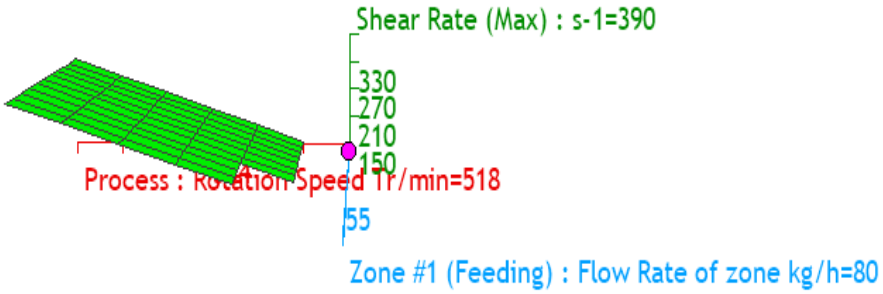

Fig 57. DoE "Shear result" at constant Barrel Temperature

Following the overall trend of the 3D curve [Fig 58], it is obvious that by increasing the barrel temperature, there is no change in the slope of the curve. This is because of the nature of the shear rate. Shear rate is a kinematic property determined strictly by the screw geometry and rotational speed, and the barrel temperature does not play a critical role in changing the shear rate. It should be noted that, although the barrel temperature does not change the shear rate, it determines the rheological behaviour of the molten polymer against the shear rate.

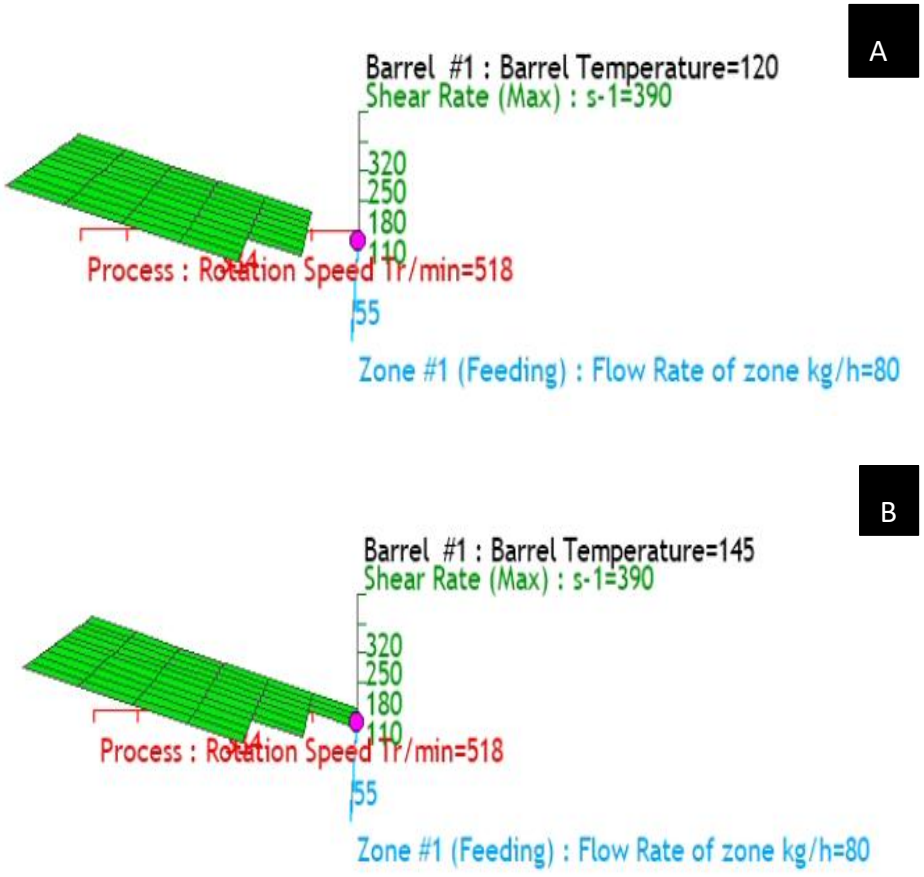

Fig 58. DoE "Shear rate result" at constant Barrel temperature at both A)120°C and B)145°C

The last important point is the processing possibility of the polymer at a constant barrel temperature. As it is demonstrated in [Fig 59], at higher barrel temperature, it is also possible to process the material at lower rotation speed and feed rate. This can be due to the reduction of viscosity of the molten polymer, which facilitates the processing even at low rotation speed. However, the processing of the material is not possible at high feed rates and low screw speeds. This limit in processing is because a higher volume of material has a higher flow resistance, and even the reduction of viscosity due to high temperature is not enough to overcome this resistance. So, a higher rotation speed is needed to provide a higher shear rate to process the

material. This is because viscosity is practically stable at constant barrel temperature; changes in shear rate are controlled by the flow that is created inside the screw channel. The material is not effectively moved forward by the screw rotation at low screw speeds because the drag flow component is weak. The system functions in low throughput conditions at low feeding rates, which increases the relative significance of pressure-driven flow to preserve continuity through the die. Strong velocity gradients form throughout the channel as a result of this combination, especially close to the barrel wall, where the no-slip condition causes the melt to drastically slow down. As a result of this intensified velocity, the shear rate value gets higher.

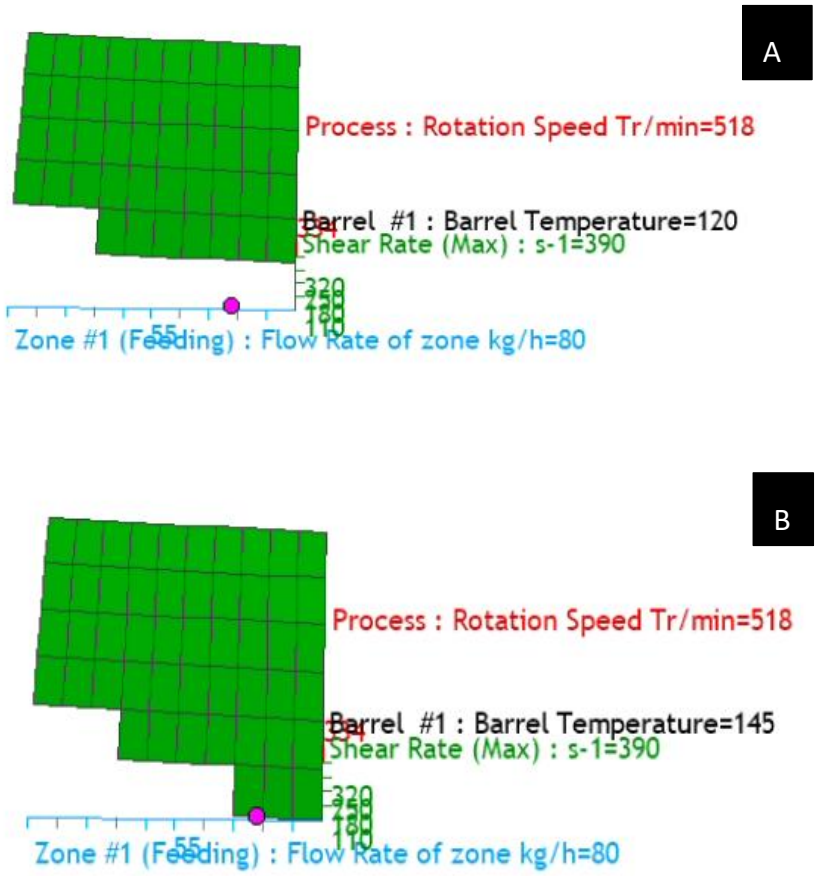

Fig 59. Comparison of the processing possibility of the material at A)120℃ and B)145℃

The next parameter, which was considered a constant, was the **Rotation Speed** [**Error! R eference source not found.**]**.** Both **the feeding rate** and **Barrel temperature** have almost zero slope, which means that their influence on the shear rate can be neglected. The reason for this shape of the curve can be found in the nature of the shear rate, which was mentioned above.

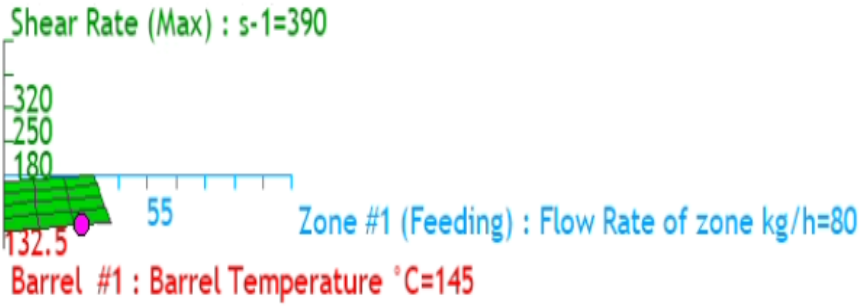

Fig 60. DoE "Shear rate result" at constant Rotation Speed

By looking at the overall trend for the 3D curve [Fig *61*], the effect of increasing rotation speed can be seen. Increasing the rotation speed causes a dramatic upward shift of the curve, which emphasises the great influence of the rotation speed on the shear rate. It is also important to say that while the increase in rotation speed changes the shear rate a lot, the effect of both the feeding rate and barrel temperature is almost nil.

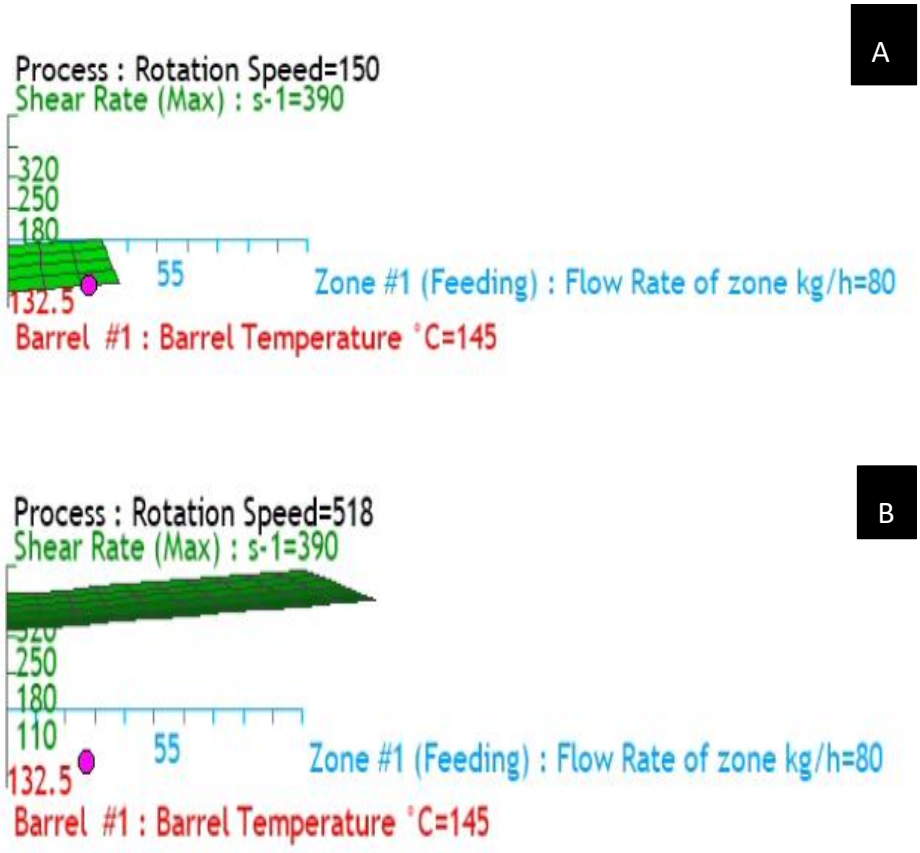

Fig 61. DoE "Shear rate result" at constant Rotation Speed, both in A)150 RPM and B)518 RPM

The last point is the possibility of processing the material at different rotation speeds [Fig *62*]. The increase of processing window by increasing the screw speed is obvious. The reason for this lies in the nature of the behaviour of the molten polymer. The increase in rotation speed increases the shear rate applied to the polymer, which allows for processing a higher amount of material. Higher screw speed provides the needed amount of shear rate to overcome the flow resistance of a greater volume of material by reducing the viscosity of the molten polymer. The other thing that should be noted is that the highest value for shear rate at constant rotation speed is when the barrel temperature is high, and the flow rate is low. To explain this, consider that viscosity is decreased by a high barrel temperature, which makes it easier for the polymer to deform and create more noticeable velocity gradients inside the screw channel. The imposed throughput is little in relation to the screw's drag conveying capacity when the feeding rate is low. The system creates a powerful counter-pressure gradient that superimposes on the drag flow to address this imbalance. Steep velocity profiles are created throughout the channel thickness as a result of this interplay between forward drag and backward pressure flow. These steeper profiles provide larger shear rates because shear rate and velocity gradient are directly correlated.

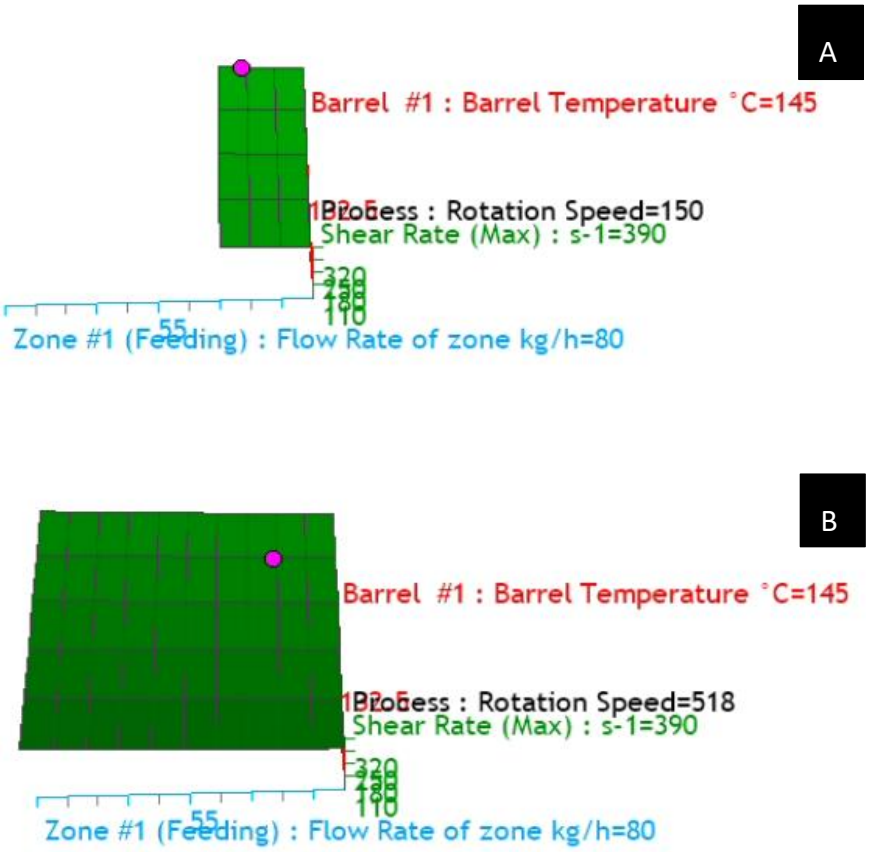

Fig 62. Comparison of the processing possibility of the material at A)150 RPM and B)518 RPM

The last parameter considered as a constraint was the **Feeding rate** [Fig *63*]. Again, a linear slope for **Barrel temperature** can be seen, which shows its negligible influence on the shear rate. On the other hand, an intense upward slope of the **Rotation speed** can be seen, which illustrates the direct relation between shear rate and the screw speed.

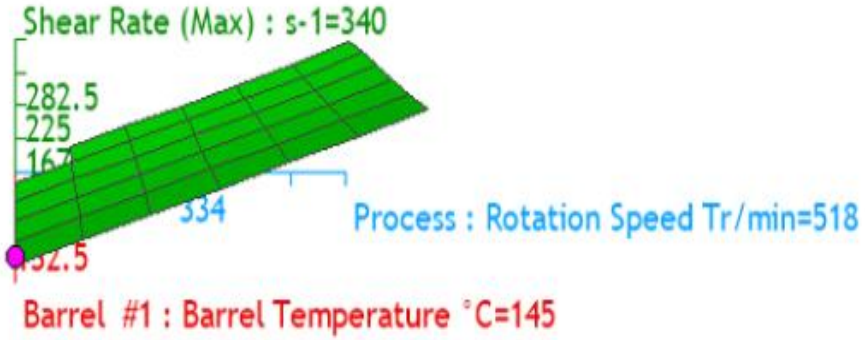

Fig 63.DoE "Shear rate result" at constant Feeding rate

The overall trend of the 3D curve [Fig 64] demonstrates that increasing the feeding rate does not affect the shear rate since the curve does not show a noticeable change. This highlights the negligible effect of the feeding rate on the shear rate once more. As previously stated, the effect of the feeding rate is on how much the screw is filled and not on the velocity gradient, which affects the shear rate.

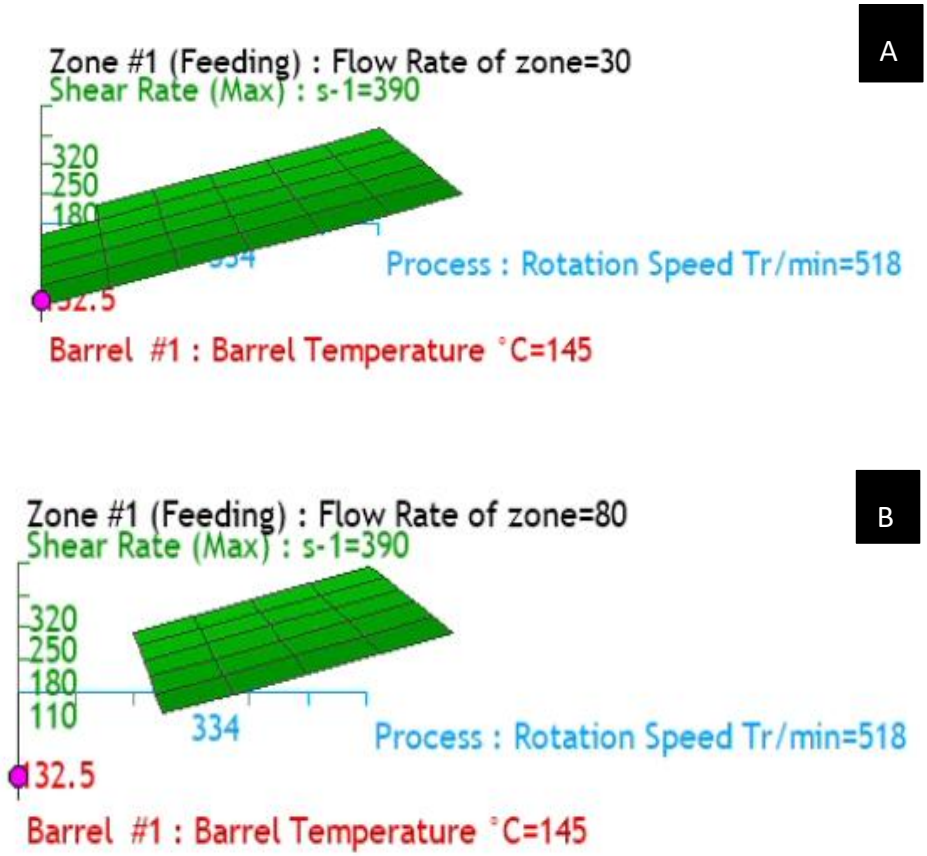

Fig 64. DoE "Shear rate result" at constant Feeding rate, both in A)30 kg/h and B)80 kg/h

The final aspect that should be investigated is the processing possibility of the material under this condition [Fig 65]. From the curve, the impossibility of processing the material at low temperatures and low rotation speed can be seen even at a low feeding rate. This is because of the minimum needed amount of both parameters for conquering the flow resistance and reducing the viscosity. It is also obvious that the increase in feeding rate causes a reduction in processing window, only at the higher screw speeds. This can be explained by the fact that a higher material volume needs a higher shear rate to lower the viscosity, which can be provided by higher rotation speeds. As can be seen, when the flow rate is constant, the maximum value of shear rate is when the barrel temperature is as high as possible, and the screw speed is low. This is because the screw's drag-induced conveyance capacity drops with decreasing screw

speed, though the mass flow rate remains constant. The system creates a powerful pressure-driven flow component that creates sharp velocity gradients across the channel in order to meet this limitation. In addition, a high barrel temperature guarantees a fully molten, homogenous phase and reduces viscosity, which enables the material to easily deform and maintain these abrupt gradients without flow instabilities. Strong pressure-driven backflow and weak drag flow combine to provide extremely non-uniform velocity profiles, especially close to the walls, which immediately raises the shear rate. Therefore, under these circumstances, the combination of pressure compensation and decreased viscosity results in the maximum shear rate despite the lower screw speed.

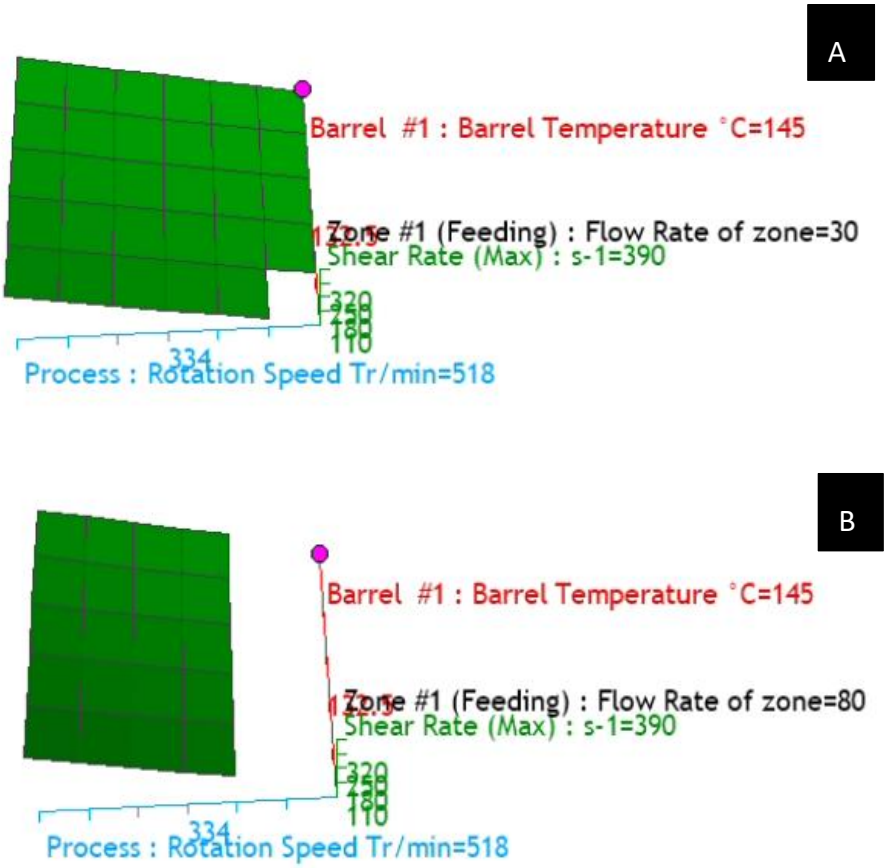

Fig 65. Comparison of the processing possibility of the material at A)30 kg/h and B)80 kg/h

Finally, by reviewing all the curves for shear rate, the most important parameter influencing it can be recognised, which is the rotation speed. This is because shear is generated by the differential movement between the rotating screw and the fixed barrel. As screw speed

increases, the tangential velocity at the screw surface rises proportionally, which steepens the velocity gradient within the polymer melt. Consequently, the shear rate scales directly with rotational speed, making it the dominant variable controlling shear deformation throughout the process.

2.2.4.1.5 *Viscosity (Pa.s)*

The other interesting result is the viscosity. The **Barrel temperature** is the first constant parameter, like before. As previously stated, the maximum viscosity was the requested result. This is because the higher viscosity requires higher stress, so finding the highest possible viscosity helps to apply the highest stress. [Fig 66] clearly shows the inverse relation between viscosity and **Rotation speed**. The reason for this relation can be explained according to 2.2.4.1.4] where the correlation between shear rate and rotation speed was analysed. In general, it can be said that as a result of increasing rotation speed, the applied shear rate on the material will be increased too. The reduction in viscosity by increasing the shear rate is due to the pseudoplastic nature of the molten polymer. At low shear rates, there is a robust physical entanglement in the macromolecular chains of the polymer, which causes extremely high resistance to flow. As the applied shear rate increases, it causes the physical de-entanglement of the chains and their subsequent orientation parallel to the flow stream. In contrast, the effect of **the feeding rate** is minimal. So, it can be said that the effect of the feeding rate can be discounted. This is totally understandable because the viscosity of a polymer melt is determined by the local temperature and the shear rate. In a screw extruder, the shear rate is a velocity gradient defined by the boundary conditions of the screw speed and the channel geometry; as long as these remain constant, the rate of molecular deformation and alignment remains unchanged regardless of the volume of the feed material.

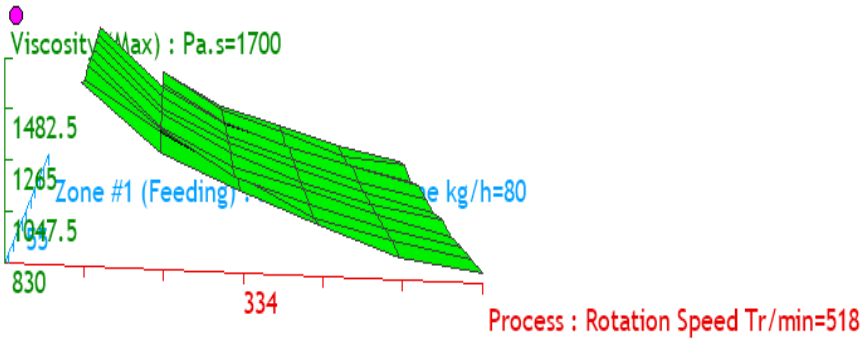

Fig 66. DoE "Viscosity result" at constant Barrel Temperature

The overall trend of the 3D curve [Fig 67], shows that increasing the temperature between 120℃ and 145℃ causes a slight downward shift of the curve, which means that increasing the temperature reduces the viscosity of the molten polymer. This can be explained by the fact that in polymers, the physical entanglements of long macromolecular chains of polymers, which produce a dense network of internal resistance, greatly hinder flow. Individual chain segments can move more freely as a result of the polymer matrix's thermal expansion, which raises the "free volume as the temperature rises. By giving the segments the activation energy they need to get past local barriers, this increase in thermal energy makes it easier for chains to slide past one another and so lowers the density of entanglements. As a result, there is less internal friction in the melt, which significantly lowers its viscosity.

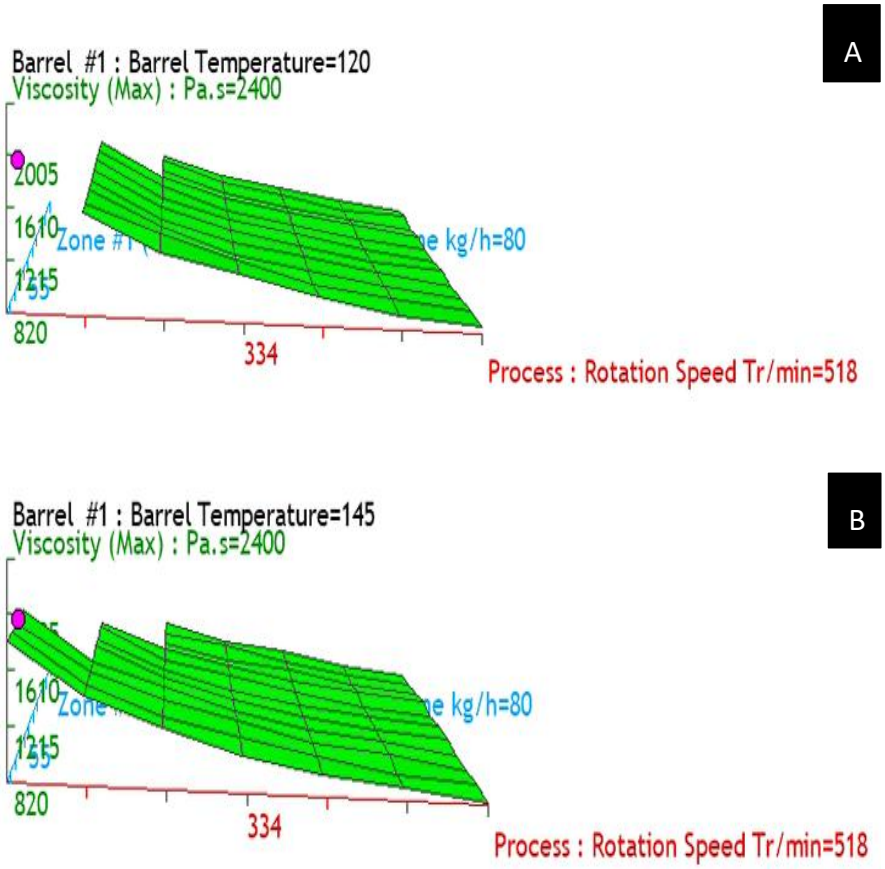

Fig 67. DoE "Viscosity result" at constant Barrel temperature at both A)120°C and B)145°C

The final point to consider when investing in viscosity under constant barrel temperature is the material's processing processability. [Fig 68] shows that increasing the barrel temperature will expand the processing window of the material to lower flow rate and rotation speed. This effect could be expected since the increase in temperature will decrease the viscosity of the material and, consequently, it is possible to reach stable processing even at a lower screw speed. But a lower screw speed has limited power and cannot overcome the flow resistance of a high amount of material, and this fact can explain why it is possible to process the material at low screw speed and low feeding rates. Since in the last part, [2.2.4.1.4], it was mentioned that the highest shear rate, at this condition, is achieved when the screw speed and feeding rate are low; it was expected not to have the highest value in this regime. However, [Fig 68] clearly shows that the highest viscosity is achieved when both the flow rate and rotation speed are low. Under this condition, low effective deformation and inefficient pressure-dominated flow combine to cause this. Because polymer melts are shear-thinning, the material tends to stay closer to its high, near-zero-shear viscosity under low screw speed and low throughput, limiting the overall deformation imposed by the screw. However, these operating circumstances also cause

pressure-driven flow with recirculation and backflow to replace effective drag-driven conveyance in the flow regime. This produces very non-uniform and unstable localised high velocity gradients and thus locally high shear rates, but it does not significantly lower the material's bulk resistance. Rather, because of poor conveyance efficiency and increased resistance to forward motion, the system needs a larger stress to maintain flow. Consequently, under constant temperature conditions, the apparent viscosity reaches its maximum at low feeding rate and low screw speed, even though local shear rates may be elevated.

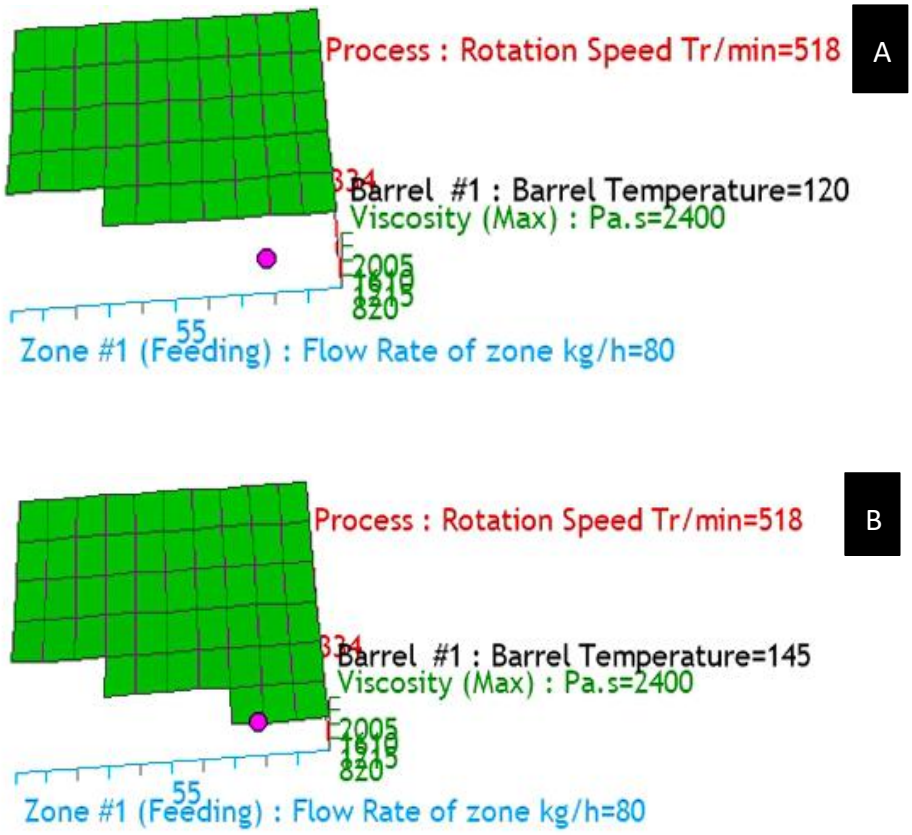

Fig 68. Comparison of the processing possibility of the material at A)120°C and B)145°C

Rotation speed is the next parameter, which was considered as a constant. As can be seen in [Fig 69], the inverse relation between the viscosity and barrel temperature is obvious, and the reason for this behaviour has been explained above. Moreover, by analysing the plot related to **the Feeding rate**, it can be seen that the slope of the curve is almost linear, which again emphasises the negligible effect of it on the viscosity of the molten polymer.

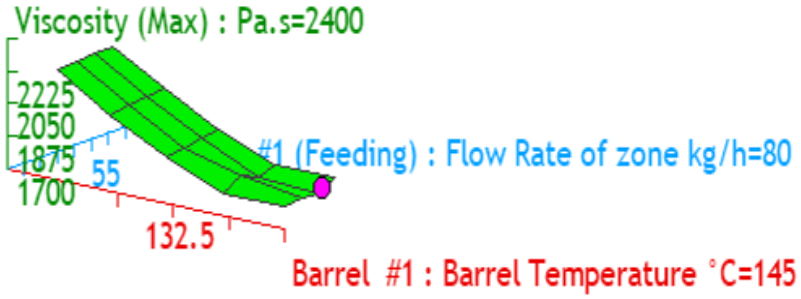

Fig 69. DoE "Viscosity result" at constant Rotation Speed

[Fig 70] illustrates the overall trend of the 3D curve, while the rotation speed varies between 150RPM and 518RPM. As observed in the transition from a rotation speed of 150RPM to 518RPM, the viscosity surface drops significantly across the processing zone. In addition, by increasing the rotation speed, the effect of both barrel temperature and the feeding rate is almost nil. The dramatic reduction in viscosity of the molten polymer as a result of the higher rotation speed is due to the generation of higher shear stress on the polymer. It was mentioned before that the molten polymer is composed of entangled macromolecular chains, and these chains continue to be highly entangled at lower rotation speeds, resulting in a substantial internal flow resistance. The polymer chains must, however, detangle and align themselves in the direction of the flow when the rotation speed increases due to the increased shear stress. As a result, the viscosity of the material will be highly decreased at higher rotation speed.

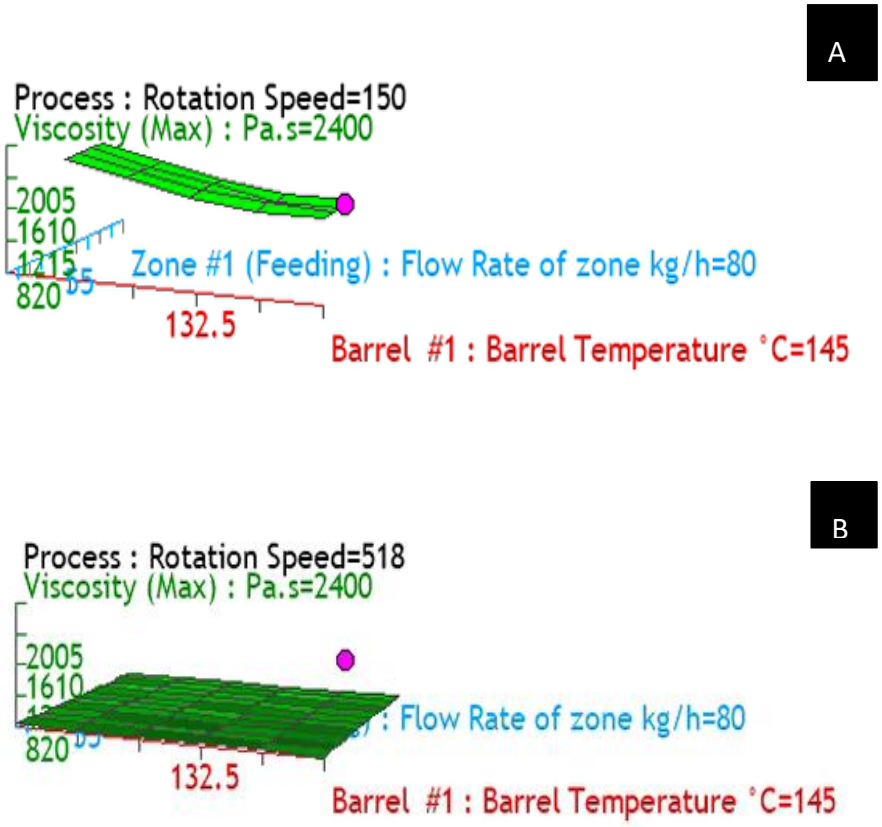

Fig 70. DoE "Viscosity result" at constant Rotation Speed, both in A)150 RPM and B)518 RPM

As anticipated, increasing the rotation speed will broaden the processing window of the material, which can be seen in [Fig 71], and the reduction in viscosity and the flow resistance are the reasons for this behaviour. It is also obvious that the highest viscosity under this condition is at a relatively high barrel temperature and low flow rate. This is because stress is effectively transmitted inside the melt, and pressure-driven flow predominates. A large counter-pressure gradient develops when the feeding rate is low because the enforced throughput is modest in relation to the screw's conveying capacity. This increases the barrier to forward flow. A high barrel temperature guarantees a totally molten and homogeneous phase in which stresses and pressure are effectively transmitted along the material without dissipation, even if it also lowers the intrinsic viscosity of the polymer by increasing molecular mobility. As a result, the system shows a greater overall flow resistance, which is represented by an increase in apparent viscosity.

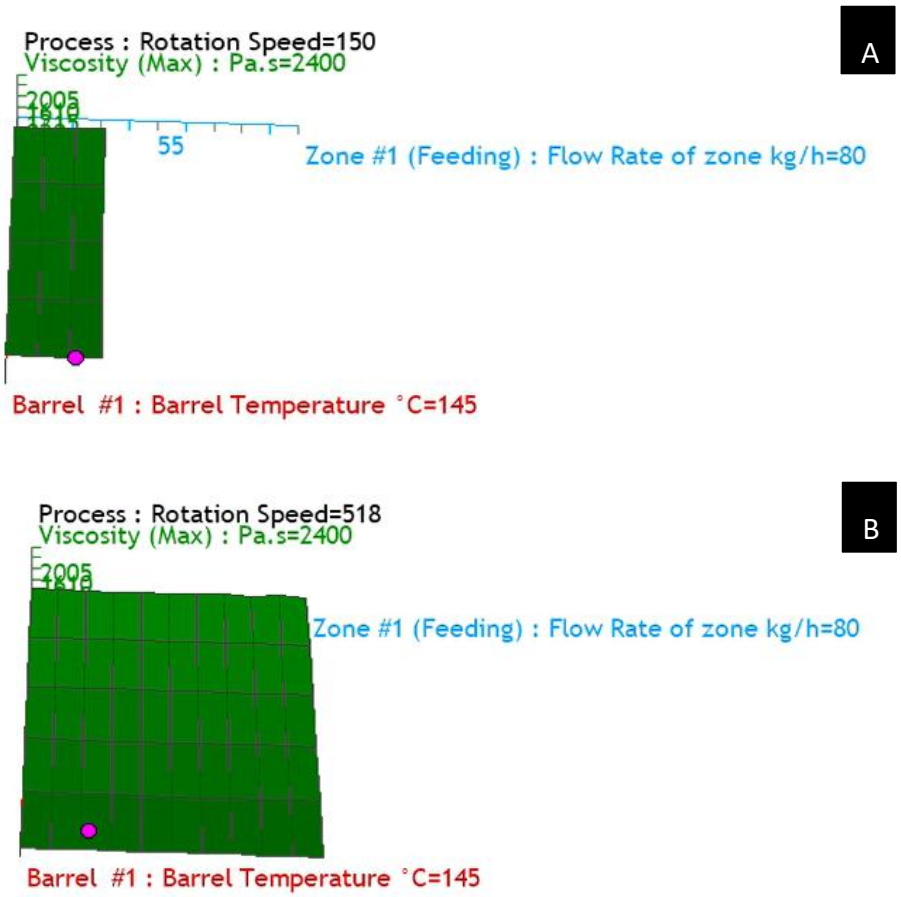

Fig 71. Comparison of the processing possibility of the material at A)150 RPM and B)518 RPM

The last parameter, which was considered a constant, was the **Feeding rate** [Fig 72]. As can be seen, when the feeding rate is constant, the effect of **barrel temperature** can be almost neglected. This is because the polymer throughput is fixed at a constant feeding rate, which limits the material flow and, as a result, the extruder's effective shear rate. Under normal processing settings, the apparent viscosity of polymer melts is mostly controlled by shear rate rather than temperature since they are substantially shear-thinning. Although an increase in barrel temperature naturally lowers the melt viscosity, this effect is mostly offset by the system's fixed kinematics. The imposed mass flow keeps the shear field along the screw constant, which restricts how much the overall flow behaviour can be affected by temperature-induced viscosity changes. Because of this, the feeding rate, via shear rate, continues to be the primary determinant of apparent viscosity, and barrel temperature becomes a secondary factor that can be safely disregarded under these circumstances. But, on the other hand, the effect of the **Rotation speed** is completely visible. This is because the applied shear rate on the molten polymer is governed by the rotation speed, as explained before.

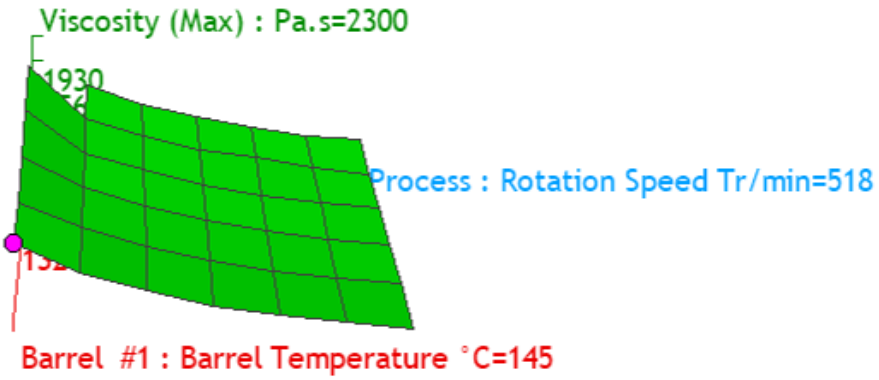

Fig 72. DoE "Viscosity result" at constant Feeding Rate

[Fig 73] demonstrate the overall 3D curve trend of the effect of the feeding rate on the viscosity. The overall curve does not exhibit any upward or downward shift as a result of increasing the feeding rate. This is because viscosity is a rheological property, and increasing the feeding rate does not change the viscosity itself.

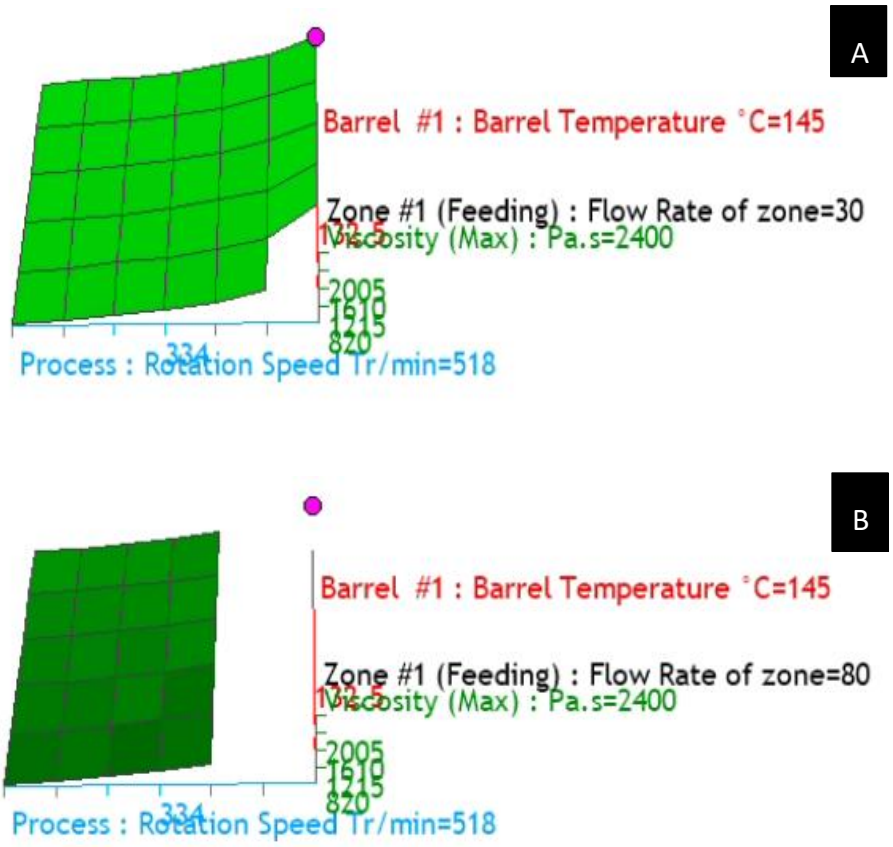

Fig 73. DoE "Viscosity result" at constant Feeding rate, both in A)30 kg/h and B)80 kg/h

The last aspect to mention is analysing the processing window at both feeding rates. [Fig 74], shows that by increasing the feeding rate, the processing of the material is possible only when the rotation speed is almost high. This is due to the increase in flow resistance of the material, which has been mentioned before. Furthermore, it can be seen that when the feeding rate is constant, high barrel temperature and low rotation speed result in the highest value of the apparent viscosity. This is because the process adjusts by creating a large pressure gradient along the barrel when the screw speed is low. After all, the drag flow produced by the screw is insufficient to transfer the fixed mass flow rate. Higher apparent viscosity is a result of this pressure build-up, which considerably raises flow resistance. In addition, a high barrel temperature guarantees a completely molten and uniform polymer phase, which permits effective transmission of pressure and stresses throughout the melt without dissipation from incomplete melting. Because of this, even while the material's inherent viscosity decreases at high temperatures, the predominance of pressure-driven flow at low screw speeds causes the overall resistance to flow to grow, reaching a maximum in apparent viscosity.

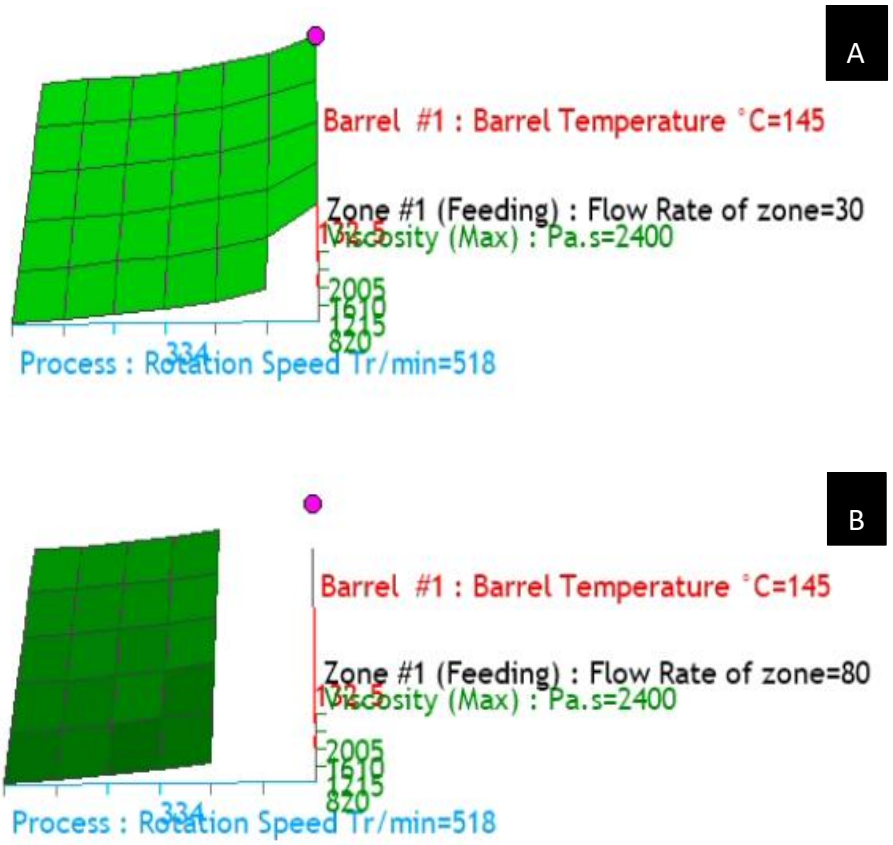

Fig 74. Comparison of the processing possibility of the material at A)30 kg/h and B)80 kg/h

So, to conclude the effect of processing parameters on the viscosity, it can be said that the **Rotation speed** had the most influence on it. To have the highest possible stress on the molten polymer, the viscosity should be kept as high as possible, which means that the rotation speed should be at the lowest possible value.

2.2.4.1.6 *Total Residence time (s)*

Total residence time is the final result, which was selected to be shown. [Fig 75] shows that total residence time has an inverse relation with both **Rotation speed** and the **Feeding rate.** This can be explained by the fact that since the extruder's internal volume is fixed, any increase in the rate of material entering the system must be balanced by a proportionate decrease in the time it spends traversing the screw length to satisfy the continuity equation. So, any increase in the feeding rate decreases the total residence time. Comparably, when the **Rotation speed** increases, the material's axial velocity and mechanical pumping efficiency both increase, pushing the melt through the screw channels more quickly and decreasing the amount of time that any particular volume element may stay inside the barrel.

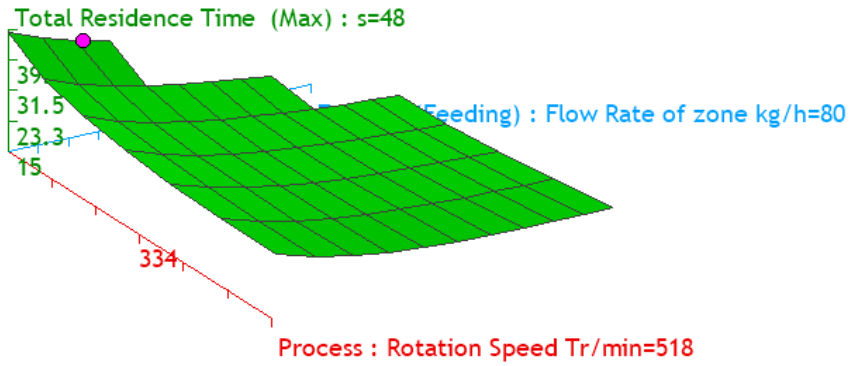

Fig 75. DoE "Total Residence time result" at constant Barrel Temperature

According to the overall trend of the 3D curve [Fig 76], it can be said that the effect of barrel temperature on total residence time is almost negligible. This is because it is well recognised that total residence time is not a thermodynamic value, but rather a kinematic one that is mostly governed by the screws' geometry and the system's mechanical push. The residence time is still mathematically related to these mechanical inputs since the screw speed and feeding rate are the factors that regulate the amount of material displaced per cycle. The degree of fill in some zones or the leakage flow over screw flights may be marginally affected by temperature changes, but these effects are usually insignificant in comparison to the motor speed's main influence and the screw profile's pump-like action.

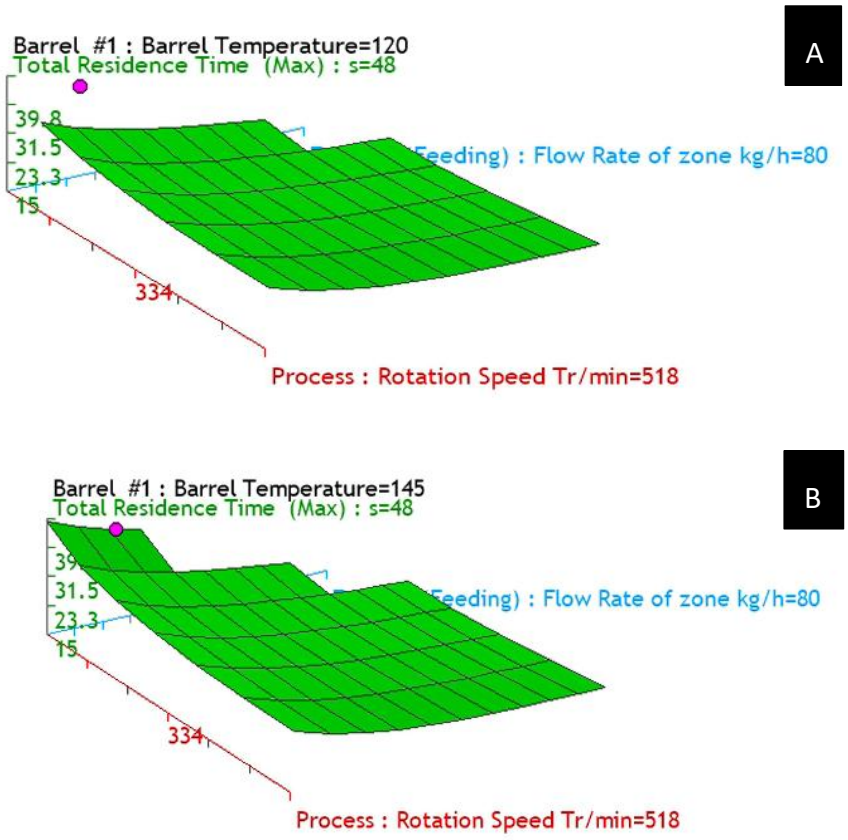

Fig 76. DoE "Total Residence time result" at constant Barrel temperature at both A)120℃ and B)145℃

The next step is to analyse the feasibility of processing the material at the lowest and highest barrel temperatures. [Fig 77] demonstrates that by increasing the barrel temperature, the possibility of processing the material will also extend to low feeding rates and rotation speed, since at higher temperatures the viscosity is lower, which assists the processing of the material. Moreover, it can be clearly seen that the highest value for residence time can also be achieved in this area. This is because the balance between mass throughput and conveying velocity within the screw influences the residence time at constant barrel temperature. The total amount of material transported through the extruder is greatly decreased when both the feeding rate and the screw rotation speed are low. A low screw speed slows down the polymer's axial movement down the barrel by reducing the drag-induced conveying capacity. Additionally, a low feeding rate lowers the mass throughput, which means that less material is forced through the system in a given amount of time. So, the combination of these two effects leads to a higher total residence time.

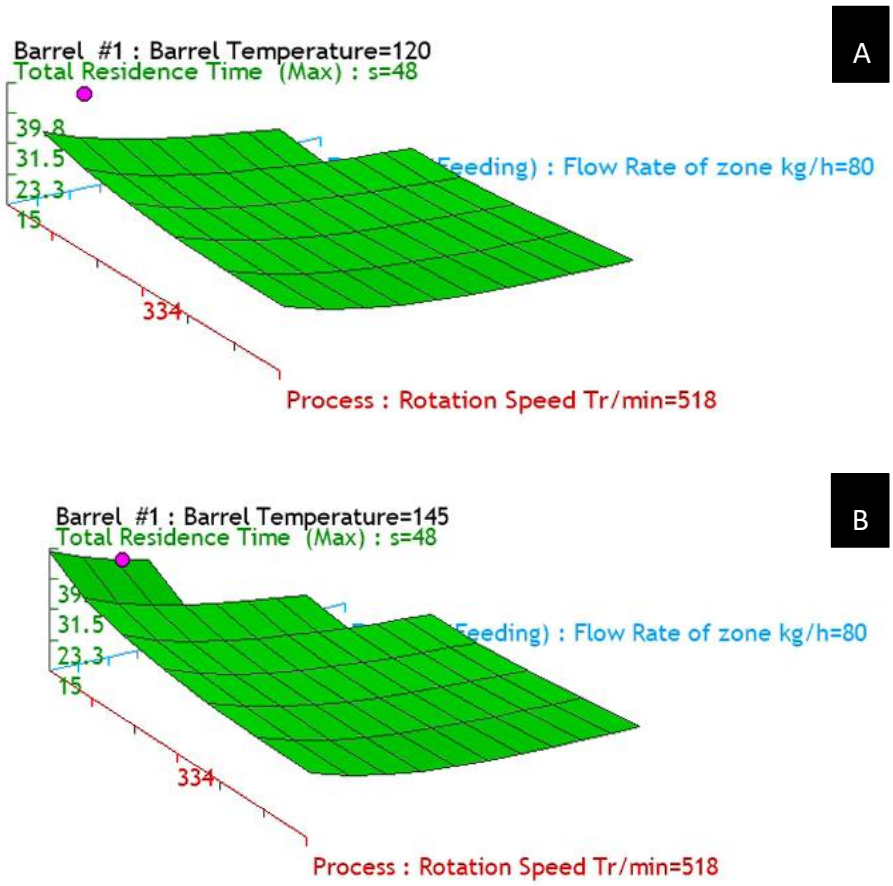

Fig 77. Comparison of the processing possibility of the material at A)120℃ and B)145℃

The next constant parameter is the **Rotation speed**. As can be seen in [Fig 78], there is a negative slope for the **Feeding rate**, which means that by increasing the feeding rate, the total residence time will be reduced. The main cause of this behaviour is an increase in mass throughput, which elevates the material's average axial velocity along the barrel. Furthermore, at greater throughputs, the forward drag flow outweighs the opposing pressure-driven backflow, leading to more efficient polymer transport with less recirculation. As a result, the material exits the extruder more quickly, reducing its total residence time. It can also be seen that the slope for the **Barrel temperature** is almost linear, which shows that this parameter does not affect the residence time. It is well known that increasing the barrel temperature lowers the viscosity of the polymer, promoting flow and improving the screw's ability to transport material. This may result in a decrease in the residence time by increasing the actual mass throughput. However, the resulting flow rate, rather than the temperature itself, remains the main determining factor. That is the reason why the effect of barrel temperature is almost nil and can be neglected.

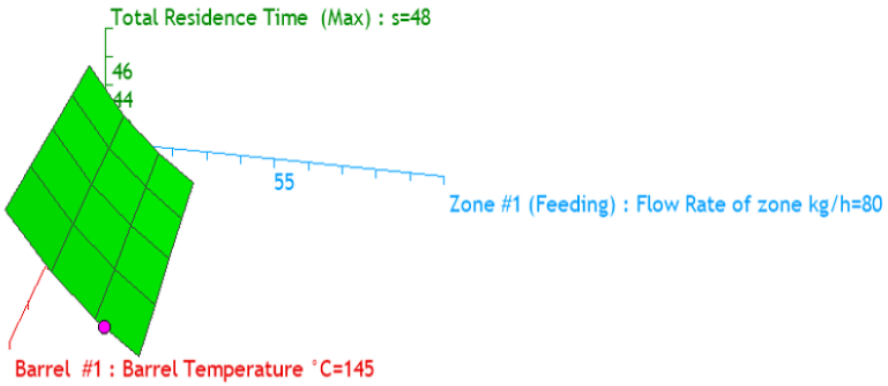

Fig 78. DoE "Total Residence time result" at constant Rotation Speed

There is a comparison between two screw speeds, the highest one and the lowest one, in [Fig 79], which clearly shows the inverse relation between the flow rate and the total residence time. Moreover, a slight downward shift of the 3D curve can be seen, which is due to the increase in the rotation speed. This behaviour makes perfect sense since the increase in rotation speed will also increase the amount of throughput. In this way, the materials have less time to remain inside the extruder, and the total residence time will be decreased.

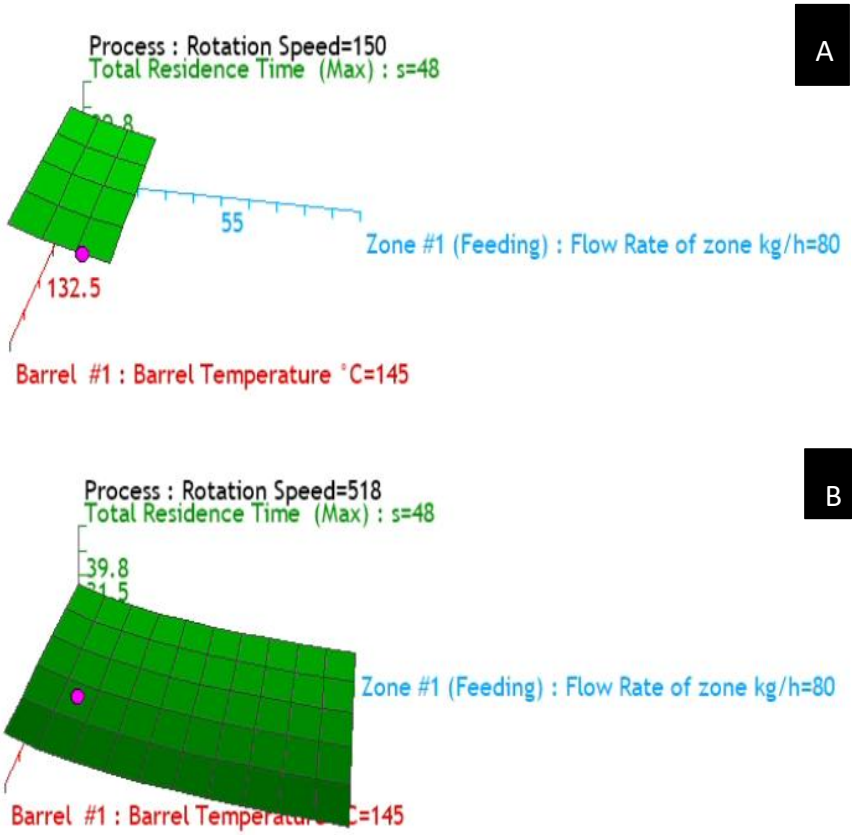

Fig 79. DoE "Total Residence time result" at constant Rotation Speed, both in A)150 RPM and B)518 RPM

The processing window of the material can be seen at [Fig 80]. An obvious expansion can be seen by increasing the rotation speed. At lower screw speeds, the amount of material that can be extruded is restricted due to the limited power of the screw for conveying the material and by increasing the rotation speed, it is also possible to extrude a higher amount of material. It can also be seen that the highest value for the total residence time at constant rotation speed is when the feeding rate is low, and the barrel temperature is relatively high. This is because a low feed rate results in a lower throughput, which causes the material to move along the screw more slowly and so extends the residence time. In addition, a high barrel temperature improves polymer flow and lowers internal resistance by lowering the melt viscosity. It should be noted that while the increase in barrel temperature means a reduction in viscosity, this reduced viscosity does not increase the throughput due to the low feed rate.

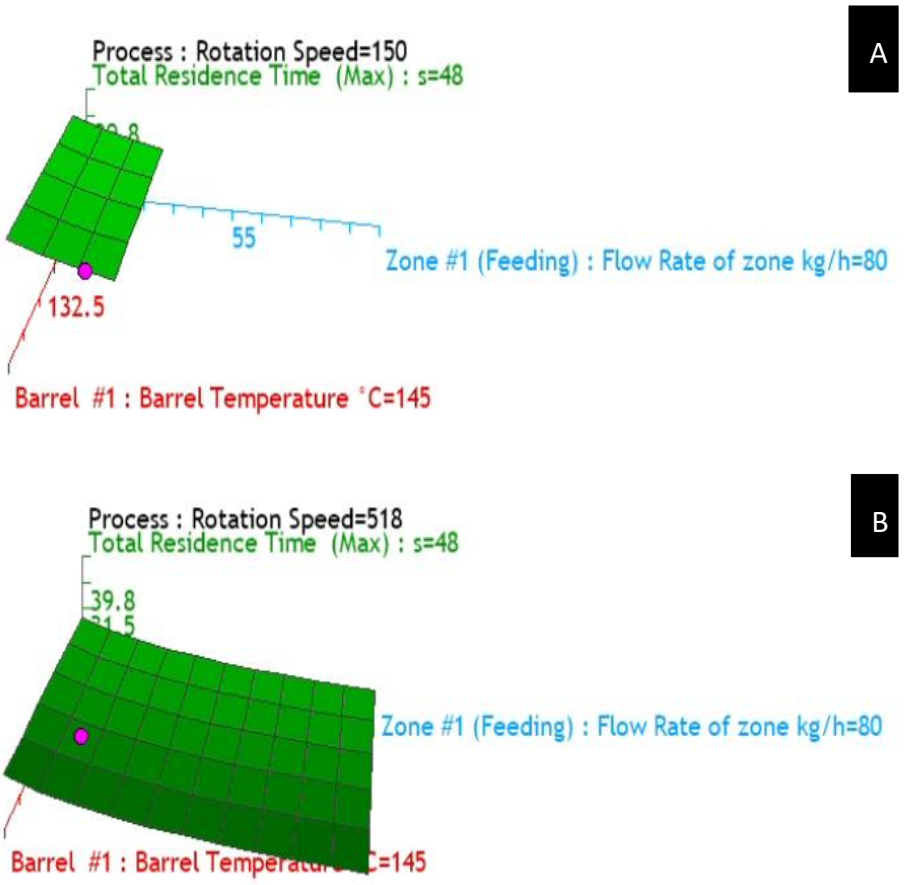

Fig 80. Comparison of the processing possibility of the material at A)150 RPM and B)518 RPM

The **Feeding rate** is the last parameter, which was considered as a constant [Fig 81]. The inverse relation between the **Rotation speed** and the residence time, which was mentioned before, can be seen here more clearly. The linear slope of the **Barrel temperature** is also obvious here, which emphasises the negligible effect of this parameter on the total residence time again.

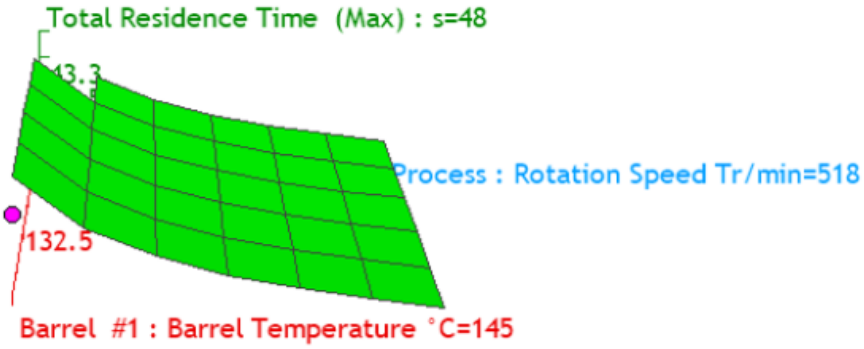

Fig 81. DoE "Total Residence time result" at constant Feeding Rate

The overall trend for the 3D curve can be seen in [Fig 82]. This curve shows that increasing the feed rate will shift the total curve slightly downward, which means a reduction in total residence time. This inverse relation is because any increase in feed rate will directly increase the screw speed and simultaneously, the amount of throughput.

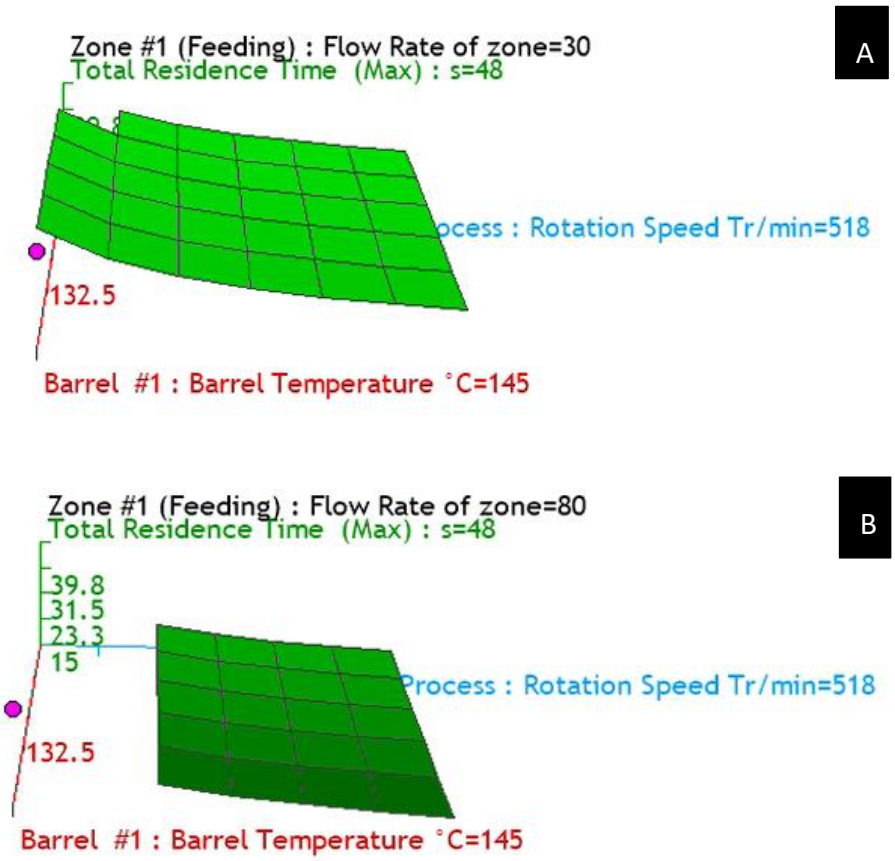

Fig 82. DoE "Total Residence time result" at constant Feeding rate, both in A)30 kg/h and B)80 kg/h

The last thing that should be mentioned is the possibility of processing the material under these conditions. As can be seen in [Fig 83], higher feed rate reduces the processing window to higher screw speeds. This is because a higher amount of material requires a higher power to be transported. In addition, it is clear that at a constant feed rate, the maximum value is when the rotation speed is low and the barrel temperature is high. This is because the axial conveying velocity of the polymer drops when the screw speed is low. The feeding rate is constant, but it moves through the barrel more slowly. This increases the amount of time the material spends inside the system by promoting longer screw channel filling. In addition, a high barrel temperature reduces the viscosity of the melt, increasing the fluidity of the polymer. Although this usually promotes flow, in low screw speed situations, it actually increases leakage and backflow over the screw flights rather than forward conveying. So, the combination of these two parameters will increase the total residence time to its highest value.

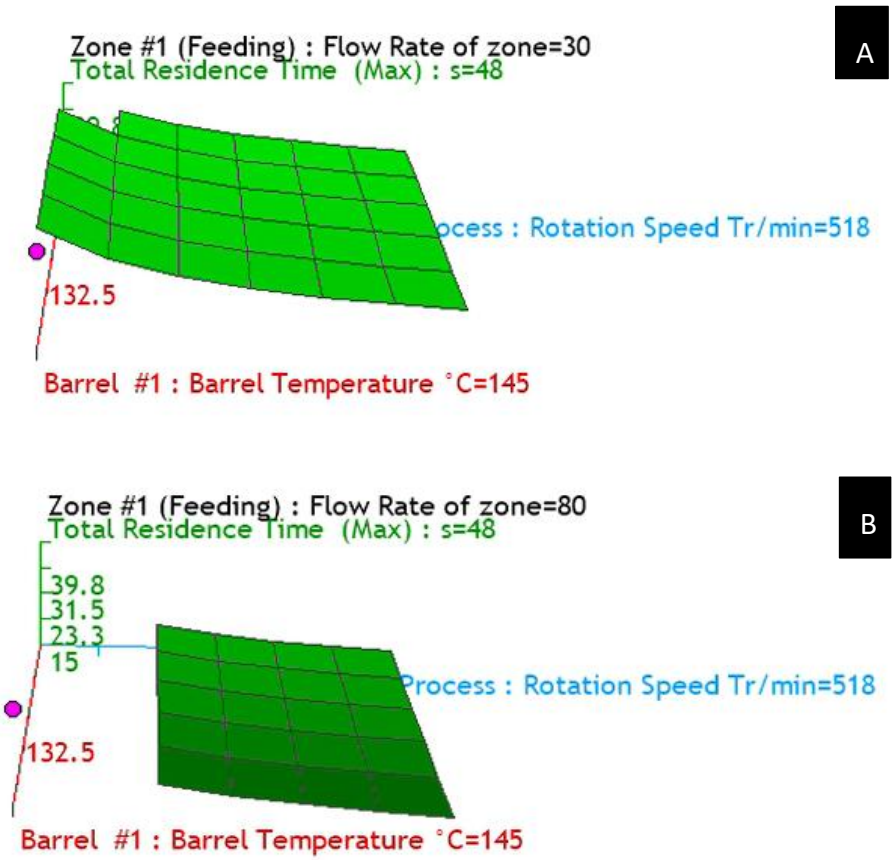

Fig 83. Comparison of the processing possibility of the material at A)30 kg/h and B)80 kg/h

In conclusion, by analysing all the curves, the **Rotation speed** was the one parameter that had the most influence on the total residence time. This means that any changes in the rotation speed cause a noticeable change in the total residence time. In order to increase the total residence time, the rotation speed must be kept as low as possible. However, higher residence time increases the risk of the degradation of the polymer. So, it should be kept in mind that although a higher residence time means that the material is under stress for a longer time, the possibility of degrading material is present.

2.2.4.2 **Summary of the DoE results**

In the DoE section, the relation between selected processing parameters and the selected results of the DoE had been studied. Please consider that the DoE was conducted to understand how the variation in selected extrusion parameters influences the parameters that introduce higher stress on the material during processing and affect the microstructure of the processed material. The table below summarises all the results that were obtained.

Table 10. Summary of the results observed from DoE

Selected DoE parameter	**Processing parameter with the most influence on the selected DoE parameter**
SME	Variation in the **Feed rate** had the most influence on SME. Lowering the feed rate increases the SME.
Torque	Variation in the **Rotation speed** had the most influence on torque. Lowering the rotation speed increases the torque.
Residence time	Variation in the **Rotation speed** had the most influence on residence time. Lowering the rotation speed increases the residence time.
Viscosity	Variation in the **Rotation speed** had the most influence on viscosity. Lowering the Rotation speed increases the viscosity.
Pressure	Variation in the **Rotation speed** had the most influence on pressure. Lowering the Rotation speed increases the pressure.
Shear rate	Variation in the **Rotation speed** had the most influence on shear rate. Increasing the **Rotation speed** increases the shear rate.

2.3 Analysing the simulation results

Now that Ludovic has demonstrated its ability to accurately predict the compounding process of a bio-based PHA blend under different processing conditions, it is time to examine how the various screw configurations affect the selected dependent variables. Temperature experienced by the polymer inside the extruder, pressure, total residence time, viscosity, shear rate, and mechanical delta T are the quantities that have been studied. As can be seen beside the thermal history of the polymer inside the extruder and mechanical delta T, all the other parameters are already discussed in the previous section, but at this part, these quantities will be studied differently. Actually, after that the simulation with the software is done, it will plot the various parameters as a function of axial distance from the hopper. This makes it possible to go further into specific parts of the machinery, whereas it is more difficult to do so following a DoE. Actually, a simulation must be used for the whole study; this final tool should only be used to establish the appropriate settings.

2.3.1 Temperature

One of the main variables that affects the final product quality is the thermal history experienced by the polymer melt inside the extruder. Melt temperature influences the viscosity, residence time distribution, mixing efficiency, potential degradation, and crystallisation kinetics in semi-crystalline polymers, which in turn determine the morphology, shrinkage, and mechanical performance of the final part. [Fig 84] demonstrates a four-phase thermal evaluation for all five trials. In the following, the three different zones of the temperature plot are explained, and please keep in mind that the X axis is the axial distance from the hopper.

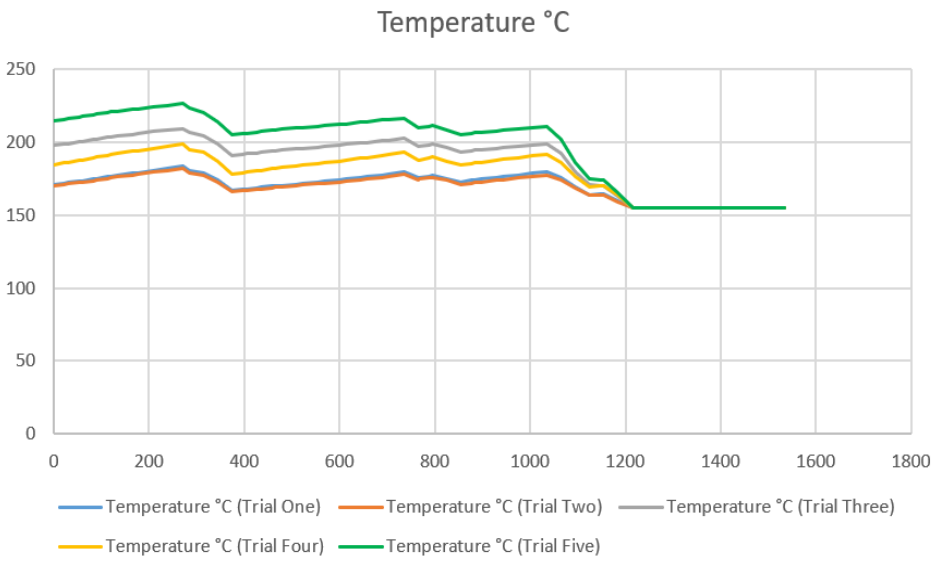

Fig 84. Comparison between the temperature plots of all the simulations

- ***Zone one: Melting and Viscose dissipation (x≈0-285 mm)***

  A temperature rise can be seen for all trials in the initial screw section, which is consistent with the combination of barrel conductive heating and viscous dissipation produced by the screw's compression and kneading geometry of the screw. The highest initial melt temperature is attained by trial 5 (approximately 214℃ at x=0). This can be due to its higher screw rotation speed with respect to other trials, which amplifies the shear rate and eventually the viscous heat dissipation. On the other hand, trials one and two, which had the lowest rotational speed, show the lowest initial melt temperature (approximately 171℃ at x=0).

  At x≈ 200-280 mm, a temperature pick can be seen for all the trials. This corresponds to the region of maximum compression and shear at the transition from the feed to the metering section and is a typical sign of viscous energy dissipation. The presence of this peak emphasises that the dominant thermal driver in the first zone is the internal heat generation, even in the absence of a high barrel temperature. As can be seen in [Fig 84], the peak amplitude is higher for the fifth trial, which supports the idea of greater dissipation under the specific processing condition.

- ***Zone two: Kneading Block / Mixing zone (x≈ 285-375 mm)***

  At approximately x≈ 285-375 mm, a slight but consistent temperature drop can be seen for all trials. This feature's uniformity under all processing conditions indicates a geometry-driven disturbance rather than a result of the processing variable being studied. This discovery is in line with physical reason. The presence of a kneading block (or reverse-pitch element) at this axial position would locally reduce the forward pumping efficiency of the screw, which increases the fill ratio but simultaneously changes how mechanical energy is distributed between dissipation and pressure generation.

- ***Zone three: Metering / plateau zone (x≈ 375-1185 mm)***

  At this zone, all the trials enter a quasi-steady plateau region in which the melt temperature is almost constant for each trial individually. In this region, again, trial 5 exhibits the upper thermal band, and trials one and two have the lowest. The near-constant slope in this region shows that thermal equilibrium has been established between viscous dissipation, conductive heat transfer to the barrel, and convection axial transport. This is the most favourable situation for reliable product quality since

variations in melt temperature lead to variations in viscosity, which in turn affects pressure at the die and melt homogeneity.

- ***Zone four: Cooling zone (x≈ 1065-1535 mm)***

  The most structurally significant and mechanically interesting feature of the dataset is the behaviour of the fifth trial beyond x≈1065 mm, since this trial undergoes the sharpest temperature reduction among all the other trials. This sharp drop in the temperature (from approximately 210℃ to 155℃) increases the viscosity at the die exit, affecting die swell and the force needed to draw down the extrudate material. The steep axial temperature gradient generates a differential thermal contraction along the die length, contributing to frozen-in orientation and residual stress in the final product.

In general, together, the five trials cover four fundamentally different heat regimes, each with unique consequences for product quality and process design. The thermal spread between the coolest trials (one and two) and the hottest trial (the fifth trial) conditions at any given axial position shows the sensitivity of the process to the experimental variables. In [Table 2], the exact conditions for each trial were mentioned. The variable which had the most difference from other trials was the screw speed in trial five (518RPM). According to this difference, it can be said that the rotation speed was the main parameter that influenced the thermal history of the material inside the extruder.

2.3.2 Pressure

[Fig 85] presents the simulated pressure experienced by the molten polymer as a function of axial distance along the extruder. The pressure profile is markedly non-uniform along the screw length and shows three distinct pressure build-up zones interspersed with regions of near-zero or atmospheric pressure.

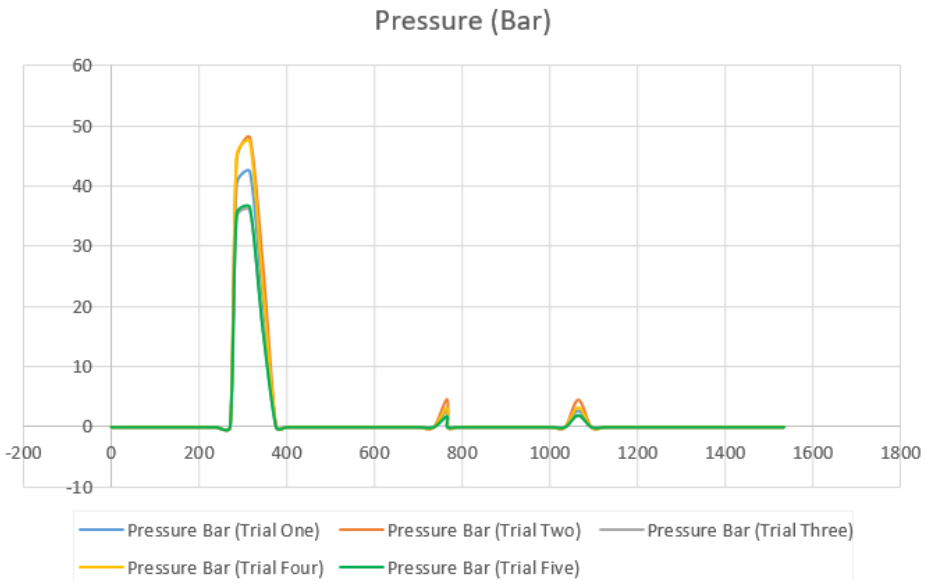

Fig 85. Comparison between the pressure plots of all the simulations

- ***Zone one: primary pressure peak (x≈ 285-375 mm)***

  The most noticeable aspect of all five pressure profiles for five trials is the dominant pressure peak located between 285 and 380 mm along the axial direction. This zone corresponds to the most critical pressurisation region within the extruder, and most likely represents a kneading block. The sharp rise and rapid drop in pressure at this location are consistent with the melt being forced through a constriction before entering a decomposition or venting zone. An important observation at this zone is that trials three and five are indistinguishable. The conditions for these two trials are quite different from each other. The fifth trial has a higher feeding rate and screw speed, and lower barrel temperature compared to the third trial. In section [2.2.4.1.3], it was mentioned that to have higher pressure, the screw speed and barrel temperature should be kept as low as possible, while the feed rate should be high. The fifth trial has a high feed rate and low barrel temperature, but the screw speed is higher than that of the third trial. According to these explanations, it can be said that the combination of these

changes and processing conditions causes the same pressure profile for both of them and the lowest pressure peak among all the trials.

In contrast to trials three and five, the second and fourth trials achieve the highest pressure peak, which indicates that they have a higher feed rate, a lower melt temperature or a combination of them. While the lower melt temperature was obvious in [Fig 84], the feed rate for trial four was higher than that of trial two. However, the screw speed for the second trial was almost half of the screw speed for the fourth trial. The combination of these conditions causes an identical pressure profile for both of them.

- ***Zone two: secondary pressure built-up (x≈ 760-770 mm)***

  The secondary, smaller pressure peak is observed for all the trials at this part of the extruder for all the trials. The overall trend for this part is almost similar to the first pressure peak. This zone likely corresponds to the second kneading block. Having a lower pressure built up at this part confirms that this element is less restrictive and is primarily designed to provide dispersive or distributive mixing rather than significant pressurising.

- ***Zone three: tertiary pressure peak (x≈ 1060-1065 mm)***

  Again, the overall trend for this pressure built up is almost the same as the two before, emphasising the fact that the same processing conditions are the dominant driver of pressure through the screw length. This zone may correspond to the final mixing or conveying section upstream of the die entry or to the last kneading element in a screw configuration.

- ***Baseline behaviour***

  The simulated pressure returns to values close to zero bar between the three pressure peaks, with slight negative deviations that are a known numerical error of the Ludovic simulation framework. These near-zero areas physically correspond to partially full or empty screw sections where the polymer melt is mostly transported by drag-induced flow as opposed to pressure-driven (Poiseuille) flow. The conveying screw sections' minimal resistance to melt transport is consistent with these zones' lack of substantial pressure.

In conclusion, it can be said that, although the combination of different processing conditions can lead to the same pressure profile, the variation between trials one, four, and five highlights the sensitivity of pressure to processing conditions.

2.3.3 Total Residence Time

In [Fig 86] the total residence time of the molten polymer inside the extruder for all the trials is demonstrated. In this context, the total residence time at a given axial position is the cumulative time the material has spent inside the extruder from the feed zone to the current position. Since not all the melt exits from the die at the same time, as shown by the Residence Time Distributions, the TRT describes the evolution of the average values. The decreasing profile observed for all the trials means that, from the beginning of the extruder, the polymer has the longest time to be spent in the extruder. It can be concluded that the polymer melt is transported gradually and without stagnation along the whole screw length, due to the uniform and almost smooth decline seen in all trials. This is a crucial sign of process stability and the lack of dead zones in the simulated extruder.

Fig 86. Comparison between the total residence time plots of all the simulations

As can be seen clearly in [Fig 86], all trials show different residence time profiles that reflect the influence of processing parameters on melt conveying velocity. The longest residence time is for trial one, with an initial value of approximately 50s and a slow reduction that extends almost to 1535mm. This indicates the lowest melt conveying velocity among all trials. This can be explained by the combination of low screw speed and feed rate that was chosen for this trial. This long residence time may be advantageous for the process or may also increase the risk of thermal degradation. For trial two, it can be said that its graph represents an intermediate to high initial residence time (~43s). Its profile decays more steeply than trial one, which means that the conveying velocity is higher for this trial. Since the screw speed was equal for both trials, the higher conveying velocity can be due to the higher feed rate that this trial had

compared to the first trial. The residence time profiles for trials three and four are very close and similar, and their TRT initial values are ~27s and ~24s, respectively. The feeding rate is higher in trial four; the screw speed is 300 RPM for both trials, and the barrel temperature is lower in the fourth trial. The similar residence profile for them means that the combination of their condition causes the same effect on the conveying velocity. In other words, the effects of their processing conditions are closely matched. The last trial, which is trial five, shows the shortest residence time of all conditions, and its starting value is ~16s. This profile corresponds to the highest average melt velocity in the extruder and indicates the most rapid conveying rate. This behaviour was predicted since this trial had the highest screw speed (518 RPM) among all the other trials.

2.3.4 Viscosity

[Fig 87] presents five viscosity curves of the trials. As can be seen, there is a similar trend for all the curves. However, the magnitude and the nature of the fluctuations for each trial are different.

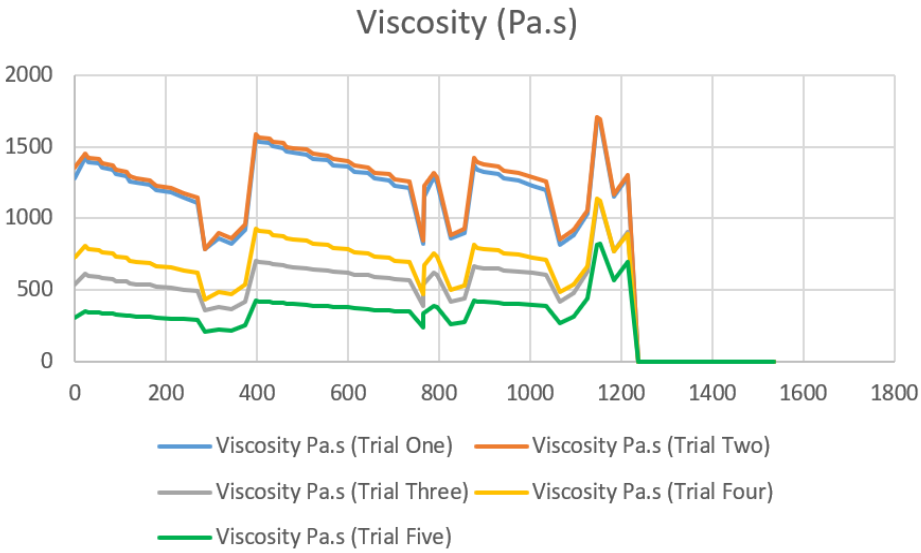

Fig 87. Comparison between the viscosity plots of all the simulations

Starting with the first trial, it should be said that the viscosity of this batch is almost 1276 Pa.s at x=0, indicating a moderately viscous melt entering the barrel. This high initial viscosity is in line with the fact that the melt is not subjected to significant shear yet. As can be seen, there is a drop in the trial one's polymer melt viscosity around x≈ 270 mm. This can be due to the entrance of the melt into the first kneading block. The increase of the shear rate and the associated viscous dissipation, which generates localised frictional heating, are the two mechanisms that cause the reduction of the viscosity at this section. The partial viscosity

recovery can be observed after x ≈ 375, which shows the transition back to a conveying section, where the shear rate decreases, and the melt is thermally stabilised. The second fluctuation occurred near x≈ 795. This drop's smaller amplitude indicates a less intense screw element or a shorter residence time in the high-shear zone. As it is obvious, there is a third drop in viscosity around x≈ 1035 mm, which can be due to a restrictive element or the pressure build-up before the die, because as the melt is compressed into the die entry, the effective shear rate increases at the die lip and produces the final drop.

Continuing with the second trial, it can be said that this trial had the highest viscosity among all the others. At x=0, the initial viscosity for this trial is almost 1358 Pa.s, indicating that the processing condition for this trial produces higher melt viscosity. As can be seen, the fluctuation pattern for trial two is similar to that of trial one but at a higher level. The first viscosity drop pattern is similar, but since the initial viscosity was higher in this trial, the viscosity drop is also larger than in the first trial. As can be seen, there is also a viscosity spike at the same position as in the first trial; besides the conveying element and possible die entry, another mechanism may be responsible for this behaviour, which is melt elasticity. At high viscosities, normal stress differences and melt elasticity become significant; while Ludovic primarily models viscous flow, the parameter sets for Trial Two may include rheological data that accentuate the viscosity peak. Similar to trial one, there is a post-spike viscosity drop, which is compatible with either the partial relaxation of the pressure-induced viscosity spike or the melt passing through the high-shear die land, where shear thinning begins.

The third trial shows relatively lower initial viscosity that trials one and two. At x=0, the initial viscosity is almost 536 Pa.s and remains well below 600 Pa.s for most of the screw length. This lower viscosity in comparison to the two other trials shows that the difference in the processing conditions had a huge influence on the viscosity. While the barrel temperature is the same for all the first three trials, there is a huge difference in the screw speed between the third trial and trials one and two. Higher screw speed (300 RPM for the third trial, which is double the screw speed for the first two trials) increased both shear rate and frictional heating simultaneously, leading to lower viscosity. Again, the fluctuation pattern is the same, and the same reason as the first trial for the first drop of viscosity can be mentioned here too. Going towards the second fluctuation, it can be seen that in comparison to the other two trials, there is a brief fluctuation, which indicates

that the melt is already well mixed and thermally equilibrium. Since there is a fully molten, homogeneous melt flowing, the curve remains almost flat after the second fluctuation. At the end, it can be said that the absence of a significant pre-die spike for the third trial means that the lower-viscosity melt generates less pressure build-up upstream of the die, which avoids the restrictive-element viscosity peak as seen in Trial Two.

Moving to trial four, an intermediate viscosity profile can be seen. At x=0, the initial viscosity is almost 721 Pa.s, and the viscosity profile is similar to all the other trials, closer to trial three. This intermediate pattern shows that the combination of the processing parameters for this trial causes a moderate behaviour of the viscosity.

The last profile is the one for the fifth trial, which begins at a very low viscosity (~ 311 Pa.s), and follows the same fluctuation pattern. This difference in the initial viscosity with respect to other trials can be explained by the higher screw speed that was chosen for this trial. The feeding rate is indeed higher than in the other trials, but the highest screw speed (518 RPM) is also for this trial, which means that the reduction in the initial viscosity is due to this high rotation speed.

In general, it can be said that by looking at the viscosity profile and comparing them together, the effect of the screw speed on viscosity can be seen clearly. Although there are differences in feed rate and barrel temperature among all the trials, the screw speed can be considered as the main processing parameter that affects the viscosity of the molten polymer.

2.3.5 Shear rate

[Fig 88] shows the shear rate profile of the five trials. Three shear rate spikes can be seen across all the trials, which confirms the presence of three kneading elements fixed in the screw configuration.

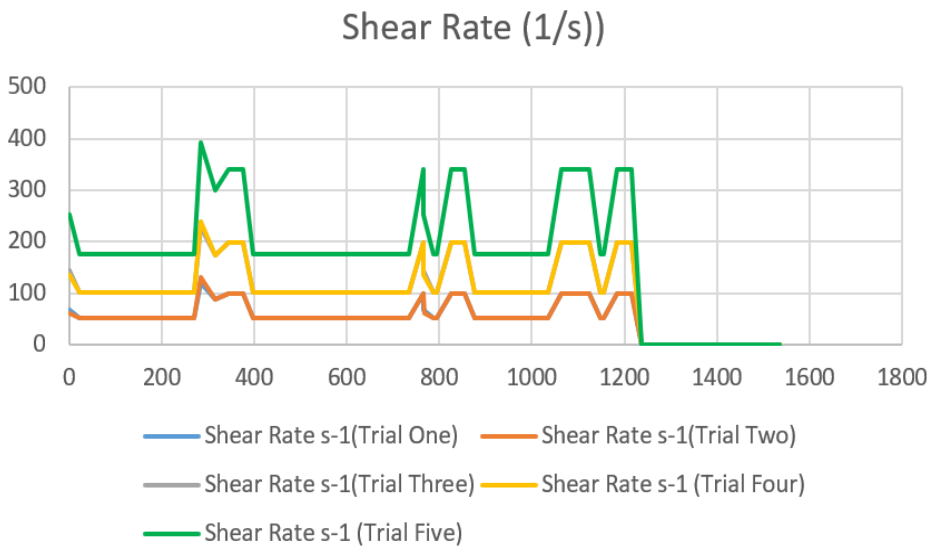

Fig 88. Comparison between the shear rate plots of all the simulations

Starting with the first trial, it can be seen that it has the same profile as trial two. The initial shear rate is almost 67 s^{-1}, and it is almost constant until the first shear rate spike, and this low shear rate is consistent with the low screw speed (150 RPM) for this trial. The identical screw speed for both trials one and two can be considered as the reason for the same share rate profile, which is seen in the shear rate profile. At all three kneading block positions, these two trials show a modest spike, which indicates that even at low screw speeds, kneading blocks impose a significantly higher local shear rate than other available elements.

The next trial is the third trial and has the same profile as the fourth trial. The initial shear rate is almost 144 s^{-1}, and this identical shear rate profile for these two trials confirms the fact that screw speed is the main processing parameter for changing the shear rate since both of them have the same rotation speed (300 RPM).

The last trial (trial five) shows a completely separate profile from the other profiles. It has the highest initial shear rate (~251 RPM), and although the pattern is the same as the other trials for the shear rate spikes, it has a higher magnitude than the others. The highest screw speed (518 RPM) for this trial is the reason for this noticeable difference between the shear rate profiles.

In general, the initial reduction in shear rate for all the trials can be due to the entrance of the molten polymer from the feed zone to a more stable conveying condition inside the extruder. A clearer reduction for the fifth trial is because the initial shear rate was too high. It can be concluded that the pattern for the shear profile confirms the dominance of screw speed in changing the shear rate on each trial.

2.3.6 Mechanical ΔT (℃) ($\Delta \mathbf{T}_{me}^{h}$)

[Fig 89] demonstrates the profile of mechanical $\boldsymbol{\Delta}$T for all five trials. Mechanical Delta T is the localised, quick temperature rise in the polymer melt, which is generated by viscous dissipation rather than by the barrel heaters. It actually represents the extra heat that the melt accumulates above the nominal barrel temperature as a direct result of the mechanical energy input from the rotating screw. Physically, intermolecular friction between polymer chains releases kinetic energy as heat when the screw rotates, and the polymer melt is deformed by shear and elongational flow. In the Ludovic simulation, the contribution of mechanical energy alone to the thermal state of the melt is measured by calculating Mechanical Delta T at each axial location along the screw. It differs from both the barrel temperature setpoint and the total melt temperature. Understanding mechanical $\boldsymbol{\Delta}$T is critical for setting the processing windows, designing screw cooling strategies, and avoiding melt degradation in extrusion processing since it gives us information about the risk of exceeding the material's thermal degradation temperature and the creation of uncontrolled temperature gradients within the melt. In the following, the analysis of the obtained mechanical $\boldsymbol{\Delta}$T profile for all the trials is given. Before starting the explanation of each trial in detail, it should be said that the graph for the five trials directly reflects the spatial distribution of shear-induced heating along the screw axis. In other words, the resulting profile illustrates how the processing conditions develop viscous heating at each zone of the extruder.

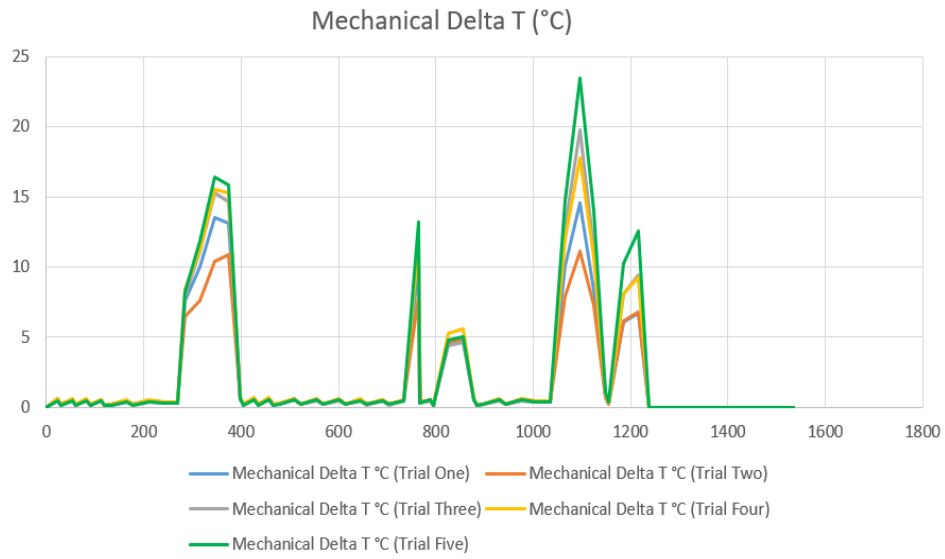

Fig 89. Comparison between the mechanical delta T plots of all the simulations

Three well-defined peaks for the $\Delta \mathbf{T}_{me}^{h}$ can be seen in all the trials, and their position is the same for all the trials. The first trial peak can be seen at x≈315 mm and reaches almost 13℃, and the second peak is located at x=825, where the $\Delta \mathbf{T}_{me}^{h}$ reaches almost 4℃. The last peak is seen at x=1065 and $\Delta \mathbf{T}_{me}^{h}$ reaches the highest value of itself, which is 10℃. As can be seen, among all these peaks, the $\Delta \mathbf{T}_{me}^{h}$ returns to zero, which indicates the efficient thermal equilibration in the conveying zones. Moving to the second trial, it can be said that the lowest peak of $\Delta \mathbf{T}_{me}^{h}$ is for this trial, with the first peak of approximately 7℃, a second peak of 11℃, and the last one of approximately 12℃. Trials three and four are nearly indistinguishable across the entire screw. The first, second and third peaks are approximately 7℃, 11℃, and 12℃, respectively. The last trial produced the most extreme $\Delta \mathbf{T}_{me}^{h}$ profile in the presented curves, and as can be seen, at each peak, it has the highest value. 8℃, 14℃, and 10℃ are the starting values for the first, second, and third peaks, respectively.

In conclusion to this part, it should be noted that the three discrete peaks, separated by near-zero inter-peak intervals, confirm that viscous heating is highly localised at the kneading blocks, while the conveying zones between them allow sufficient heat dissipation.

2.3.7 Conclusion for all the simulation results for each trial

In this part, each trial is analysed individually to determine how the six output variables (melt temperature, pressure, total residence time, melt viscosity, shear rate, and mechanical delta T) interact along the screw to produce a well-organised picture of thermo-mechanical processing. Three mechanically active zones are identified across all trials, which refer to kneading block elements in a screw configuration.

2.3.7.1 **Trial one**

When the six variables are examined together, trial one can be identified as the condition with high melt viscosity, the longest residence time, moderate-to-high pressure peaks, limited shear rate, and no extreme mechanical heating in the kneading zones.

The melt temperature for this trial is one of the lowest of all five trials. At the conveying zone, the profile is largely flat, which confirms that the barrel temperature dominates the thermal state of the melt in this region. Low screw speed at this trial can be one of the reasons for the low melt temperature. As a result of a low screw speed, less shear heating is introduced to the material, keeping the melt temperature lower. In addition, at the three kneading blocks position, a small but visible rise in temperature can be seen. These localised increases are due to the viscous dissipation in the mentioned zones, which is also captured in the $\Delta \mathbf{T}_{me}^{h}$ graph.

The pressure profile of this trial has its first peak at the first position of the kneading blocks, followed by two smaller peaks at the second and third kneading blocks. The large primary pressure peak is directly due to the high melt viscosity of Trial One. As the highly viscous melt is forced through the restrictive kneading block geometry, high pressure must build up to force the molten polymer to move forward. The lower second and third pressure peaks indicated that the relative kneading elements introduce less resistance to the molten polymer.

This trial also shows the longest residence time, which is the direct consequence of its low screw speed, since molten polymer is transported forward slowly. The polymer melt in this trial is subjected to continuous thermo-mechanical loading for the longest period of time among the five trials due to the extended time within the extruder.

Trial one also shows one of the highest melt viscosities. This high viscosity is a result of a lower screw speed, which results in less shear thinning, meaning the melt retains a higher viscosity compared to high screw speed conditions. At each kneading block, the viscosity drops sharply due to the local increase in shear rate. When the melt enters the conveying zone after

each kneading block, the polymer melt partially recovers its viscosity since shear rate returns to a lower value.

When it comes to the shear rate, as expected, one of the lowest values is for trial one due to its low screw speed. At the conveying zones, the shear rate is at its minimum, and the material is mainly transported forward with limited mechanical work. At three kneading block positions, the shear rate increases locally, which can be seen as the visible peaks on [Fig 88]. These peaks are the primary reasons for the viscosity drop and mechanical heating observed at the same axial positions.

The last point that should be mentioned about the trial one is the $\Delta \mathbf{T}_{me}^{h}$ profile. Three distinct peaks can be seen in its profile. It should be said that the combination of high melt viscosity and the shear rate introduced by the kneading elements is responsible for the mechanical heating. Despite the relatively low shear rates of this trial, the high viscosity is sufficient to produce a meaningful local mechanical heating rise.

Generally speaking, the first trial can be considered a low-energy processing condition. The low screw speed keeps the viscosity high, which in turn generates the second highest pressure peak. The low screw speed also produces minimal shear rates, resulting in mechanical heating events at the kneading blocks that are small but highly localised. Lastly, this trial had the longest residence time of all trials, which means that the melt spends the greatest amount of time in the extruder and accumulates mechanical energy gradually over a prolonged period.

2.3.7.2 **Trial two**

Trial two has the same barrel temperature and screw speed as the first trial. When all six variables are analysed together, this trial can be considered as the most viscous and highest-pressure processing condition of all five trials, which means that this trial is the most demanding mechanical loading state within the extruder.

The melt temperature of this trial has an almost identical profile to that of the first trial. Small, localised increases at the three kneading zones are visible, which are in line with the viscous dissipation events at these positions. It can be said that the melt temperature behaviour of trial two is governed almost entirely by the barrel setpoint, with only minimal contributions from mechanical heating. Despite having the highest viscosity and high pressure of all trials, the low screw speed maintains the melt in a high-resistance rheological state throughout the screw.

As mentioned, this trial has the highest-pressure peak, which is a consequence of its highest melt viscosity, because the greater the resistance of the molten polymer to flow, the higher the

pressure needed to transfer the material forward. The high first pressure peak in trial two causes this trial to be considered the most mechanically demanding condition on the extruder. Again, the small secondary and tertiary peaks of the pressure in this trial confirm the fact that the downstream kneading elements cause less restriction on the molten polymer.

The second longest total residence time is for the second trial. The slightly lower residence time compared to trial one is due to the higher throughput of this trial, since the screw speed is the same for both trials. The combination of long residence time and the highest melt viscosity means that the molten polymer in trial two undergoes the most sustained viscous stress loading of any trial over the screw length.

As said before, the highest value of viscosity is for this trial. At each kneading zone, the shear rate increases locally, and the viscosity of the molten polymer decreases as a result of the shear-thinning behaviour. However, after the kneading elements, the molten polymer recovers to its high value since the shear rate is reduced.

The shear rate profile is the same for the first and second trials because the screw speed is the same in both. Localised increases of shear rate at the kneading zones are responsible for the viscosity drops described above. The combination of low shear rate and the highest viscosity of all trials results in the largest viscous stress product, which causes the pressure build-up visible in the pressure profile.

Lastly, the mechanical ΔT profile shows three peaks at the kneading zones. Compared to trial one, although the viscosity is higher in the second trial, the mechanical ΔT values are lower. This can be due to the balance between the viscosity and the shear rate in determining the viscous dissipation. Both trials have the same and relatively low shear rate, which results in different local dissipation.

To conclude trial two, it can be claimed that the overall picture is that this trial is one of the most internal mechanical loading, and the extruder must work at its hardest to process it. This results in the highest-pressure demand while maintaining a relatively low melt temperature and significant viscous heating at the kneading zones.

2.3.7.3 **Trial three**

When all six output variables are examined together, trial three presents a distinctive profile compared to the first and second profiles. It has moderate viscosity, lower pressure build-up, higher shear rate, intermediate total residence time, and higher mechanical heating at the kneading zones.

The melt temperature profile for this trial shows a small, localised increase in the kneading zones, highlighting the viscous dissipation events. Since the barrel temperature is the same as previously described trials, the higher screw speed is the reason for the higher melt temperature in this trial.

In comparison to trials one and two, the pressure profile for the third trial is lower. This can be due to the higher screw speed, which was selected for this trial. The screw speed is twice that of the previous trials, indicating that the reduction in viscosity reduces pressure build-up in kneading zones.

The third trial shows an intermediate total residence time, shorter than trials one and two due to its higher screw speed. The melt spends a reasonable amount of time in the extruder due to its moderate residence time, which allows the kneading elements to act on the molten polymer several times as it moves forward, but for a shorter total duration than in Trials One or Two.

The viscosity profile of trial three shows a noticeable reduction compared to trials one and two, which was expected due to its higher screw speed. This significant reduction in viscosity highlights the fact that higher screw speed introduces a higher shear rate, which increases the viscous dissipation and, as a result, the melt temperature. Eventually, higher melt temperature decreases the viscosity, and in this way, the reduction in viscosity will become the dominant reason for lower pressure build-up.

As mentioned above, higher screw speed produces higher shear rate, and according to this explanation, the higher shear rate profile for the third trial compared to trials one and two is completely understandable.

Mechanical ΔT is the last profile that should be discussed for this trial. As can be seen in [Fig 89] trial three shows one of the highest peaks at the kneading zones. This can be due to the combination of a higher shear rate and viscous dissipation for this trial.

In conclusion, the third trial has moderate viscosity, a higher shear rate than the previous trials, evident mechanical heating, relatively low-pressure build-up, and shorter total residence time. Since the only huge difference between this trial and trials one and two is the screw speed, it can be said that a higher screw speed is responsible for this variation in the mentioned profiles.

2.3.7.4 **Trial four**

By analysing the six output variables together for the fourth trial, a moderate viscosity, intermediate shear rate, high pressure build-up, moderate total residence time, intermediate melt temperature, and relatively high mechanical heating can be seen.

The melt temperature profile for the fourth trial is higher than that of the first and second trials, while the barrel temperature is lower. This can be due to the higher screw speed for the fourth trial than trials one and two, which can increase the shear rate and viscous dissipation. By comparing the fourth trial melt temperature profile with trial three, it can be seen that trial four shows a lower melt temperature along the screw. While the screw speed is the same for both, the barrel temperature is lower, which can be considered the main reason for this difference.

Moving to the pressure profile, it is clear that trials two and four have almost identical behaviour and show the highest peak among all trials. In the fourth trial, a higher feed rate and screw speed are responsible for the high pressure built up. Higher feed rate causes the accumulation of material, which compresses the material ahead of the screw, and at this point, the die acts as a restriction, and this compression directly increases the pressure built up in the molten polymer. Moreover, high screw speed increases the drag flow component. Higher screw speed increases the amount of melt flow to be transported forward, and again, the die will act as a restriction, and a high-pressure peak can be seen. By comparing the third and fourth trials, it should be mentioned that although the screw speed is the same, the feed rate is higher in the fourth trial, which is the reason that this trial shows a higher-pressure peak.

Trial four has the second shortest total residence time. This is understandable due to the high rotation speed, which aids the transfer of molten polymer. It was mentioned that trials three and four have the same screw speed, but the total residence time is shorter in trial four. This is because the barrel temperature is lower in this trial. When the barrel temperature is high, the material needs a longer time to transfer the heat through itself, and a reduction in the barrel temperature will reduce this time.

The viscosity profile for trial four is lower than that of trials one and two, and higher than that of trial three. Higher melt temperature in trial four than in trials one and two, and lower-barrel temperature of the fourth trial than that of trial three, are the reasons for this behaviour, respectively.

The shear rate profile is identical to trial three, which is due to the similar screw speed in these trials. This identical pressure profile emphasises the dominance effect of the screw speed on the shear rate profile.

Lastly, while the mechanical ΔT for the fourth trial is almost similar to that of the third trial (which is understandable due to the different melt temperature, TRT, viscosity profiles and the same shear rate and pressure profiles), it shows a higher peak than trials one and two.

In conclusion, trial four provides a processing state that is reflective of a balanced processing condition since temperature, viscosity, shear rate, and pressure are all at intermediate, evenly distributed levels.

2.3.7.5 **Trial five**

Trial five had the most mechanically intensive processing condition of all five trials, and when all six output variables are considered together, this trial presents the most energetically intense and fastest-processing condition in the simulation.

The melt temperature for this trial shows the highest profile of all trials, which was predictable due to its high screw speed (518 RPM). When the screw speed is high, the molten polymer experiences a higher shear rate, and, as a result, viscous dissipation increases, eventually raising the melt temperature of the material.

For the pressure profile, it is exactly opposite. Trial five shows the lowest pressure profile, similar to trial three. This is due to the dominant effect of viscosity on pressure. The very low viscosity of this trial, which will be explained in the following, means that at high shear rates, the flow resistance through the kneading block restrictions is lower than the high viscosity ones (trials one, two, and four). In other words, pressure can be considered as a product of viscosity and feed rate through a restriction. The low viscosity of this trial results in a lower peak, although the feed rate is higher.

As was expected, the total residence time of this trial is the lowest profile of all trials, and the highest screw speed is the reason for this behaviour, which transports the material through the extruder at the greatest rate. Low residence time of the molten polymer means that, despite the very high shear rates, the cumulative thermal and mechanical exposure of the melt is limited by the shortness of its time in the extruder.

The viscosity profile of trial five is the lowest of all other trials, which can be considered as a direct result of the combination of high melt temperature and high shear rate. High melt temperature reduces the flow resistance, and the highest shear rate further reduces viscosity through shear thinning. Trial five viscosity profile also shows the lowest drop in the kneading zones, and after each kneading, the viscosity recovers partially.

Trial five shows the highest shear rate of all trials by far. This extreme shear rate is a direct consequence of the highest screw speed of this trial. The highest shear rates at the kneading zones are responsible for a severe viscosity drop and the large mechanical ΔT events for trial five.

Lastly, the mechanical ΔT profile of trial five is the most intense one. This represents the maximum mechanical energy dissipation event across all trials and all zones. As stated before, the extremely high shear rate of this trial is the reason for the large mechanical ΔT profile.

Generally speaking, trial five marks the conclusion of the Ludovic software's simulation of processing conditions. A processing condition that is together the most thermally elevated, the most mechanically intense in terms of shear and viscous dissipation, and the least viscous is produced by combining the highest screw rotational speed with the highest shear rates and shortest residence time. Despite the rapid throughput, minimal peak pressure is achieved because the low melt viscosity lowers the pressure needed to push the melt through the screw. The highest absolute melt temperatures in the simulation are produced by imposing the largest Mechanical ΔT events, which are produced by the extremely high shear rates at the kneading zones, on top of the high baseline temperature. Although the rate of thermo-mechanical energy input is the highest of all trials, the short residence period restricts cumulative exposure. Thus, in this simulation study, Trial Five establishes the maximum processing intensity.

To conclude this part, it should be said that the final results of the Ludovic simulation again show that the screw speed had the most influence on pressure, shear rate, viscosity and total residence time, as was stated before in [2.2.4.1]. In addition, its influence on Mechanical ΔT and melt temperature was concluded. The disintegration test of the trials will be described in the sections that follow.

2.4 Disintegration Test

In order to determine the degree of disintegration of G713 samples, an incubator in the MAIP company was used. The whole test was conducted based on ISO/DIS20200:2022, where the degradation of the selected bio compound will be examined when exposed to a laboratory-scale composting environment. It should be said that laboratory-scale composting is a process designed to produce compost at a laboratory scale under environmental conditions simulating those experienced in an industrial compost pile. A synthetic solid waste mixed with mature compost from an industrial or municipal composting facility makes up the solid matrix. This formed solid matrix is incubated with pieces of the G713. There are two types of incubation methods. In type one, for 84 days, the reactors must be kept at a steady temperature of 58 °C. The second type requires a first 56-day incubation period at 58 °C, followed by a second 84-day incubation period at 45 °C. In order to replicate a declining temperature profile over time that is comparable to the one established for the standard test method ISO 16929:2021, a second method has been implemented. After a composting cycle, the final matrix is sieved through a 2 mm sieve to recover the leftovers that have not dissolved in order to measure the degree of disintegration. To determine the degree of disintegration, the test sample's mass decrease is regarded as disintegrated material.

In this study, the first type was used to analyse the disintegration percentage of the selected material.

Aerated compost from a municipal or industrial aerobic composting plant is used as the inoculum. The compost inoculum must be homogeneous and free from large inert objects. Therefore, these objects should be removed manually and then sieve the compost on a screen of mesh aperture between 0.5cm and 1cm. To provide a suitable diversity of microorganisms, the organic part of solid municipal garbage should be composted using plants. Compost from plants that treat farmyard trash, or from blends of garden waste and solid municipal waste, can be utilised if such compost is unavailable. Note that the compost cannot be more than four months old [24].

In the table below, the composition of the synthetic waste used in this method is described.

Table 11. Composition of synthetic solid waste

Material	Dry mass (%)	Humidity (%)	Grams (dry)	Grams (wet)	H_2O (present)
Sawdust	40	9.42	3969	4382	413
Rabbit-feed	30	11.87	2977	3378	401
Ripe compost	10	56.96	992	2305	1313
Corn starch	10	15.33	992	1172	180
Saccharose	5		496	496	
Cornseed oil	4		397	397	
Urea	1		99	99	

The prepared solid waste and the samples should be placed inside a composting reactor. The most suitable composting reactor is a typical plastic box measuring 30cm × 20cm × 10cm (length, width, and height, respectively). To prevent excessive evaporation, the box must have a lid that ensures a tight seal. Adhesive tape can also be used to close any space between the box and lid. To facilitate gas exchange between the internal atmosphere and the external environment, a hole measuring 5mm in diameter must be constructed in the centre of the two 20cm wide sides of the box, about 6.5cm from the bottom. Other containers with a volume between 5 1 and 20 1 can be used, but in this study, a typical plastic box was used.

Before putting the samples inside the composting reactor, they should be cut into a defined dimension, which is given in the [Table 12].

Table 12. dimensions of the pieces of the test material used in the disintegration test

Thickness of test material	Dimensions of pieces (mm)
<5mm	(25 to 50) × (25 to 50) × original thickness
≥5mm	(15 to 25) × (15 to 25) × thickness from 5mm to 15mm)

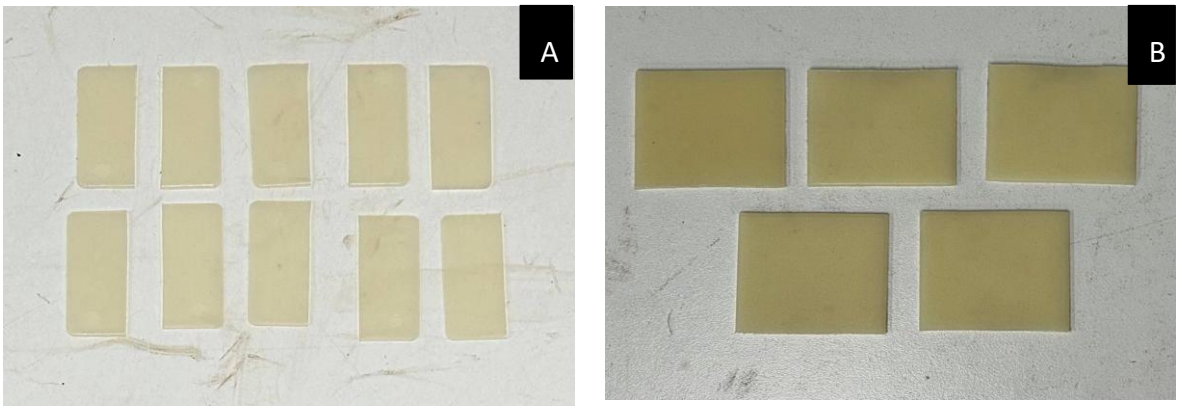

Fig 90. The cut samples with the thickness of A)1mm and B)2mm

It should be noted that, to place the samples in the composting reactor, first, the box should be filled with solid waste to form a homogeneous layer, then the samples should be placed on it, and eventually, the samples should be covered with the mixture. Please consider that the layer should not be compressed to allow efficient gas exchange with the interior of the bed.

Fig 91. The placement of 1mm samples inside the composting reactor

In general, there are two methods for incubation. In method one, the reactors are incubated at a constant temperature over time and in method two, they are incubated at two different temperatures. In this study, the first type was used to incubate the reactors. Type one of the incubation is also known as a ***constant thermophilic incubation,*** in which each reactor is closed, weighed, and placed in an air circulation oven maintained at a constant temperature of 58±2℃ for a minimum time of 45 days and a maximum of 84 days. Maintaining appropriate environmental conditions is essential for a successful composting process. The table below, [Table 13], shows the methodology used in this study. This process keeps the

composting matter's water content sufficient while aerating it. At the start of the composting process, the gross mass of the reactor containing the mixture is calculated. The reactor is weighed at each scheduled time, and if necessary, the initial mass is restored entirely or partially by adding distilled water, deionised water, or tap water free of chlorine. Distilled water was used in this examination. It is crucial to remember that when the composting matter is wet, but there is no free water, the optimum water concentration is achieved. This indicates that the maximum ability to absorb water has not been reached. A regular spoon or a lab spatula can be used to mix the composting material. Proper care must be used during this process to avoid damaging the test material pieces in the compost. Aerating the mass and remixing the water are the goals of mixing, but it's crucial to prevent any mechanical damage to the test material.

Table 13. Composting procedure

Time from start Days	**Operation**
0	Record the initial mass of the reactor
1,2,3,4,7,9,11,14	The reactor should be weighed, and if needed, water should be added to restore the initial weight. The composting should also be mixed.
8,10,16,18,21,23,25,28	The reactor should be weighed, and if needed, water should be added to restore the initial weight. The composting should NOT be mixed.
30,45	The reactor should be weighed, and if needed, water should be added to restore the 80% of the initial weight. The composting should also be mixed.
From 30 to 56, twice a week	The reactor should be weighed, and if needed, water should be added to restore the 80% of the initial weight. The composting should also be mixed.
From 56 to the end, twice a week	The reactor should be weighed, and if needed, water should be added to restore the 70% of the initial weight. The composting should also be mixed.

It should be said that it is better to weigh the samples at the end of each month. This weighting is not accurate since the compost is attached to the samples, and it's not possible to fully remove it from the samples.

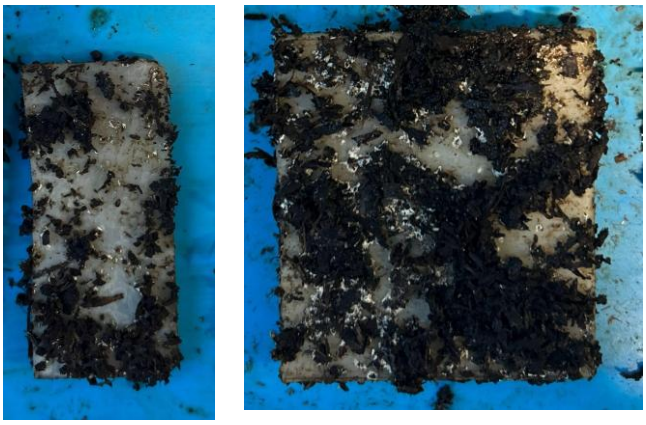

Fig 92. The initial stages of the creation of the bacterial film on the samples

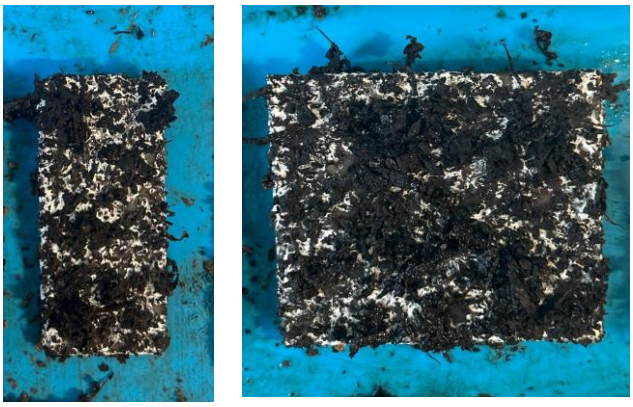

Fig 93. The samples are almost covered with the bacterial film

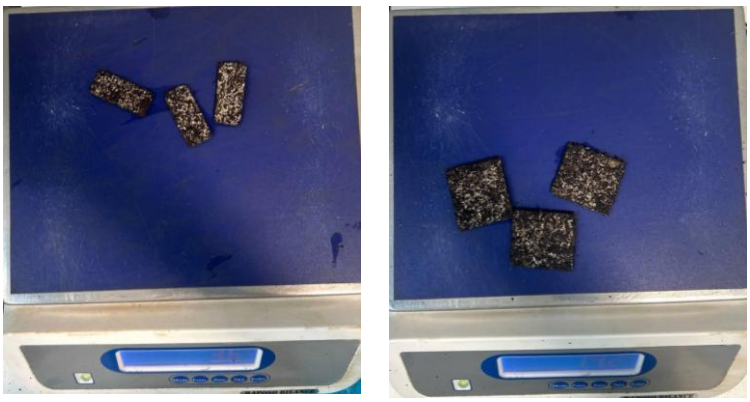

Fig 94. weighting of the samples

After the test is finished, each reactor's lid should be taken off to determine the degree of disintegration. If the content is too moist and might block the sieves, the reactors should be left at room temperature for two to three days to dry the contents. It is necessary to break up any large pieces of compost, and at this stage, special care must be taken to avoid damaging any test material pieces that may remain inside. Each reactor's compost must be sieved using standard sieves in accordance with ISO 3310-1, starting with a 10 mm sieve. The fraction that does not pass through this sieve should be checked. The particles should be allowed to pass through the sieve to collect the fraction smaller than 10 mm. Any fragments of test material that are retained on the 10 mm sieve should be collected and stored. The compost should then be sieved using a 5 mm sieve, followed by a 2 mm sieve, applying the same procedure used for the 10 mm sieve. The test material fragments collected during the different sieving stages should be combined, any remaining compost should be removed, and, if necessary, the fragments should be washed by being immersed in water. To prevent any unintentional loss of test material, the cleaning and washing process must be carried out with extreme caution. Lastly, the test material should be dried under vacuum to constant mass in an oven set at (40±2)°C. The materials that pass the sieve process are regarded as disintegrated materials, whereas the materials that are collected are regarded as non-disintegrated materials. To calculate the degree of disintegration, a specific formula, [Equation 2], should be used:

$$D = \frac{m_i - m_r}{m_i} \times 100$$

Equation 2. The formula for calculating the disintegration percentage

Where:

m_i is the initial weight of the samples

m_r is the dry mass of the remaining test samples collected after the sieving process

The degree of disintegration should be calculated for each composting reactor independently.

[Fig 95] illustrates all the collected samples after the sieving process. As can be observed, all of the 2mm samples are still remaining, but they are excessively fragile and damaged, and all of the 1mm samples have completely disintegrated.

Fig 95. Non-disintegrated dried samples

[Table 14] and [Table 15] provides an overview of all the information obtained from the disintegration test for both G713 bio-compounds, which were moulded at 20℃ and 50℃, respectively. Please consider that G713-1 in the tables means G713 trial one and so on.

As previously stated, weighing the samples at the end of each month is mainly a recommendation and does not provide a precise weight measurement. This is because a bacterial film has formed on the samples' surface, and the compost is still attached to the samples. Therefore, the two previously mentioned factors can account for the samples' weight rise each month.

The results of the disintegration test show a clear difference between the 1mm and 2mm samples. This indicates that the thickness was one of the most important variables. Every 1mm sample was completely disintegrated in both mould temperatures. The 2mm samples were not completely disintegrated, but they show an obvious difference in the degree of disintegration at different temperatures. While none of the 2mm samples exceeded 70% disintegration, the degree of disintegration is higher in the samples which were moulded at 20°C. This means that the mould temperature is another important parameter which influences the disintegration percentage of the samples.

As can be seen in both [Table 14] and [Table 15], there is also a difference in the disintegration percentage in samples with the same mould temperature. This means that the processing parameters, which were different in extruding the samples, have their own influence too. By simply looking at the results, it is not possible to identify the exact impact of each parameter on the disintegration degree; however, with the use of Minitab software, it is possible to identify the parameters that cause this difference in the final disintegration degree. This will be discussed in detail in the following section of this study.

So, in general, by looking at the results, it can be said that thickness and mould temperature were the main factors that influenced the disintegration percentage. The difference in the samples with the same mould temperature shows that each variable in the processing parameters also changes the disintegration degree, which will be examined with the use of Minitab software and explained in detail.

Table 14. Disintegration Test results for G713 moulded at 20℃

	The total weight of the reactor (g)	80% of the total weight of the reactor (g)	70% of the total weight of the reactor (g)	Initial weight of three samples (g)	Three samples' weights after one month (g)	Three samples' weights after two months (g)	Initial weight of all the samples (g)	Final weight of all the samples (g)	The degree of disintegration of the samples (%)
G713-1 (1mm)	1230	984	861	3	3.1	2.9	10	0	100
G713-1 (2mm)	1230	984	861	12.5	15.5	13.3	20.9	6.3	70
G713-2 (1mm)	1230	984	861	3	3.5	2.4	10.1	0	100
G713-2 (2mm)	1230	984	861	12.5	14.1	12.5	20.9	6.7	68
G713-3 (1mm)	1230	984	861	3	3.6	2.8	10.1	0	100
G713-3 (2mm)	1230	984	861	12.6	14	11.9	21	6.7	68
G713-4 (1mm)	1230	984	861	3	3.6	2.5	10.1	0	100
G713-4 (2mm)	1230	984	861	12.5	13.4	12.8	20.8	7.7	63
G713-5 (1mm)	1230	984	861	3.1	3.1	1.8	10.2	0	100
G713-5 (2mm)	1230	984	861	12.5	14.4	12.7	20.9	8	62

Table 15. Disintegration Test results for G713 moulded at 50°C

	The total weight of the reactor (g)	80% of the total weight of the reactor (g)	70% of the total weight of the reactor (g)	Initial weight of three samples (g)	Three samples' weights after one month (g)	Three samples' weights after two months (g)	Initial weight of all the samples (g)	Final weight of all the samples (g)	The degree of disintegration of the samples (%)
G713-1 (1mm)	1230	984	861	3.1	3.5	3	10.3	0	100
G713-1 (2mm)	1230	984	861	12.5	14.2	12.6	20.8	7.6	63
G713-2 (1mm)	1230	984	861	3.1	3.2	3.1	10.2	0	100
G713-2 (2mm)	1230	984	861	12.4	13.3	12.5	20.7	8	61
G713-3 (1mm)	1230	984	861	3	3.2	3	10.1	0	100
G713-3 (2mm)	1230	984	861	12.5	13.9	12.8	20.8	9.5	54
G713-4 (1mm)	1230	984	861	3	3.5	3.2	10.1	0	100
G713-4 (2mm)	1230	984	861	12.5	13.9	13.7	20.8	8.9	57
G713-5 (1mm)	1230	984	861	3	3.6	3.1	10.1	0	100
G713-5 (2mm)	1230	984	861	12.5	13	12.5	20.9	8.4	60

The next chapter contains the analysis of the disintegration results and gives an overall conclusion of all the analyses in this study.

3 Chapter 3

3.1 Statistical analysis with Minitab software

Minitab is statistical software widely used in process engineering, developed at Penn State University in 1972. This software provides a comprehensive suite of statistical tools designed to enable researchers and engineers to analyse complex datasets, identify patterns, build predictive models, and make data-driven decisions without requiring advanced programming knowledge. At its core, Minitab offers an interactive worksheet environment where data can be entered and organised in a column-based format, similar in appearance to a spreadsheet. However, unlike general-purpose spreadsheet tools, Minitab is specifically engineered to perform accurate statistical analyses, with built-in procedures that follow validated methodologies consistent with internationally recognised statistical standards.

Among the many analytical capabilities of Minitab, its Design of Experiments (DOE) module is particularly relevant to the present study. DOE is a systematic method for planning experiments so that the resulting data can be statistically analysed to produce reliable, valid, and objective conclusions. Through DOE, it is possible to identify which factors significantly influence a response variable, determine the magnitude of those effects, and detect interactions between factors that may not be apparent through one-factor-at-a-time testing. Minitab supports several DOE methodologies, including full factorial designs, fractional factorial designs, response surface designs, and mixture designs. In the present investigation, a factorial regression approach was employed. This method fits a linear model to the experimental data, incorporating main effects and interaction terms, and evaluates which terms are statistically significant in explaining the variation observed in the response variable, which in this study is the disintegration rate of G713.

The software provides several indicators to assess model quality, including the coefficient of determination (R-squared), adjusted R-squared, the standard error of regression (S), variance inflation factors (VIF) for detecting multicollinearity, analysis of variance (ANOVA) tables, and residual plots. These tools collectively allow the researcher to evaluate the validity and reliability of the fitted model before drawing conclusions from it. Minitab also generates graphical outputs such as Pareto charts of effects, normal probability plots of effects, main effects plots, interaction plots, contour plots, and surface plots, all of which are invaluable for communicating findings clearly and for identifying optimum operating conditions. The regression equation produced by Minitab can then be used to predict the response at any combination of factor levels within the experimental space, making it a highly practical tool for process optimisation.

Given the large number of potential factors and the limited number of experimental runs (n = 10), a Stepwise Selection procedure was applied in Minitab to identify the most statistically relevant predictors. Stepwise selection is an automated model-building technique that iteratively adds or removes terms from the model based on their statistical significance. The selection criteria used were α=0.15. The significance level (α) is a pre-defined probability threshold used in statistical hypothesis testing to determine whether an observed effect is statistically significant or likely due to random chance. In this study, α stands for the highest possible probability that a processing parameter looks meaningful just by coincidence but has no actual impact on the disintegration percentage. A factor is kept in the model when its observed effect is unlikely to be random, as shown by a p-value < α. In this analysis, a significance level of α = 0.15 was applied for both entry and removal of terms during the stepwise selection procedure. This threshold was selected in place of the conventional α = 0.05 due to the relatively small number of experimental runs (n = 10), as smaller datasets produce less statistical power, making it more difficult to detect real effects at stricter thresholds. The use of α = 0.15 is an accepted practice in exploratory experimental studies where the primary objective is to identify the most influential factors rather than to confirm effects with a high degree of certainty.

Table 16. Selection Criteria

Criterion	Value	Meaning
α to enter	0.15	A term is added to the model if its p-value is below 0.15
α to remove	0.15	A term is removed from the model if its p-value rises above 0.15

One important table present in the Minitab result is the Coded Coefficient table [Table 17]. The coded coefficients table shows how each processing parameter affects the disintegration percentage, and how accurate the shown effect is. Before running the analysis, Minitab converts all the factor values into a standardised scale ranging from -1 to +1, regardless of their original units. This is done simply because the factors are measured in completely different units. As an example, feed rate is in kg/h and Screw speed is in RPM and converting them to the same scale makes it possible to fairly compare how much influence each one has on the result.

The table contains several columns, and each of them gives different information. The Effect column shows the total change in disintegration percentage when a factor is moved from its lowest tested value to its highest tested value. Both factors in this model have negative effects, meaning that increasing either feed rate or mould temperature causes the disintegration percentage to decrease. The Coefficient is simply half of the effect value and represents the slope of the relationship between each factor and the response. The Standard Error (SE Coef) indicates how precise that coefficient estimate is. The smaller it is relative to the coefficient, the more reliable the estimate. Next is the T-Value, which is calculated by dividing the coefficient by its standard error, and it reflects how strong the evidence is that a factor has a real effect. Based on this explanation, it can be said that the larger the T-Value, the more accurate the analysis is. Another column in the table is the P-Value, which translates the T-value into a probability, specifically, the probability that the observed effect happened by random chance. In this model, Mould Temperature has a p-value of 0.006, meaning there is only a 0.6% chance its effect is coincidental, while Feed Rate has a p-value of 0.077, meaning a 7.7% chance. Both fall below the significance threshold of $\alpha = 0.15$ and are therefore considered statistically significant. Finally, the VIF (Variance Inflation Factor) value of 1.00 for both factors confirms that the two predictors are completely independent of each other and do not interfere with one another's estimates.

Table 17. Coded Coefficient Table

Term	Effect	Coefficient	SE Coef	T-Value	P-Value	VIF
Constant	—	62.239	0.952	65.37	0.000	—
Feed Rate (kg/h)	-5.65	-2.82	1.37	-2.07	0.077	1.00
Mould Temperature (°C)	-7.200	-3.600	0.936	-3.85	0.006	1.00

Another important table available in the result file is the Model Summary [Table 18]. This table provides four key statistics that describe how well the regression model fits the experimental data. The first is S, also known as the Residual Standard Error, which represents the average distance between the actual measured disintegration values and the values predicted by the model. In this study, S = 2.960, meaning that on average, the model's predictions deviate from the real measurements by approximately 2.96 percentage points. The second statistic is R^2, which indicates the percentage of the total variation in disintegration percentage that is explained by the model. An R^2 of 73.15% means that 73.15% of the differences observed between experimental runs can be accounted for by the factors selected by the model, while the remaining 26.85% is attributed to other sources of variation not captured by the model. The third statistic is R^2(adjusted), which is a more reliable version of R^2 because it restricts the model from having additional predictors that do not improve the fit. The R^2(adjusted) value of 65.48% is therefore the most appropriate measure of model fit to report, as it accounts for the number of predictors relative to the number of observations. The fourth statistic is R^2(predicted), which estimates how well the model would perform if used to predict disintegration percentages for new experimental runs that were not part of the original dataset. A value of 39.53% reflects the limited predictive power of the model beyond the original data, which is expected given the small number of experimental runs and the presence of some variability in the dataset.

Table 18. Model Summary

S	R-sq	R-sq (adj)	R-sq (pred)
2,95981	73,15%	65,48%	39,53%

The next table is the Analysis of Variance (ANOVA), which is a statistical method used to determine if the variation observed in the experimental results is caused by the processing parameters in the model, or it is due to random experimental error.

The fundamental idea behind ANOVA is that the total variation measured across all experimental runs can be split into two parts. The variation that is explained by the model and the variation that remains unexplained, which is referred to as error. By comparing these two portions against each other, ANOVA produces an F-Value, which is a ratio of the variation explained by the model to the variation caused by random error.

A large F-Value indicates that the model explains substantially more variation than random error does, which is a sign that the factors in the model have a genuine and meaningful effect on the response. This is then translated into a p-value for the overall model, which in this study is 0.010, meaning there is only a 1% probability that the relationships identified between the processing parameters and the disintegration percentage occurred by chance. In general, ANOVA confirms that the regression model as a whole is statistically significant and that the variation in disintegration percentage is not simply the result of random experimental noise. Other available terms in the table are DF (Degrees of Freedom), which is the number of independent pieces of information used to estimate each source of variation. The model has 2 DF (one per predictor), the error has 7 DF, and the total has 9 DF (n−1 = 10−1). Adj SS (Adjusted Sums of Squares) is the next visible term, which is the amount of variation in the response attributable to each source, adjusted for the presence of the other terms in the model. It is used instead of sequential SS because the design is not orthogonal. The next term is Adj MS (Adjusted Mean Square), which is Adj SS divided by DF. It represents the average variation per degree of freedom for each source. All this information is available in [Table 19].

Table 19. Analysis of Variance

Source	DF	Adj SS	Adj MS	F-Value	P-Value
Model	2	167,08	83,538	9,54	0,010
Linear	2	167,08	83,538	9,54	0,010
Feed rate (kg/h)	1	37,48	37,477	4,28	0,077
Mould Temperature (°C)	1	129,60	129,600	14,79	0,006
Error	7	61,32	8,760		
Total	9	228,40			

As can be seen in the [Table 19], only feed rate and the mould temperature were the main parameters that affect the disintegration percentage of G713. Please consider that in this analysis, the selection of significant factors was not performed manually but was carried out automatically by Minitab through the stepwise selection procedure. All the processing parameters (barrel temperature, feed rate, screw speed, and mould temperature) were initially entered into the analysis as candidate factors. Minitab then automatically evaluated the statistical significance of each factor by comparing its p-value against the pre-defined significance threshold of $\alpha = 0.15$. Factors whose p-value exceeded this threshold were automatically removed from the model, as they did not demonstrate a statistically significant relationship with the disintegration percentage. This procedure continued until the model contained only the variables that contributed to explaining the response's fluctuation. As a result, Feed Rate and Mould Temperature were retained as the only statistically significant predictors. Another important row in the table is the linear row. This indicates the relation between the remaining parameters and the disintegration percentage of the material.

Based on all this information, the final regression equation, which is given by the Minitab software, can be seen in [Equation 3].

$$Disintegration\ \%\ (2mm) = 76.85 - 0.1129\ Feed\ rate\ (\frac{kg}{h}) - 0.2400\ Mould\ temperature\ (℃)$$

Equation 3. Regression Equation in Uncoded Units

This equation can be used directly to predict the disintegration percentage for any combination of fed rate and mould temperature, and it uses the actual measured values of the predictors. As can be seen, both of the main parameters have a negative sign, and since both of them have a linear relation with the disintegration percentage, it can be said that increasing each of the parameters will decrease the percentage of disintegration. In [Table 20], all the parameters available in the equation are explained in more detail.

Table 20. Explanation of the terms in the equation

Term	Value	Interpretation
Intercept	76.85	The predicted disintegration percentage when both Feed Rate and Mould Temperature are equal to zero. This is a mathematical baseline and does not represent a physically meaningful operating condition.
Feed Rate coefficient	−0.1129	If the mould temperature is considered as a constant parameter, for every 1 kg/h increase in feed rate, the disintegration percentage decreases by 0.1129 percentage points.
Mould Temperature coefficient	−0.2400	If the feed rate is considered as a constant parameter, for every 1°C increase in mould temperature, the disintegration percentage decreases by 0.2400 percentage points.

It should be noted that Minitab identified Observation 8 (G713-4 (2mm)) as having a high residual, indicating a 5.43-percentage-point difference between the model's predicted value (59.43%) and the actual measured value (54.00%). Minitab highlights the standardised residual of -2.06 for attention because it is greater than the traditional threshold of ±2.0 [Table 21].

This observation could be the result of an uncontrolled variable, measurement error for that specific run, or natural experimental variability. Its existence should be taken into consideration when analysing the results, although it does not invalidate the model.

Table 21. Fits and Diagnostics for Unusual Observations

Obs	Disintegration % (2mm)	Fit	Resid	Std Resid	
8	54,00	59,43	-5,43	-2,06	R

As mentioned before, Minitab also provides a Pareto chart, a graphical tool that shows the magnitude and statistical significance of each factor's effect [Fig 96]. The chart confirms visually what the numerical analysis shows quantitatively. Mould Temperature (E) produces the longest bar, extending to approximately 3.85, well beyond the significance threshold. This makes it the dominant factor controlling disintegration percentage in this experiment. Feed Rate (B), with a bar extending to approximately 2.07, also crosses the threshold and is the second significant factor.

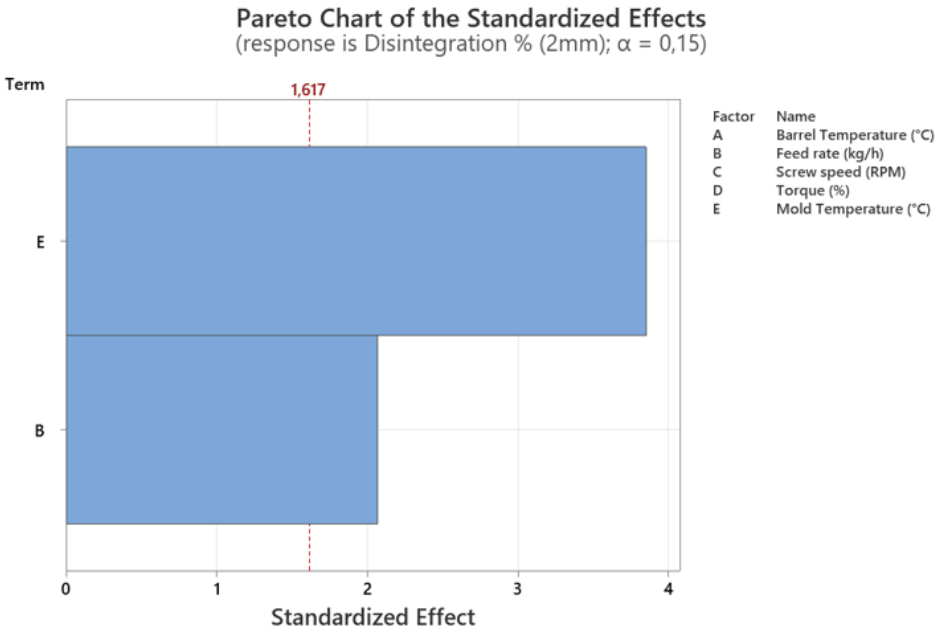

Fig 96. Pareto Chart of the standardised effects

As can be seen in [Fig 96], all the other factors do not appear in the chart because they were eliminated during the stepwise selection process due to having standardised effects below the threshold. This confirms that within the range of tested conditions in this study, neither barrel temperature nor screw speed had a statistically detectable influence on disintegration.

3.2 Conclusion

After having the statistical results from the Minitab software, it can be estimated that among all the independent variables for the processing condition (the barrel temperature, the feed rate, and the screw speed), only feed rate had a meaningful and significant effect on the disintegration percentage of the material, and it has a direct negative effect, meaning that increasing the federate will decrease the disintegration percentage of the material. This result is in line with what has been seen in [Table 14], [Table 15]. As can be seen, trial one, which had the lower feed rate, has the highest disintegration percentage regardless of its mould temperature. It should be mentioned that, with the use of the Ludovic software [2.2.4.1.1], the effect of these processing parameters on six dependent variables was studied. In Minitab, none of these dependent variables was identified as an important parameter affecting the disintegration percentage.

Moving forward, the mould temperature in injection moulding is the most important parameter that affects the disintegration percentage, and it also has a direct inverse effect, meaning that increasing it will reduce the disintegration percentage, which is again in line with the results mentioned in [Table 14], [Table 15].

Another parameter, which is not considered a processing parameter but has an effect on the disintegration of the material, is the thickness of the samples. As was mentioned before, 1mm samples have been disintegrated completely, indicating that, besides processing parameters, the dimension of the material is another important thing that should be considered. The table below summarises all the findings of the analysis in this study.

Table 22. Summary of the results

Objective	**Federate**	**Mould temperature**	**Thickness**
Maximising the disintegration	Lower the feed rate	Lower mould temperature	Lower thickness
Minimising the disintegration	The higher the feed rate	Higher mould temperature	Higher thickness

In conclusion, in this study, five trials of G713 were extruded, then moulded at two different temperatures with an injection moulding machine. The independent processing parameters that varied among the trials were feed rate, barrel temperature, and screw speed. Then, with the Ludovic software, the relation and effect of these parameters on dependent variables (SME, torque, pressure, viscosity, shear rate, and residence time) were investigated. It should be said that these parameters were selected due to their relation to the stress that the material will experience inside the extruder. Meanwhile, the disintegration test for the trials was conducted at the MAIP Compounding Srl. At the end, when all the needed information was collected, and the disintegration test had been done, the statistical analysis with the Minitab software was accomplished, in which only feed rate, moulding temperature, and thickness had a notable and relevant effect on the disintegration percentage of the material.

4 References

[1] F. Zeng, L. Luo, X. Huang, and N. Pradhan, “Polyhydroxyalkanoates (PHA) based biopolymers: properties, applications and biodegradation,” *Advances in Bioenergy*, vol. 10, pp. 101–127, Jan. 2025, doi: 10.1016/bs.aibe.2025.03.003.

[2] J. N. Lalonde, G. Pilania, and B. L. Marrone, “Materials designed to degrade: structure, properties, processing, and performance relationships in polyhydroxyalkanoate biopolymers,” Oct. 15, 2024, *Royal Society of Chemistry*. doi: 10.1039/d4py00623b.

[3] “D. Nath, E. Pesaranhajiabbas, A. K. Pal, B. Ramarao, M. Misra, and A. K. Mohanty, ‘Polyhydroxyalkanoates (PHAs) Advancements in blends, biocomposites, and their commercialization,’ in Polyhydroxyalkanoates (”.

[4] R. E. Martínez-Herrera, M. E. Alemán-Huerta, O. M. Rutiaga-Quiñones, E. de J. de Luna-Santillana, and T. O. Elufisan, “A comprehensive view of Bacillus cereus as a polyhydroxyalkanoate (PHA) producer: A promising alternative to Petroplastics,” Jun. 01, 2023, *Elsevier Ltd*. doi: 10.1016/j.procbio.2023.03.032.

[5] S. H. Hadri, N. Tareen, A. Hassan, M. Naseer, K. Ali, and H. Javed, “Alternatives to conventional plastics: Polyhydroxyalkanoates (PHA) from microbial sources and recent approaches – A review,” Mar. 01, 2025, *Institution of Chemical Engineers*. doi: 10.1016/j.psep.2025.106809.

[6] H. Park, H. He, X. Yan, X. Liu, N. S. Scrutton, and G. Q. Chen, “PHA is not just a bioplastic!,” Mar. 01, 2024, *Elsevier Inc.* doi: 10.1016/j.biotechadv.2024.108320.

[7] J. C. C. Yeo *et al.*, “Innovative biomaterials for food packaging: Unlocking the potential of polyhydroxyalkanoate (PHA) biopolymers,” *Biomaterials Advances*, vol. 163, Oct. 2024, doi: 10.1016/j.bioadv.2024.213929.

[8] Y. X. Weng, Y. Wang, X. L. Wang, and Y. Z. Wang, “Biodegradation behavior of PHBV films in a pilot-scale composting condition,” *Polym. Test.*, vol. 29, no. 5, pp. 579–587, Aug. 2010, doi: 10.1016/j.polymertesting.2010.04.002.

[9] M. Salomez *et al.*, “A comparative study of degradation mechanisms of PHBV and PBSA under laboratory-scale composting conditions,” *Polym. Degrad. Stab.*, vol. 167, pp. 102–113, Sep. 2019, doi: 10.1016/j.polymdegradstab.2019.06.025.

[10] P. K. Shin, M. H. Kim, and J. M. Kim, “Biodegradability of Degradable Plastics Exposed to Anaerobic Digested Sludge and Simulated Landfill Conditions,” 1997.

[11] P. Lyshtva *et al.*, “Degradation of a poly(3-hydroxybutyrate-co-3-hydroxyvalerate) (PHBV) compound in different environments,” *Heliyon*, vol. 10, no. 3, Feb. 2024, doi: 10.1016/j.heliyon.2024.e24770.

[12] R. Bellache, D. Hammiche, A. Bettache, and A. Boukerrou, “Enzymatic degradation of prickly pear seed (PPS)/Polyhydroxy(butyrate-co-valerate) (PHBV) biocomposite,” in *Materials Today: Proceedings*, Elsevier Ltd, 2022, pp. 113–116. doi: 10.1016/j.matpr.2021.12.419.

[13] S. M. Emadian, T. T. Onay, and B. Demirel, “Biodegradation of bioplastics in natural environments,” Jan. 01, 2017, *Elsevier Ltd*. doi: 10.1016/j.wasman.2016.10.006.

[14] C. Frank, A. Emmerstorfer-Augustin, T. Rath, G. Trimmel, M. Nachtnebel, and F. Stelzer, “Bio-Polyester/Rubber Compounds: Fabrication, Characterization, and Biodegradation,” *Polymers (Basel).*, vol. 15, no. 12, Jun. 2023, doi: 10.3390/polym15122593.

[15] J. Y. Cho *et al.*, “Polyhydroxyalkanoates (PHAs) degradation by the newly isolated marine Bacillus sp. JY14,” *Chemosphere*, vol. 283, Nov. 2021, doi: 10.1016/j.chemosphere.2021.131172.

[16] M. J. Getahun, B. B. Kassie, and T. S. Alemu, “Recent advances in biopolymer synthesis, properties, & commercial applications: a review,” Oct. 01, 2024, *Elsevier Ltd*. doi: 10.1016/j.procbio.2024.06.034.

[17] D. V. A. Ceretti, M. Edeleva, L. Cardon, and D. R. D’hooge, “Molecular Pathways for Polymer Degradation during Conventional Processing, Additive Manufacturing, and Mechanical Recycling,” Mar. 01, 2023, *MDPI*. doi: 10.3390/molecules28052344.

[18] R. R. de Sousa Junior, C. A. S. dos Santos, N. M. Ito, A. N. Suqueira, M. Lackner, and D. J. dos Santos, “PHB Processability and Property Improvement with Linear-Chain Polyester Oligomers Used as Plasticizers,” *Polymers (Basel).*, vol. 14, no. 19, Oct. 2022, doi: 10.3390/polym14194197.

[19] G. Janowski, W. Frącz, Ł. Bąk, and T. Trzepieciński, “The Effect of the Extrusion Method on Processing and Selected Properties of Poly(3-hydroxybutyric-co-3-hydroxyvaleric Acid)-Based Biocomposites with Flax and Hemp Fibers,” *Polymers (Basel).*, vol. 14, no. 24, Dec. 2022, doi: 10.3390/polym14245370.

[20] C. H. Lee, S. H. Lee, A. Khalina, S. M. Sapuan, and R. A. Ilyas, "Development and Processing of PLA, PHA, and Other Biopolymers," in *Advanced Processing, Properties, and Applications of Starch and Other Bio-based Polymers*, Elsevier, 2020, pp. 47–63. doi: 10.1016/B978-0-12-819661-8.00005-6.

[21] C. Vanheusden *et al.*, "Extrusion and injection molding of poly(3-hydroxybutyrate-co-3-hydroxyhexanoate) (phbhhx): Influence of processing conditions on mechanical properties and microstructure," *Polymers (Basel).*, vol. 13, no. 22, Nov. 2021, doi: 10.3390/polym13224012.

[22] L. J. Vandi, C. M. Chan, A. Werker, D. Richardson, B. Laycock, and S. Pratt, "Experimental data for extrusion processing and tensile properties of poly(hydroxybutyrate-co-hydroxyvalerate) (PHBV) polymer and wood fibre reinforced PHBV biocomposites," *Data Brief*, vol. 22, pp. 687–692, Feb. 2019, doi: 10.1016/j.dib.2018.12.084.

[23] S. A. Thompson and R. O. Williams, "Specific mechanical energy – An essential parameter in the processing of amorphous solid dispersions," Jun. 01, 2021, *Elsevier B.V.* doi: 10.1016/j.addr.2021.03.006.

[24] Plastics — Determination of the degree of disintegration of plastic materials under composting conditions in a laboratory-scale test, ISO/DIS Standard 20200:2022, 2022